

NORTH-WEST UNIVERSITY
YUNIBESITI YA BOKONE-BOPHIRIMA
NOORDWES-UNIVERSITEIT

THE APPLICABILITY OF AN EXISTING TUBE CONDENSER MODEL WHEN USED WITH REFRIGERANT R-407C

GERRIAAN WESSELS B. Eng.

Dissertation submitted in partial fulfilment of the requirements
for the degree Master of Engineering
at the
North-West University

Supervisor: Dr. M. van Eldik
November 2007
Potchefstroom Campus

ACKNOWLEDGEMENTS

"Nothing is impossible for God" (Luke 1:37), therefore I am capable to accomplish anything. I would like to thank my Heavenly Father for His support, inspiration and love, especially during this study.

To my parents, thank you for all your love, support, guidance, care and constant availability throughout this life. I really appreciate it all, tons of love from me to you.

A special word of thanks goes to Dr Martin van Eldik, my promoter, for his exceptional guidance, support, patience and advice. Thank you and the School of Mechanical Engineering for the financial support, which made it possible to complete the study.

I would like to thank Robbie Arrow for his enthusiasm, humour and assistance in helping me with the experimental test facility.

ABSTRACT

Title:	The applicability of an existing tube condenser model when used with Refrigerant R-407C
Author:	Gerriaan Wessels
Supervisor:	Dr. M van Eldik
School:	School of Mechanical Engineering
Degree	Master of Engineering

The Montreal Protocol resulted in the phase out of ozone depleting refrigerants like chloroflourocarbons (CFC) and hydrochloroflourocarbons (HCFC) used in refrigeration and heat pump applications. In heat pump applications the environmentally friendly refrigerant mixture, R-407C, usually replaces these refrigerants. The use of these zeotropic refrigerant mixtures has technical implications when the performance of refrigeration systems in industry is evaluated. These zeotropic mixtures display a temperature glide during the condensation process, which can be exploited to improve heat exchanger performance.

In the past decade, research also focused on the enhancement of the heat transfer area by applying passive schemes. Limited information is available on the condensation characteristics of R-407C inside fluted tube annuli. Nevertheless, Rousseau *et al.* (2003) claimed that their correlation could be used to simulate a zeotropic mixture inside fluted tube annuli. Therefore, a need exists to investigate the applicability of the correlation by Rousseau *et al.* (2003) for R-407C condensation inside fluted tube annuli.

In order to evaluate the correlation, experimental data was gathered from a fluted tube test facility. The test section consists of a pre-, test- and sub-cooler. The refrigerant's mass flow rate, temperature and pressure were measured at each inlet and outlet of the condensers as well as the water's temperature and mass flow rate. The experimental results proved that the correlation of Rousseau *et al.* (2003) was only 48% accurate in predicting the pressure drop and 95% accurate for the heat transfer of R-407C during the condensation process inside fluted tube annuli. Due to this inexactness, new enhancement factors for pressure drop and heat transfer were derived from comparing the experimental data against the simulation results.

These newly generated enhancement factors were implemented in the correlation of Rousseau *et al.* (2003) and predicted the theoretical pressure drop with a 90.48% accuracy and the heat transfer with a 99.48% accuracy. Thus, this method is acceptable to predict the data for design applications.

UITTREKSEL

Titel: Die bruikbaarheid van 'n huidige *fluted tube* kondenser model wanneer verkoelingsmengsel R-407C gebruik word.
Outeur: Gerriaan Wessels
Studieleier: Dr. M van Eldik
Skool: Skool vir Meganiese Ingenieurswese
Graad Magister in Ingenieurswese

Die Montreal Protokol het gelei tot die uitfasering van verkoelingsgasse soos chloorfluoridekoolstof (CFC) en waterstof-chloorfluoriedkoolstof (HCFC) wat die osoonlaag verdun en dikwels in verkoelings- en hitte-pomp toepassings gebruik word. In hitte-pomp toepassings word hierdie verkoelingsgasse meestal deur die omgewingsvriendelike verkoelingsmengsel R-407C vervang. Die gebruik van hierdie zeotropiese verkoelingsmengsels het egter tegniese implikasies wanneer verkoelingstelsels se werkverrigting in die industrie geëvalueer word. Dié zeotropiese mengsels toon temperatuurverplasings tydens die kondensasieproses. Die temperatuurverplasings kan egter gebruik word om die vertoning van hitte-uitruiling te verbeter.

Gedurende die laaste dekade het navorsing ook op die verbetering van die hitte-oordrag area gefokus, deur passiewe skemas toe te pas. Daar is egter beperkte inligting oor die kondensasie eienskappe van R-407C binne die geriffelde pypringe beskikbaar. Rousseau *et al.* (2003) is van mening dat hul korrelasie gebruik kan word om die zeotropiese mengsel binne die geriffelde pypringe te stimuleer. Daar is dus 'n behoefte ge-identifiseer om die toepassing van Rousseau *et al.* (2003) se korrelasie op R-407C kondensasie binne die geriffelde pypringe te ondersoek.

Eksperimentele data is deur die gebruik van 'n geriffelde-pyp toetsfasiliteit ingesamel ten einde die korrelasie te evalueer. Hierdie toetsfasiliteit het uit 'n voor-, toets- en sub-verkoeler bestaan. Die verkoelingsgas se massavloei tempo, temperatuur en druk is by elke in- en uitlaat van die kondenseerder gemeet. Die water se temperatuur en massavloei tempo is ook

bepaal. Eksperimentele resultate het getoon dat Rousseau *et al.* (2003) se korrelasie slegs 48% akkuraat is om die drukval te voorspel en 95% akkuraat is om die hitte-oordrag van R-407C gedurende die kondensasieproses binne die geriffelde pypringe te voorspel. Daarom is nuwe verbeterde faktore vir drukval en hitte-oordrag verkry deur die eksperimentele data met die simulasie resultate te vergelyk.

Hierdie nuut gegenereerde, verbeterde faktore is in Rousseau *et al.* (2003) se korrelasie geïmplementeer met die gevolg dat dit die teoretiese drukval 90.48% akkuraat voorspel en die hitte-oordrag met 99.45%. Dus, is hierdie metode aanvaarbaar om data vir ontwerptoepassings te voorspel.

TABLE OF CONTENTS

ACKNOWLEDGEMENTS ..... **I**

ABSTRACT ..... **II**

UITTREKSEL ..... **IV**

TABLE OF CONTENTS ..... **VI**

LIST OF FIGURES ..... **X**

LIST OF TABLES ..... **XII**

NOMENCLATURE ..... **XIII**

CHAPTER 1 ..... **1**

INTRODUCTION **1**

1.1 BACKGROUND 1

1.2 NEED FOR THIS STUDY 3

1.3 PROBLEM STATEMENT 5

1.4 METHOD OF INVESTIGATION 5

1.5 CONTRIBUTION OF THIS STUDY 6

CHAPTER 2 ..... **7**

LITERATURE STUDY **7**

2.1 INTRODUCTION 7

2.2 CHARACTERISTICS OF REFRIGERANT MIXTURES 7

2.2.1 Description of refrigerant mixtures *7*

2.2.2 Temperature glide of zeotropic mixtures *10*

2.2.2.1 Dew and bubble point *10*

2.2.2.2 Temperature glide *11*

2.2.3 The effect of temperature glide of zeotropic mixtures on refrigerant systems *13*

2.2.4 Steady-state efficiency improvement *18*

2.3 HEAT TRANSFER CHARACTERISTICS OF ZEOTROPIC MIXTURES 19

2.3.1 Two - phase flow patterns *19*

2.3.2 Internal forced convective boiling *20*

2.4. TECHNIQUES USED TO IMPROVE THE HEAT TRANSFER OF ZEOTROPIC MIXTURES 21

2.4.1 Techniques used to improve heat transfer *22*

2.4.1.1 Fluted tubes *22*

2.4.1.2 Finned tubes *24*

2.4.1.3 Microfin tubes *24*

2.4.1.4 Herringbone tubes *25*

2.5 SUMMARY 26

CHAPTER 3 ..... **27**

THEORETICAL BACKGROUND **27**

3.1 INTRODUCTION 27

3.2 FLUTED TUBES 27

3.2.1 Theory of fluted tubes *28*

3.2.1.1 Parameters of a fluted tube *28*

3.3 CORRELATION OF ROUSSEAU 29

3.3.1 Single-phase region *29*

3.3.1.1 Single-phase pressure drop *29*

3.3.1.1.1 Pressure drop in the inner fluted tube *29*

3.3.1.1.2 Pressure drop in the outer fluted tube *30*

3.3.1.2 Single-phase heat transfer coefficient *31*

3.3.1.2.1 Heat transfer in the inner fluted tube *31*

3.3.1.2.2 Heat transfer in the annulus *32*

3.3.2 Two-phase region *33*

3.3.2.1 Two-phase pressure drop *33*

3.3.2.2 Two-phase heat transfer coefficient *33*

3.4 THE SIMULATION MODEL OF ROUSSEAU ET AL. (2003) 34

3.4.1 Simulation model no.1 ..... *34*

3.4.2 Simulation model no.2 ..... *36*

3.4.3 Counter-flow configuration *36*

3.5 SUMMARY 37

CHAPTER 4 ..... **38**

EXPERIMENTAL FACILITIES **38**

4.1 INTRODUCTION 38

4.2 MANUFACTURING PROCESS 38

4.2.1 Workbench *39*

4.2.1.1 Chuck and grooving wheels *40*

2.4.1.2 Basic manufacturing procedure *41*

4.3 LAYOUT OF ORIGINAL TEST BENCH 43

4.4 TEST BENCH ALTERATIONS 45

4.4.1 New testing configuration *45*

4.4.2 Test bench components *47*

4.4.2.1 Compressor *47*

4.4.2.2 Suction accumulator *48*

4.4.2.3 Expansion valves *48*

4.4.2.4 Heat exchanger *48*

4.4.2.5 Test section heat exchanger *48*

4.4.2.6 Water supply to heat exchanger *49*

4.5. MEASUREMENT AND DATA ACQUISITION SYSTEM 50
4.5.1 Measuring equipment *50*
4.5.1.1 Temperature measurement *50*
4.5.1.2 Pressure measurement *51*
4.5.1.3 Mass flow measurement *52*
4.5.2 Acquisitioning equipment *53*
4.5.2.1 Temperature acquisitioning *53*
4.5.2.2 Pressure and flow data acquisitioning *53*
4.6 UNCERTAINTY ANALYSIS 53
4.7 CALIBRATION OF THE INSTRUMENTATION WITH R22 56
4.8 SUMMARY 58

CHAPTER 5 ..... **59**
EXPERIMENTAL INVESTIGATION **59**
5.1. INTRODUCTION 59
5.2 TEST FACILITY 59
5.2.1 Experimental set-up *59*
5.2.2 Controlled variables *61*
5.2.2.1 The refrigerant mass flux *61*
5.2.2.2 The refrigerant inlet conditions to the test condenser *62*
5.2.2.3 The refrigerant heat flux *62*
5.2.2.4 Data reduction procedure *62*
5.2.3. Test Matrix *63*
5.2.4 Data sampling *65*
5.3 EXPERIMENTAL RESULTS 65
5.3.1 Pressure loss *66*
5.3.1.1 Refrigerant pressure loss in the single-phase region *66*
5.3.1.2 Refrigerant pressure loss in the two-phase region *67*
5.3.1.3 Effect of refrigerant mass flow rate on the pressure loss *68*
5.3.1.4 Effect of flute pitch on the pressure loss *69*
5.3.2 Heat transfer *69*
5.3.2.1 Effect of refrigerant mass flow rate *70*
5.3.2.2 Effect of water mass flow rate *70*
5.3.2.3 Effect of the cooling water inlet temperature *71*
5.3.2.4 Effect of the condensing process in the two-phase region *71*
5.3.2.5 Effect of flute pitch *71*
5.4 SUMMARY 71

CHAPTER 6 ..... **73**
SIMULATION MODEL VERIFICATION **73**
6.1 INTRODUCTION 73
6.2 MODEL ACCURACY 73

6.2.1 Accuracy of existing correlation *73*
6.2.2 Derived new enhancement factors *75*
6.2.2 Deriving average enhancement factors *77*
6.3. ACCURACY OF CORRELATION WITH NEW ENHANCEMENT FACTORS *79*
6.3.1 Results for Fluted Tube no.1 ..... *79*
6.3.1.1 Fluted tube no.1: Pressure drop results *80*
6.3.1.2 Fluted tube no.1: Enthalpy drop results *81*
6.3.1.3 Fluted tube no.1: Heat transfer results *81*
6.3.1.4 Fluted tube no.1: LMTD results *82*
6.3.2 Results for Fluted Tube no.2 ..... *84*
6.3.2.1 Fluted tube no.2: Pressure drop results *84*
6.3.2.2 Fluted tube no.2: Enthalpy drop results *85*
6.3.2.3 Fluted tube no.2: Heat transfer results *86*
6.3.2.4 Fluted tube no.2: LMTD results *87*
6.3.3 Results for Fluted Tube no.3 ..... *89*
6.3.3.1 Fluted tube no.3: Pressure drop results *89*
6.3.3.2 Fluted tube no.3: Enthalpy drop results *89*
6.3.3.3 Fluted tube no.3: Heat transfer results *90*
6.3.3.4 Fluted tube no.3: Enthalpy drop results *91*
6.4 COMPARISON OF ENHANCEMENT FACTORS 92
6.5 SUMMARY 94

CHAPTER 7 ..... **95**
CONCLUSION AND RECOMMENDATIONS **95**
7.1 INTRODUCTION 95
7.2 SUMMARY OF THE STUDY 95
7.3 CONTRIBUTION OF THIS STUDY 97
7.4 RECOMMENDATIONS FOR FURTHER WORK 97

REFERENCES **99**

APPENDIX A **A.1**

APPENDIX B **B.1**

APPENDIX C **C.1**

APPENDIX D **D.1**

APPENDIX E **E.1**

APPENDIX F **F.1**

LIST OF FIGURES

Figure 1.1: Fluted Tube Configuration (Rousseau *et al.*, 2003:37) 3
Figure 2.1: Pressure-molar fration of ideal binary mixture (De Vos, 2006:9) 9
Figure 2.2: Pressure-mass fraction behaviour of real binary mixtures. (Venter, 2000:8) 10
Figure2.3: Binary zeotropic mixture: Variation in bubble point and dew point temperature and composition (Venkataratham, 1996:362) 11
Figure 2.4: Vapour pressure-temperature chart of R22 12
Figure 2.5: The cold fluid being the minimum heat capacity 13
Figure 2.6: The hot fluid being the minimum heat capacity 13
Figure 2.7: The minimum temperature difference between the streams (Venkataratham, 1996:206). 14
Figure 2.8: The maximum temperature difference between the streams (Venkataratham, 1996:206) 15
Figure 2.9: Process of heat pump efficiency improcement (De Vos, 2006:14) 19
Figure 2.10: Flow patterns of horisontal co-current two-phase flow (Mills, 1995:649) 20
Figure 2.11: Flow regimes inside a horizontal evaporator 20
Figure 3.1: Illustration of fluted tube dimensions (Christensen *et al.*, 1993). 28
Figure 3.2: Temperature-Enthalpy diagram of the test evaporator part of the refrigeration cycle (Rousseau *et al.*, 2003:237). 35
Figure 3.3: Counter-flow fluted tube geometry 37
Figure 4.1: Schematic illustration of workbench. 39
Figure 4.2: Chuck of workbench. 40
Figure 4.3: Grooving wheels of workbench. 41
Figure 4.4: Magnetic dial gauge on chuck. 41
Figure 4.5: Illustration of a grooving wheel with markings. 42
Figure 4.6: Layout of the evaporation test bench; refrigeration circuit (Venter, 2000:37). 43
Figure 4.7: Layout of the evaporation refrigerant test section (De Vos, 2006:31). 44
Figure 4.8: Layout of the modified test facility 46
Figure 4.9: Temperature-Entropy diagram of the cycle. 47
Figure 4.10: Layout of the condensing Test Section. 49
Figure 4.11: Pt 100 grade A three-wire with thermowell probe 51
Figure 4.12: Pt 100 grade A four-wire. 51
Figure 4.13: PREMA 3040 scanner and logger (3040 Precision Thermometer, 1998) 51
Figure 4.14: Endress + Hauser PMC731 pressure sensor (Endress + Hauser, 2006). 52
Figure 4.15: Endress + Hauser Promass 63F flow meter (Endress + Hauser, 2005). 52
Figure 4.16: Micromotion RTF9739 flow meter 53
Figure 5.1: Positioning of measuring equipment on the test condenser. 60
Figure 5.2: Example of recorded data set 65
Figure 5.3: Comparison pressure drop through the two-phase region 67

Figure 6.1: Simulation of the heat transfer by using the new enhancement factors on fluted tube no.1. 80
Figure 6.2: Simulation of the enthalpy drop by using the new enhancement factors on fluted tube no.1..... 81
Figure 6.3: Simulation of the heat transfer by using the new enhancement factors on fluted tube no.1. 82
Figure 6.4: Simulation of the enthalpy drop by using the new enhancement factors on fluted tube no.1..... 83
Figure 6.5: Simulation of the enthalpy drop by using the new enhancement factors on fluted tube no.2..... 85
Figure 6.6: Simulation of the heat transfer by using the new enhancement factors on fluted tube no.2. 86
Figure 6.7: Simulation of the enthalpy drop by using the new enhancement factors on fluted tube no.2..... 87
Figure 6.8: Simulation of the heat transfer by using the new enhancement factors on fluted tube no.2. 88
Figure 6.9: Simulation of the pressure drop by using the new enhancement factors on fluted tube no.3. 89
Figure 6.10: Simulation of the enthalpy drop by using the new enhancement factors on fluted tube no.3..... 90
Figure 6.11: Simulation of the heat transfer by using the new enhancement factors on fluted tube no.3. 91
Figure 6.12: Simulation of the LMTD by using the new enhancement factors on fluted tube no.3. 92

LIST OF TABLES

Table 4-1 Experimental Fluted Tube Geometry Results. 42
Table 4-2 Uncertainty on the measuring equipment 54
Table 4-3 Average and maximum uncertainty of the heat transfer (Q_w) on the water side 55
Table 4-4 Average and maximum uncertainty of the heat transfer (Q_r) on the refrigerant side 56
Table 4-5 Determining the accuracy of the measuring equipment with R22 57
Table 5-1 Test Matrix 63
Table 5-2 Experimental results from Fluted Tube no.1 with refrigerant mass flow = 0.05kg/s) 66
Table 5-3 Refrigerant pressure drop on fluted tube no.2 for different mass flow rates 68
Table 5-4 The effect of pitch on the pressure drop for a refrigerant mass flow = 0.02kg/s. 69
Table 5-5 Heat transfer on the three fluted tubes with a refrigerant mass flow = 0.02kg/s 69
Table 6-1 Accuracy of existing enhancement factors. 74
Table 6-2 Enhancement factors and heat transfer on the three fluted tubes with a fixed refrigerantion mass flow flow 0.05kg/s) 75
Table 6-3 Genrating "First Set" of enhancement factors 78
Table 6-4 The three sets of enhancement factors. 79
Table 6-5 The theoretical results compared to the experimental results for Fluted tube no.1 84
Table 6-6 The theoretical results compared to the experimental results for Fluted tube no.2 88
Table 6-7 The theoretical results compared to the experimental results for Fluted tube no.3 92
Table 6-8 Outlet results of the theoretical results compared to the experimental results from Figure 6.18. 93
Table 7-1 The newly generated enhancemant factors. 97

NOMENCLATURE

A	Area	m^2
C_p	Specific heat	kJ/kgK
C	Constant value	
D, d	Diameter	m
D_h	Hydraulic diameter	m
ΔT_{sat}	Super heat, $T_{wall} - T_{sat}$	°C
ΔT_{lm}	Log mean temperature difference	°C
Δp_{sat}	Difference in vapour pressure corresponding to ΔT_{sat}	kPa
e	Surface finish	
e_h, E	Enhancement factor	
e	Flute depth	m
e^*	Non-dimensional flute depth	
e_f	Pressure drop enhancement factor	
e_h	Heat transfer enhancement factor	
f	Friction factor	
$f_{helical}$	Helical coil friction factor	
$f_{straight}$	Straight tube friction factor	
F	Forced convective heat transfer enhancement factor	
Fr	Froude number	
g	Acceleration of gravity	m/s^2
G	Mass flux	kg/m^2s
h	Heat transfer coefficient	W/m^2K
$h_{helical}$	Heat transfer coefficient for helical coils	W/m^2K
$h_{straight}$	Heat transfer coefficient for straight coils	W/m^2K
k	Thermal conductivity	W/mK
L	Length	m
$\dot{m}$	Mass flow rate	kg/s

M	Molecular weight	mol
n	Constant value	
N	Number of flute starts	
Nu	Nusselt number	
P	Pressure	kPa
p	Flute pitch	m
Pr	Prandtl number	
P_r	Reduced pressure	kPa
pr	Pressure ratio	
p^*	Non-dimensional flute pitch	
q	Heat flux	W/m^2
Q	Heat transfer rate	J/s or W
r	Radius	m
Re	Reynolds number	
R_w	Thermal resistance of the wall	m^2K/W
R_{ev}	Vapour properties of the refrigerant	
S	Suppression factor	
t	Wall thickness	m
T	Temperature	°C
U	Overall heat transfer coefficient	W/m^2K
V	Velocity	m/s
Vol	Volume	m^3
wt	Weight	
x	Quality	

Greek symbols

β	Aspect ratio	
θ	Helix angle	°
θ^*	Non-dimensional helix angle	
λ	Latent heat	J/kg
μ	Kinematic viscosity	Ns/m^2

π	Constant (3.141592654)
ρ	Density
ϕ_f	Two-phase friction multiplier
ε	Effectiveness

Subscripts

c	Cold
cal	Calculated value
Cu	Copper
e	Equivalent
exp	Experimental value
h	Hot
i	Variable
i	Inside
in	At the inlet
l, *liq*	Liquid
m	Mean value
n	Variable
o	Outside
out	At the outlet
pool	Pool boiling
r	Refrigerant
R407C	R407C
tot	Total value
tp	Two-Phase
theo	Theoretical data
v	Vapour
vi	Inside volume
vo	Outside volume
w	Water
wall	Property at the wall

Mathematical Symbols

Min	Minimum
Max	Maximum

CHAPTER 1

INTRODUCTION

1.1 *BACKGROUND*

With the environmental protection of the earth being a concern, forty-six countries signed the Montreal Protocol "Substances that Deplete the Ozone Layer" on 16 September 1987 (Department of Environmental Affairs and Tourism, 2006:7). The effect of the Montreal Protocol is the phase out of halogenated refrigerants like chloroflourocarbons (CFC) and hydrochloroflourocarbons (HCFC) used in refrigeration systems. The reason for the phase-out of CFC is the fact that it contains chlorine and fluorine and these components are the main cause of ozone depletion. HCFCs contain hydrogen in addition to the other components. The application of hydrogen makes it less damaging to the ozone layer than CFC in the long term.

The phasing out of these ozone-depleting substances in various sectors had immense technical implications on the performance of refrigeration systems, especially in First World countries. This resulted in extensive international experimental and analytical research studies to find non-ozone depleting refrigerant mixtures such as hydrofluorocarbons (HFCs).

On the subject "Substances that Deplete the Ozone Layer", the Montreal Protocol agreed in 1992 to the total ban of production and use of Halons in First World countries by January 1994, and that of CFCs by January 1996. For developing countries the phase out is more lenient with HCFCs only scheduled for 2015. At South Africa's request in 1995, it was decided that the use of HCFC in South Africa had to be scaled down by the year 2010 to 35%

of the total amount used in 1989. The scaling down should continue to 10% in 2015 and 0.5% in 2020. By 2030 there should be a total phase-out of HCFC (UNEP, 2000).

Over the past few decades to the present-day, the azeotropic refrigerant R22 was generally used in refrigeration systems and heat pumps. Several refrigerant mixtures were evaluated over the years to determine their potential to replace R22, including Douglas *et al.* (1999:107). A refrigerant mixture composed by mass of R32 (23%), R125 (25%) and R134A (52%), known as R-407C has been identified as a strong replacement candidate in many refrigeration, air conditioning and heat pump applications.

However, until recently, limited experimental data was available on the characteristics of non-azeotropic (zeotropic) mixture for passive replacement and application in refrigeration systems. An intensive study by Sami *et al.* (2000:1120) reported an increased degradation of performance when used in refrigeration units. The performance is influenced by the critical temperature and differences in the shape of the two-phase dome on the temperature-entropy diagram.

It is currently of utmost importance to determine whether the existing systems should be redesigned differently when using zeotropic refrigerant mixtures like R-407C, with no ODP (ozone depleting gasses), in order to reach the maximum possible coefficient of performance (Gabriellii *et al.*, 1998). However, when an azeotropic refrigerant is replaced with a zeotropic mixture, refrigerant systems and heat pumps have shown degradation in heat transfer performance, especially during the condensation process (Ebisu, 1998:1044). This is due to the temperature glide during the phase change (evaporation and condensation process) of the zeotropic refrigerant mixture.

There is evidence that it should be possible to exploit the temperature glide of a zeotropic refrigerant mixture to reduce the exergetic losses in refrigeration systems. The performance of these systems could also be improved by matching the temperature glide of the refrigerants to that of the heat-transfer fluid (Venkatarathnam *et al.*, 1996:361).

Furthermore, it is probable that the heat exchangers of a heat pump should be adapted by using passive schemes to accommodate the advantages of zeotropic mixtures. A passive scheme is a method whereby the geometry of the heat transfer area is altered including

artificially roughened surfaces, extended surfaces and swirl flow devices. This increases the contact area between the fluid and the pipe wall, resulting in an increased heat transfer area. Passive schemes also enhance convective heat transfer by introducing swirl into the bulk flow and disrupting the boundary layer at the tube surface, due to repeated changes in the surface geometry (Srinivasan *et al.*, 1994:820). With the variety of passive schemes, numerous ways exist to change the geometry of heat exchangers, resulting in more compact heat exchangers.

Recently, most of the leading studies on passive schemes focused on zeotropic and azeotropic refrigerants mixtures applied inside micro-fin tubes (Lee *et al.* (2002), Bukasa (2002), Dongsoo *et al.* (2003) and Honda *et al.* (2004)). However, there is limited information on the use of zeotropic mixtures inside enhanced tubes, known as fluted tubes.

A fluted tube is mainly used to improve the condensation heat transfer of zeotropic refrigerant mixtures in refrigerant-to-water heat exchangers. Fluted tube condensers compared to smooth-tubes are able to produce higher heat transfer coefficients on both sides of the transfer surface by enhancing the flow conditions. Figure 1.1 is an illustration of a fluted-tube used in a heat pump for heating sanitary hot water.

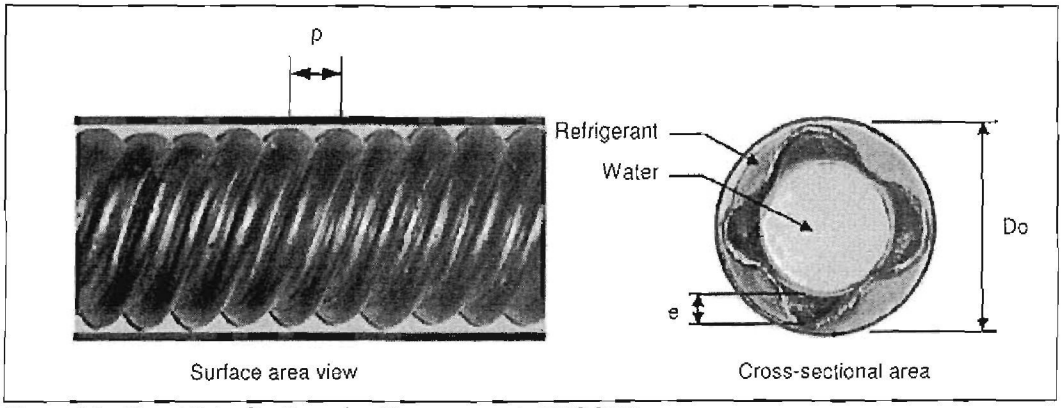


Figure 1.1: Fluted Tube Configuration (Rousseau *et al.*, 2003:233)

Presently, a need exists to further investigate this field to obtain useful information for practical application in the heat pump and refrigeration industry.

1.2 NEED FOR THIS STUDY

Since the early 90's, a few in-depth studies were done on single-phase behaviour inside fluted tubes (Srinivasan *et al.* (1994); Srinivasan and Christensen (1992)). Yet, there has been

limited research into the two-phase characteristics of refrigerants inside this tubing. Sami and Schnolate (1992), and Sami *et al.* (1994) obtained average heat transfer coefficients on the two-phase boiling of zeotropic mixtures, using a single horizontal spirally fluted tube. A shortcoming of their studies was that only the effect of mass flow rate was investigated and not the effects of heat flux, local quality, pressure loss and flute pitch and depth. From this, it is evident that limited information is available on refrigerants applied inside fluted tubes. Another area of research is the effects of flute pitch on the heat transfer. Christensen (1993) has done leading research on the thermal hydraulic characteristics of flow through spirally enhanced fluted tubes in heat exchangers. His research was limited to liquid water flowing through the tubes.

Only Rousseau *et al.* (2003:232) shows a correlation for two-phase flow inside the annulus of a fluted-tube condenser. This correlation is based on R22 data obtained from a series of commercially available fluted tubes. A simulation model was developed to predict the heat transfer characteristics of R22 in a fluted tube condenser. Due to the lack of accuracy of the model, the authors developed two enhancement factors to predict the heat transfer and pressure drop more precisely. The research of Rousseau *et al.* (2003:239) was restricted by two factors, namely the effect of flute pitch and the limited information on the experimental characteristics of the refrigerant inside fluted tubes.

De Vos (2006) produced the latest work on fluted tubes and did experimental work on the forced convective boiling heat transfer coefficients of R-407C in fluted tubes annuli. The best correlations from his viewpoint to predict the experimental heat transfer of R-407C on fluted tubes, is the correlation of Rousseau *et al.* (2003) with different enhancement factors used and the correlation of Gungor and Winterton (1987). The average deviation of the measured Nusselt number to the calculated Nusselt number for R-407C, according to the correlation of Rousseau *et al.* (2003:239), was 3.83%. The research by De Vos (2005:105) was limited to only one pitch configuration for forced convective boiling.

There exists a need to determine if the correlation of Rousseau *et al.* (2003) can be used to predict the pressure drop and condensation heat transfer of R-407C inside fluted tubes.

1.3 PROBLEM STATEMENT

The aim of this study is to investigate the applicability of the model developed by Rousseau *et al.* (2003), for the pressure drop and heat transfer predictions of R-407C inside fluted tube annuli. If the model, when evaluated, is not sufficiently accurate, the aim of this study will be to improve the enhancement factors of the original model in order to increase the accuracy of the model to predict the pressure drop and heat transfer on the refrigerant side.

Determining the zeotropic two-phase condensation heat transfer coefficients is a complex process. Accurate experimental measurements are required, since the heat transfer coefficient is a function of the vapour quality. In the case of zeotropic mixtures, determining the heat transfer coefficient is being complicated by the temperature glide. Since this temperature glide is not necessarily linear, precise measurements are required. To implement the model of Rousseau *et al.* (2003) for predicting the characteristics of R-407C inside the annuli of fluted tubes, an intensive experimental and simulation study had to be conducted.

Subsequently, the experimental investigation was carried out using an existing test bench fully equipped with temperature, pressure and mass flow rate-measuring equipment. To gain more information on the effect of the flute pitch, different fluted tube configurations had to be manufactured for use on the test bench. For this an existing manufacturing bench was refurbished and modified to produce fluted tubes with different pitches. The experimental data and the theoretical data were compared. If needed, the heat transfer and pressure drop enhancement factors of Rousseau *et al.* (2003) were altered to improve the model's accuracy.

1.4 METHOD OF INVESTIGATION

In order to reach the aim of this study the following method had to be implemented:

- Alterations had to be made to the existing test bench, fully equipped with measuring equipment. The main alteration was to convert the bench from an evaporation test facility to a condensation test facility.
- Fluted tubes with three different flute pitches were tested individually on the test bench to determine the effect of the flute pitch.
- Before the R-407C tests commenced, a few tests with R22 were done to verify the accuracy of the measuring equipment.

- R-407C tests for the three different flute pitches were conducted according to a test matrix covering a wide range of operation. Conditions altered include:
    (a) Mass flow rate of the refrigerant.
    (b) Mass flow rate of the water.
    (c) Inlet temperature of the water.
    (d) Condensing pressure of the refrigerant.
    (e) Pitch of the fluted tubes.
- Experimental pressure drop and heat transfer were compared to the calculations of Rousseau *et al.* (2003).
- Based on the accuracy of the results obtained with the existing correlation, modifications and enhancements were proposed and implemented.

1.5 CONTRIBUTION OF THIS STUDY

The contributions made by this study can be summarised as follows:

1. Validation of an existing fluted tube model including enhancements to improve the accuracy of the model.
2. Additional experimental data on the heat transfer characteristics and pressure drop of R-407C inside fluted tube annuli.

CHAPTER 2

LITERATURE STUDY

2.1 *INTRODUCTION*

The forced convective condensation of substances is a complex process. This chapter opens with a detailed discussion of the fundamental characteristics of azeotropic and zeotropic mixtures. The characteristics reviewed, include the dew point and bubble point, composition mixture, temperature glide, steady-state efficiency improvement and the effects of pinch points of zeotropic mixtures.

The chapter continues with a presentation of a thermodynamic and thermo physical comparison of R22 and R-407C. A description of the different methods that could improve the heat transfer coefficient of zeotropic mixtures inside heat exchangers then follows. The chapter concludes with several studies that were done on the heat transfer characteristics of refrigerants and mixtures.

2.2 *CHARACTERISTICS OF REFRIGERANT MIXTURES*

2.2.1 *DESCRIPTION OF REFRIGERANT MIXTURES*

Refrigerant mixtures used in air conditioning and heat pump applications can be divided into three main groups:

- Azeotropic mixtures: Work like a homogeneous substance.
- Near-azeotropic mixtures: Have a temperature glide less than 2.8°C during evaporation and condensation.

- Zeotropic mixtures: Have a distinct temperature glide of more than 2.8°C during evaporation and condensation.

The benefit of a zeotropic mixture over an azeotropic refrigerant is that it can be formed to obtain specific thermodynamic properties. Through intensive research, it became evident that environmentally friendly zeotropic mixtures have similar thermodynamic and transport properties than azeotropic refrigerants. If the temperature glide of a zeotropic mixture is exploited correctly, it will give an improvement in the COP (coefficient of performance) of the refrigeration systems (Gabrielii *et al.*, 1997). Therefore, zeotropic mixtures were proposed as replacement candidates for the banned azeotropic refrigerants.

However, these zeotropic mixtures have advantages and disadvantages with regard to the performance of heat exchangers in refrigeration systems when compared to azeotropic technology.

The advantages according to Venkatarthnam *et al.* (1996:361) include:

- If the temperature glides (the process that occurs during the phase change (evaporation and condensation)) of the refrigerant and heat transfer fluid in the condenser matches, a reduction in entropy will be generated.
- The composition of zeotropic mixtures can be selectively varied on-line to regulate the capacity of the system.

A disadvantage according to Venkatarthnam *et al.* (1996:363 and 1999:206) is:

- When zeotropic refrigerant mixtures are used in condensers and evaporators, temperature pinch points may occur. This happens due to the large non-linear variation of two-phase enthalpy with temperature during phase change in some zeotropic mixtures.

The characteristics of the three main group refrigerant mixtures will now be discussed in more detail. For ideal mixtures the bubble point curve is a straight line as illustrated in Figure 2.1. According to Raoult's law, explained in detail by De Vos (2005:9), the bubble point curve with the straight line is due to the linearity relation to molar concentration between the vapour pressure curves of each component. For real mixtures all of the lines have a curve either deviating over or under the ideal.

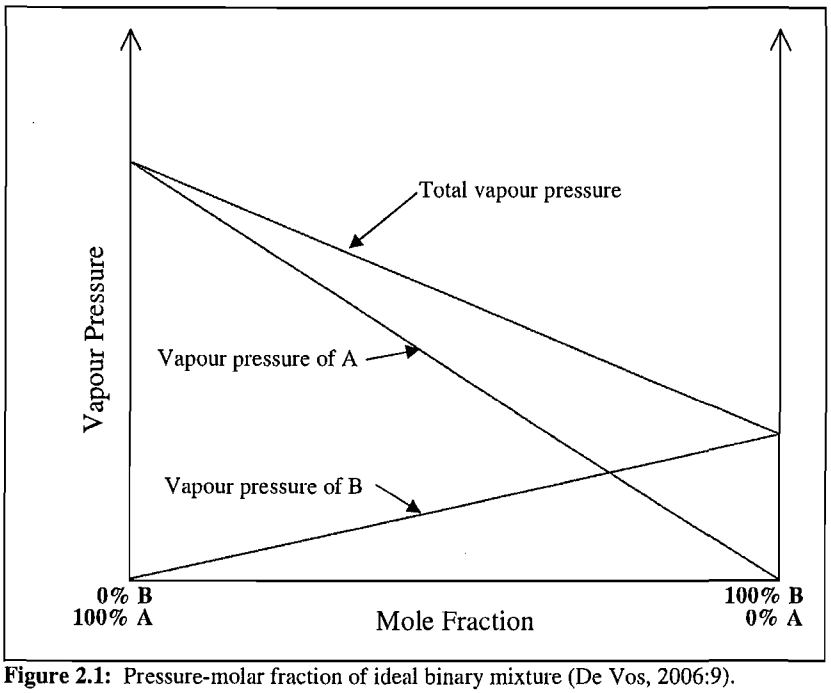


Figure 2.1: Pressure-molar fraction of ideal binary mixture (De Vos, 2006:9).

Real mixtures (Venter, 2000:9) have three different behaviours at a constant temperature as illustrated in Figure 2.2.

- *Curve 1*: At a given concentration the vapour pressure is higher for the mixture than for any one of the pure components. Such a mixture has a positive azeotropic composition at the colliding point (p) in the curve. Examples of such mixtures are R502 (R-22/R-115) and R-410 (R-32/R-125).
- *Curve 2*: At a given concentration the vapour pressure is lower for the mixture than for any one of the pure components. Such a mixture has a negative azeotropic composition at the colliding point (q) in the curve. An example of such a mixture is R-507 (R-125/ R-143a).
- *Curve 3*: In this mixture the vapour pressure curve of the mixture lies between the curves of the pure components over the entire range of the concentration. An example of such a mixture is R-407C (R-32/R-125/R-134a).

Points p and q on curves 1 and 2 are colliding points. Here the dew point and bubble point curves have the same pressure and during phase-change no transformation will occur in concentration. At these colliding points the given mixture reacts as a pure substance during phase-change.

Curve 3 does not have this phenomenon and is therefore defined as a zeotropic mixture. During the phase-change process a zeotropic mixture shows concentration shifts and temperature glides.

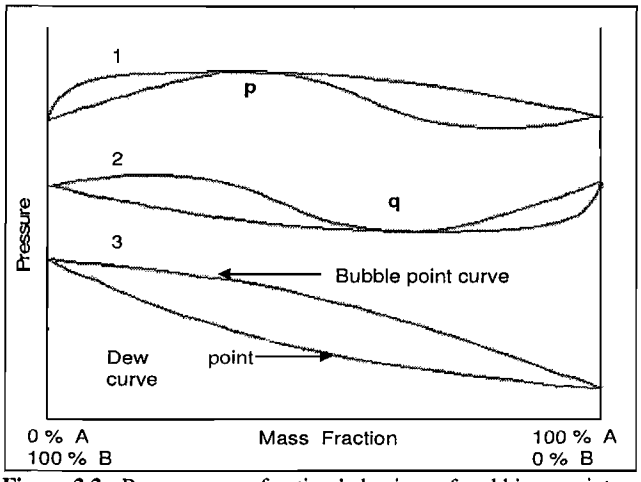


Figure 2.2: Pressure-mass fraction behaviour of real binary mixtures (Venter, 2000:8).

2.2.2 TEMPERATURE GLIDE OF ZEOTROPIC MIXTURES

2.2.2.1 DEW POINT AND BUBBLE POINT

Figure 2.3 illustrates a temperature-mixture composition diagram, during phase-change, of a typical binary mixture at a constant pressure. As the vapour is cooled, liquid starts to form at the dew point (T_d) and condensation is complete only at the bubble point (T_b). Similarly, when the liquid is heated, vapour starts to form at the bubble point (T_b) and the vaporisation is complete at the dew point (T_d) (Venkatarthnam *et al.*, 1996:362).

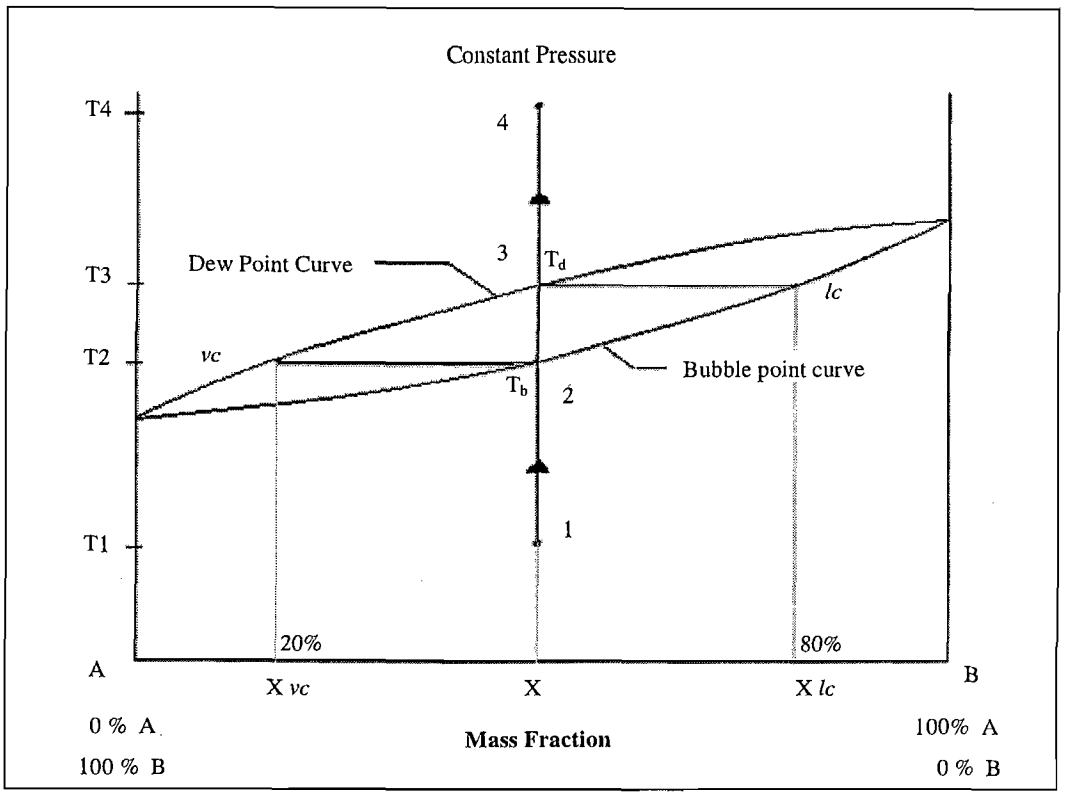


Figure 2.3: Binary zeotropic mixture: Variation in bubble point and dew point temperature and composition (Venkatarathnam, 1996:362).

2.2.2.2 TEMPERATURE GLIDE

To explain the temperature glide of a zeotropic mixture the vapour pressure and the composition mixture of an azeotrope (R22) will firstly be described. When the pressure is kept at a constant value during condensation, the temperature will also remain constant as illustrated in Figure 2.4. The reason for the temperature and pressure remaining constant is due to the phase-change temperature related to the pressure by means of a vapour pressure function that is presented as a vapour pressure curve. In contrast to this, the temperature at which phase-change occurs with a zeotropic mixture (R-407C) will not only be a function of the pressure, but also of the mixture composition.

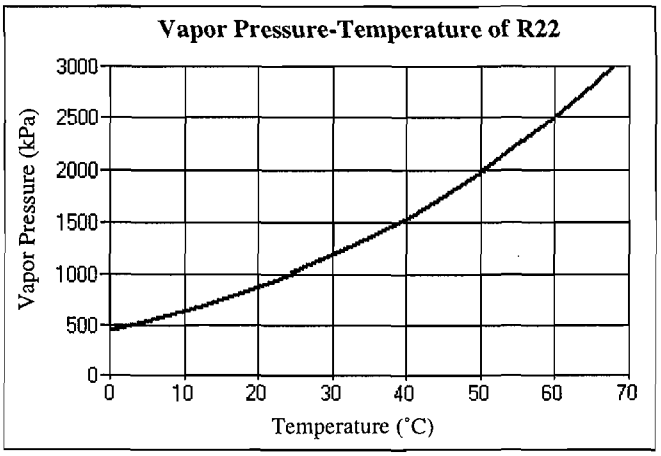


Figure 2.4: Vapour pressure-temperature chart of R22.

The condition of constant pressure, illustrated in Figure 2.3, is more or less similar to the evaporator and condenser of a refrigeration system or heat pump. The boiling process for a binary mixture with composition X is illustrated. The refrigerant mixture at point 1 with temperature T_1 is in a sub cooled liquid form. Here the binary mixture consists of 50% A composition and 50% B composition. When heat is applied to the process, the mixture's temperature rises to T_2, where it starts to boil as the first vapour bubble forms at this point. This vapour bubble has a composition of 20% A (x_{vc}) and 80% B (x_{lc}) with the liquid composition still at 50% A and 50% B. Thus, the vapour in this bubble has a different composition, x_{vc}, to that of the original liquid mixture. The phase-change process will continue when more heat is supplied. The temperature will increase until it reaches point 3 as the last drop of liquid evaporates at temperature T_3. The composition of the remaining liquid phase will follow the bubble point curve from point 2 to point ℓ_c. In the same way, the composition of the vapour phase will follow the dew point curve from point v_c to point 3. The last remaining liquid droplet, with composition ℓ_c, will evaporate at point 3. At this point 3 the last drop of liquid will have a composition of 80% A (x_{lc}) and 20% B (x_{vc}) with vapour composition the original composition of 50% A and 50% B. From point 3 to point 4, the vapour mixture will have the same composition as the liquid mixture between points 1 and 2. The temperature difference between points 2 and 3 is called the temperature glide of the mixture and its magnitude is dependent on the original mixture composition. The temperature glide may improve the efficiency of refrigeration systems and heat pumps if it is applied correctly; meaning that more energy is transferred between the refrigerant and heat-transfer fluid.

2.2.3 *THE EFFECT OF TEMPERATURE GLIDE OF ZEOTROPIC MIXTURES ON REFRIGERANT SYSTEMS*

By matching the glide of the refrigerant with that of the heat-transfer fluid, it reduces the entropy generated in the heat exchangers during phase change. The reduction of the entropy generation leads to an increase in the efficiency of refrigeration systems. According to Venkatarathnam (1999:208) the temperature difference between the two fluids must be constant over every section to obtain perfect glide matching.

If the fluid specific heat (C_p) is constant at a constant pressure and independent of the temperature in an unbalanced ($v < 1$) heat exchanger, the minimum temperature difference between the fluid streams will occur at one of the ends (Venkaratarathnam, 1996:363). It can be noticed from Figures 2.5 and 2.6 that the maximum temperature difference can occur at other ends of the fluid streams.

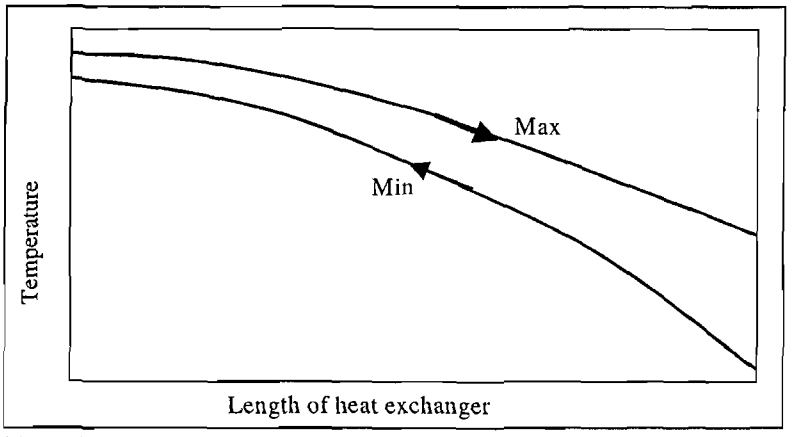


Figure 2.5: The cold fluid being the minimum heat capacity rate

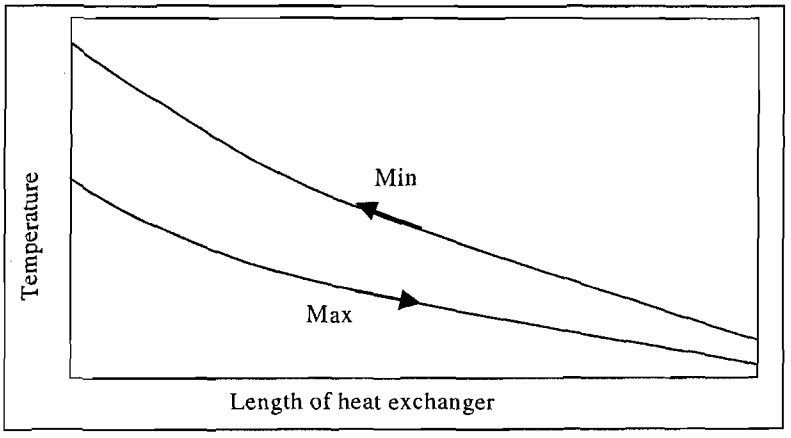


Figure 2.6: The hot fluid being the minimum heat capacity rate

Temperature pinch points can occur when zeotropic refrigerant mixtures are used in condensers and evaporators. This makes it difficult to achieve perfect glide matching. The reason for temperature pinch points is due to the fact that the heat capacity rate or specific heat of one or both of the fluids, change. Then, it is possible that the minimum heat capacity rate fluid at one end can became the maximum heat capacity rate fluid at the other end as illustrated in Figure 2.7 and 2.8.

Heat capacity rate: $v = \frac{(\dot{m}C_p)_{\min}}{(\dot{m}C_p)_{\max}}$

In Figure 2.7 the cold fluid is the minimum heat capacity rate at the cold end, but it becomes the maximum heat capacity rate fluid at the hot end.

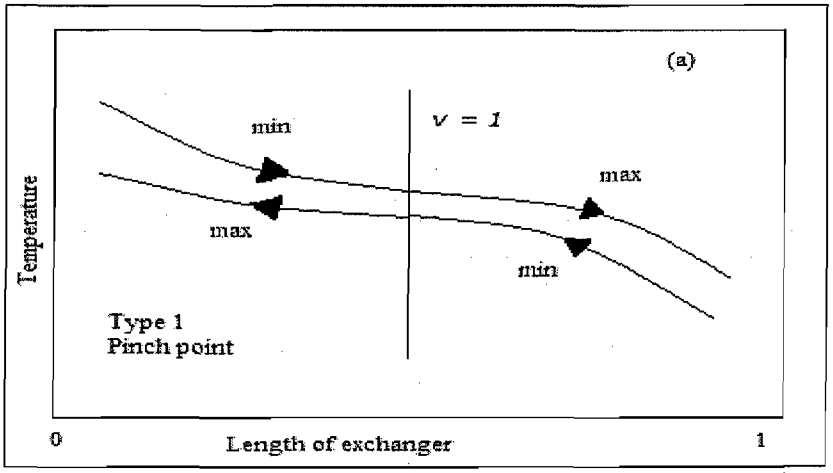


Figure 2.7: The minimum temperature difference between the streams (Venkataratham, 1996:206).

In Figure 2.8 the cold fluid is the maximum heat capacity rate fluid at the cold end and becomes the minimum heat capacity rate fluid at the hot end. As illustrated, the maximum temperature difference will occur within the ends.

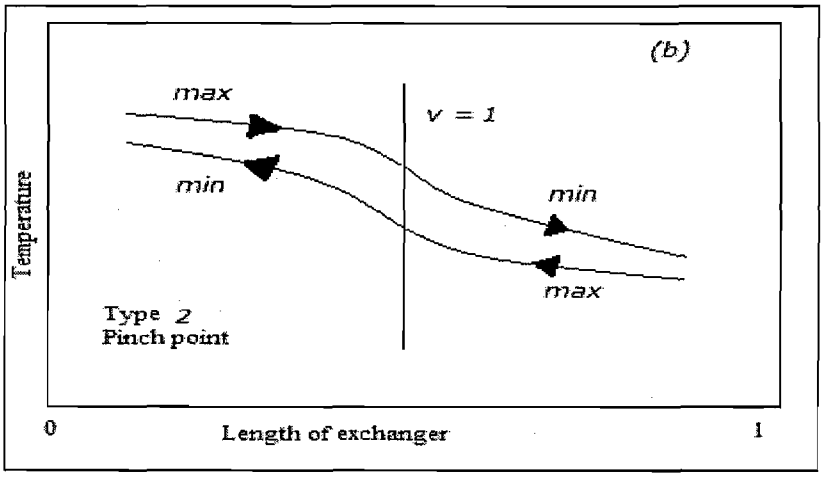


Figure 2.8: The maximum temperature difference between the streams

The enthalpy change during phase change (Δh_r) in a condenser is calculated with Equation 2.1.

Condenser: $\Delta h_r = h_d - h_b$ (2.1)

h_d – Enthalpy at the dew point

h_b – Enthalpy at the bubble point

The system design, the heat exchanger type, the system running conditions, as well as the temperature glide of the refrigerant mixture affect the magnitude of the concentration shift in a given system. The benefits of these zeotropic refrigerant mixtures compared to pure refrigerants are:

- Higher condensing temperatures.
- Lower pressures.
- The potential to increase capacity, which automatically leads to an improvement in efficiency.

For a mixed refrigerant application it is important to understand the concentration shift phenomena (Albrecht, 1996). The concentration shift is caused by the following phenomena:

- Leakage of refrigerant mixture out of the system.
- Differential solubility of the components of refrigerant mixtures in the lubrication oil.

Numerous studies were done on refrigeration systems, to determine what the effect in performance is, when these new zeotropic mixtures are used as the refrigerant. In the following paragraphs the most relevant studies are briefly discuss.

Chen *et al.* (1997:149) developed an air conditioning simulation model, where the concentration shifts of refrigerant mixtures R-404A, R-32/134A, and R-407C were included. Furthermore, this computer model predicted the concentration shift and associated performance changes. Later Venkatarathnam *et al.* (1999:206) proved that perfect glide matching of heat transfer fluid and the refrigerant is difficult in condensers and evaporators for many zeotropic mixtures. A simple method for predicting the occurrence of pinch points was presented. The thermodynamic analysis showed that various applications rather opt for the multi-component mixtures over that of the many boiling binary mixtures that focus on pinch points and glide matching.

Jung *et al.* (1993:201) developed a correlation to predict the heat transfer coefficients and pressure drops of R22 replacements. The results proved that heat transfer prediction is more sensitive to the properties of liquid than vapour.

Hwang *et al.* (1997:103) experimented on the heat transfer and pressure drop of zeotropic mixtures, CFCs and HCFCs in a heat pump application. They used the experimental data that was obtained from the heat pump to develop a simulation to predict the characteristics of CFCs and HCFCs. Furthermore, they improved the performance of these zeotropic mixtures by making use of the following methods:

(1) Change the geometry of the heat exchanger.

(2) Switch to a counter flow heat exchanger, improving performance by 10%.

Gabrielii *et al.* (1997:440) investigated whether the optimal distribution of the heat exchanger area between the evaporator and the suction gas heat exchanger, at a given cost, will change when R22 is replaced with the zeotropic mixture R-407C. For R-407C, in most cases it was favourable to move some heat exchanger area from the evaporator to the suction gas heat exchanger. The improvement in the coefficient of performance (COP) of the heat exchanger can be up to 3.4%. It was observed that the optimal area distribution for R-407C corresponds to the maximum use of the glide in the evaporator. Gabrielii *et al.* (1998:518) followed with a performance study on a tube-and-shell evaporator. The study used a simulation program to

determine the performance of a tube-and-shell evaporator under several sets of test conditions. It was found that the characteristics of R-407C were very similar to that of R22. One disadvantage of R-407C is that it had a larger pressure drop due to a lower evaporation temperature, resulting in a lower COP.

Douglas *et al.* (1999:107) developed a general-purpose method for comparing alternative refrigerants. The method utilised a single performance index based upon minimum cost for a simplified system operating with a given cooling capacity and efficiency. They also evaluated the performance of several leading R22 replacement candidates for window air conditioners. They concluded that the two leading R22 replacement candidates, R-407C and R-410A had optimal costs that were nearly identical to R22.

A year later Kusaka *et al.* (2000:55) focused their study on developing a higher performance refrigeration system with R-407C, using a technique of capacity control by varying the zeotropic refrigerant composition. They improved the system efficiency by capacity saving by about 26%.

In the same year Sami *et al.* (2000) examined the performance of R22 and its possible replacements in refrigerant units. Previous studies reported an increased degradation in performance for fluids replacing R22, which have a low critical temperature. An attempt was made to explain this behaviour. The refrigerants that were used included: R22, R-134A, R-290, R-410A and R-407C. The examined refrigerants exhibited different critical temperatures and differences in the shape of the two-phase dome on the temperature-entropy diagrams, which explained the different performance trends for the refrigerants.

Jeng *et al.* (2001:863) investigated the effect of lubrication on the vapour pressure of R-407C in refrigeration systems. Their study concluded that the change of vapour pressure with oil concentration is relatively small due to the zeotropic nature of R-407C.

Thome (2002:27) concentrated on the methods of that period to predict the heat transfer coefficients of refrigerants in refrigeration systems. The study attempted to correct the previously incorrect use of the flow pattern maps.

Later De Monte (2002:315) did a theoretical evaluation of the thermodynamic properties of R-407C and R-410A in the superheated vapour state. The modelling was based on the Martin-Hou equation of state. Both R-407C and R-410A are well-investigated refrigerants. Therefore, the analytical procedure focused on the following thermodynamic properties: compressibility factor, isentropic and isothermal compressibility, volume expansiveness, isentropic and isothermal exponent, speed of sound and Joule–Thomson coefficient. These properties may be used as a theoretical basis for research into the optimal HFC-mixture for compressor efficiency and for performing cycle calculations in the vapour-phase region for systems working with R-407C and R-410A.

2.2.4 STEADY-STATE EFFICIENCY IMPROVEMENT

By reducing the enclosed area of the cycle on a temperature-entropy diagram, the efficiency of any thermodynamic cycle can be improved (Johannsen, 1992). The enclosed area can be reduced by the following three methods:

- Reducing the refrigerant superheat at the outlet of the compressor by selecting a suitable refrigerant.
- Reducing the temperature difference between the refrigerant and the outside source by increasing the heat transfer surface or by increasing the flow rate of the outside fluid.
- The T-s diagram (Figure 2.9) can also be reduced if the temperature profile of the refrigerant in the heat exchanger is matched to the temperature of the outside fluid. This is where the temperature glide of the zeotropic refrigerant mixtures can play a major role to improve the system effectiveness.

Figure 2.9 illustrates how the temperature glide can be used to improve the system efficiency. Diagram 1 illustrates the operation of the most common isothermal vapour compression cycle for pure refrigerants. Diagram 2, which is a Lorenz vapour compression cycle, illustrates how applying temperatures in an ideal process, can reduce the enclosed area. Ideal processes do not exist and the possibility for pinch point is too great. Thus this situation is avoided.

With the use of a zeotropic refrigerant mixture, Diagram 1 can be swivelled on the points as illustrated in Diagram 3. Diagram 4, illustrates that this does not result in a reduction of the enclosed area on the T-s diagram but it enables both phase change processes to be shifted towards the temperature gradient of both exit fluids. This reduces the enclosed area in the T-s diagram for the cycle while maintaining the same exit temperatures of the fluids. The

temperature glide of the zeotropic refrigerant mixture during phase change reduces the possibility for pinch points to occur and allows the heat transfer process to be shifted closer together.

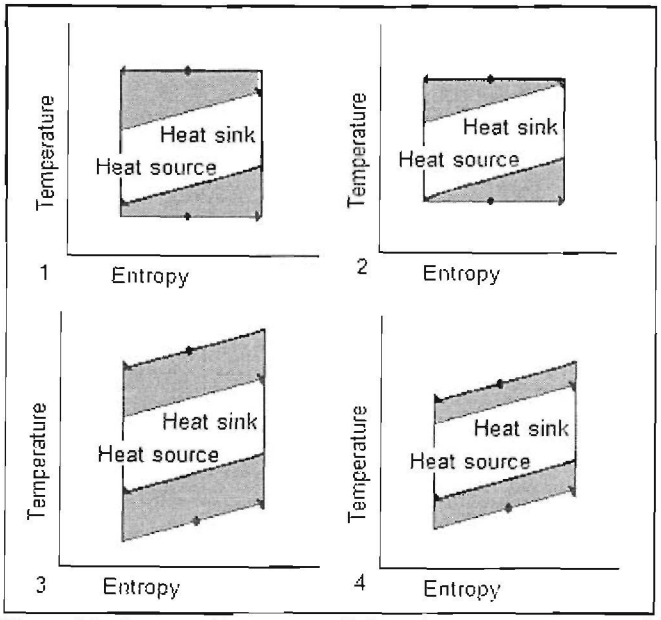


Figure 2.9: Process of heat pump efficiency improvement (De Vos, 2006:14).

2.3 *HEAT TRANSFER CHARACTERISTICS OF ZEOTROPIC MIXTURES*

2.3.1. *TWO - PHASE FLOW PATTERNS*

There exist a variety of flow patterns during the evaporation and condensation processes of refrigerant mixtures. The most ordinary flow patterns include: bubbly flow, slug flow and annular flow. The actual flow pattern encountered in the system depends mainly on the flow velocity and the relative amounts of liquid and vapour. Therefore, it is very difficult to determine the flow-pattern, pressure drop and heat transfer for a specified system.

Figure 2.10 illustrates the different horizontal flow pattern characteristics in the two-phase substance (Mills, 1995:647). The gravity force perpendicular to the flow causes certain differences from that of flow in a vertical tube, especially at low flow rates. De Vos (2006:16) describes the different flow patterns in more detail.

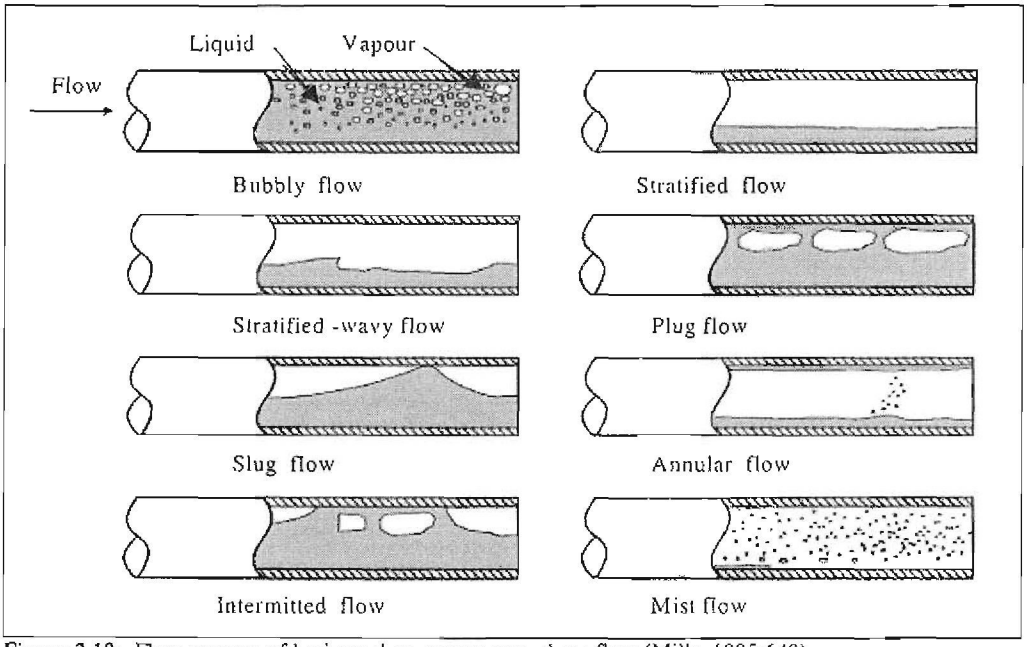


Figure 2.10: Flow patterns of horizontal co-current two-phase flow (Mills, 1995:649).

2.3.2 *INTERNAL FORCED CONVECTIVE BOILING*

Figure 2.11 illustrates a refrigerant flowing through a horizontal pipe during the condensation process. Initially, the refrigerant is in the annular flow regime; meaning that the liquid film is on the perimeter of the wall, the vapour is in the centre core and some liquid droplets are entrained in the vapour from the tips of waves on the interface of the film. As condensation continues to take place, the vapour velocity decreases, resulting in a decrease in vapour shear on the interface. This leads to the liquid film becoming thicker at the bottom of the tube than it is at the top. New condensate forming adds to the thickness of the liquid film. As the quality of the liquid increases along the tube, slug flow is encountered and still further along all the vapour is finally converted to liquid.

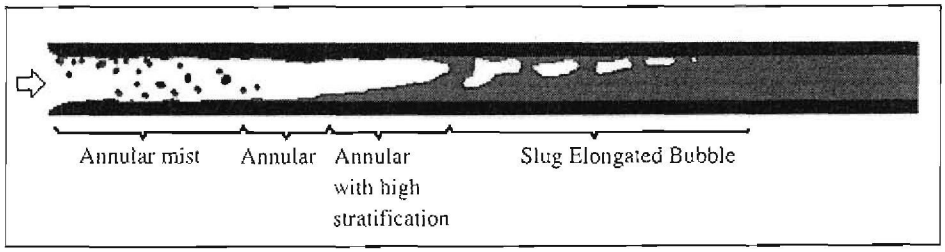


Figure 2.11: Flow regimes inside a horizontal condenser.

The study of Wang *et al.* (1997:395) focused on the flow pattern and friction characteristics of R22, R-134A and R-407C inside a smooth tube. The tests were done with a mass flux range between $50\,kg/(m.s^2)$ and $700\,kg/(m.s^2)$. Results from their tests showed that flow pattern transition for R-407C indicated a considerable delay compared to R22 and R-134A.

A new correlation for the heat transfer coefficient was derived from the experimental heat transfer characteristics of R22 and R-407C (Choi *et al.*, 2000:3660). The absolute average deviation between the predicted and measured data was 13.2% on 2971 data points.

Cavalinni *et al.* (2001:73) measured experimental heat transfer coefficients and pressure drops during condensation inside a smooth tube while operating with pure HFC refrigerants (R-134A, R125, R236ea, R32) and the nearly azeotropic HFC refrigerant blend R-410A. Experimental runs were carried out at saturation temperatures ranging between $30\,°C$ and $50\,°C$, and mass velocities varying from $100\,kg/(m.s^2)$ to $750\,kg/(m.s^2)$ over the vapour quality range of 0.15 to 0.85. The effects of vapour quality, mass velocity, saturation temperature as well as temperature difference between saturation and tube wall on the heat transfer coefficient were investigated by analysing the experimental data. Their experimental results, when compared to the theoretical model, had a deviation within 10%.

Karlsson *et al.* (2004:561,858) did a detailed examination on the performance of a shell-and-tube condenser when R22 is replaced with zeotropic mixtures. Their calculations showed that the mass transfer resistance in the vapour phase causes a decrease in duty between 10% and 20% calculated at constant pressure when neglecting liquid phase resistance. The higher value corresponded to a low duty. Mass transfer resistance in the liquid phase caused a decrease in duty between 15% and 65% calculated at constant pressure. .

2.4. *TECHNIQUES USED TO IMPROVE THE HEAT TRANSFER OF ZEOTROPIC MIXTURES*

In recent years researchers and engineers focused on improving heat exchangers to accommodate new zeotropic mixtures as the cooling liquid. The zeotropic mixtures replacing the traditional refrigerants have a degradation effect on the heat exchangers. Efforts have been made to design heat exchangers that operate more effectively and also in size reduction, subsequently leading to a material cost reduction. This has led to the extensive use of heat

transfer enhancement technologies aiming to improve heat exchanger capacities (Bukasa, 2001:1).

2.4.1 TECHNIQUES USED TO IMPROVE HEAT TRANSFER

Various augmentation methods have been developed and applied to different types of heat exchangers in order to improve their heat transfer performance. The most important enhancement technique is the passive technique (Vijayaragham *et al.*, 1994). Passive schemes include techniques such as the use of artificially roughened surfaces, extended surfaces, swirl flow devices and inlet vortex generators. Passive techniques include finned-tubes, microfin tubes, herringbone tubes and fluted tubes. This study focuses on heat augmentation by means of fluted tubes. Due to the surface geometry of fluted tubes, the swirl disrupts the boundary layer at the tube surface. Therefore, the swirl flow enhances the convective heat transfer.

The next section reviews the most relevant studies, arranged according to different kinds of tubes.

2.4.1.1 FLUTED TUBES

Sami *et al.* (1992:37) investigated the boiling and condensation of ternary refrigerant mixtures for internally and externally enhanced surfaces, such as double-fluted tubes. A model was derived to predict the characteristics of the ternary refrigerants, showing a ±20% deviation for the heat transfer and ±15% deviation for the pressure drop.

Das (1993:972) generalised a correlation for predicting the frictional pressure drop across rough transparent PVC helical coils. The entire test was conducted for turbulent conditions. A correlation was derived for predicting the pressure drop through the tubes with a 95% confidence interval. An important factor for all pipe flow calculations is the accuracy of the relative roughness.

Sami *et al.* (1994:755,756) executed an experimental study on the heat transfer characteristics of the two-phase flow boiling of zeotropic mixtures inside water and refrigerant horizontal enhanced surface tubing. A correlation was developed to predict the boiling heat transfer coefficient and pressure drop as a function of the flow key parameters. The correlation had a mean deviation of approximately 30% for the pressure drop and about 20% for the heat transfer.

A correlation was developed for the heat transfer as a function of the inclination angle of a fluted tube (Kang *et al.*,1997:1112). They analysed the heat transfer in a fluted tube with a twisted insert for different inclination angles. The tests were carried out with a water-ethyl alcohol solution down the fluted tube while air-flows in the counter flow direction upwards.

R-134A demonstrated an increase in heat transfer performance of 10% to 20% over R22 in spirally fluted tubes. The study done by MacBain *et al.* (1997:65) investigated the heat transfer and pressure drop characteristics of flow boiling in a horizontal deep spirally fluted tube.

Wang *et al.* (2000:993) investigated the heat transfer in a carbon steel spirally fluted tube. The experimental results showed that although the total heat transfer coefficient of the carbon steel spirally fluted tube is between 10% and 17%, higher than that of the carbon steel smooth tube, it is almost equal to that of a copper smooth tube. Therefore, it is feasible to use carbon steel spirally fluted tubes to replace copper smooth tubes when the following refrigerants are used: R22, R-134A and R-407C.

However, this study mainly focuses on Rousseau *et al.* (2003:232) who developed a detailed model to simulate fluted tube refrigerant-to-water condensers. The model allowed the surface area to be divided into any number of sections in the length, for which all the refrigerant and water properties can be evaluated. This allows for the extension of the model to simulate heat exchangers for cycles employing zeotropic refrigerant mixtures. For the waterside, existing friction and heat transfer empirical equations were used. However, on the refrigerant side no correlations were available in the literature to calculate friction and heat transfer coefficients. Rousseau *et al.* (2003) used existing smooth tube correlations combined with enhancement ratios based on correlations available for helical coils as well as enhancement factors based on empirical data for fluted tube condensers. The model was validated by the results of independent tests on two commercial fluted tube heat exchangers. The average difference between the simulated and measured pressure drops was 7.27% and the average difference for the log mean temperature difference (LMTD) was 4.41%.

Fluted tubes use their spiralled walls to generate a swirling motion. This improves the drag reduction and reduces energy consumption. It also decreases the size of pumps, pipes and fittings inflow systems such as district heating and cooling. While fluted tubes enhance the

heat transfer from the fluid to the tube wall, there is a penalty in the form of an increased pressure drop of the fluid flowing through the heat exchanger when compared to a smooth tube. Fluted tubes produce the heat transfer enhancement by enlarging the contact heat transfer surface area and thinning the condensation film based on the surface tension effect (Bukasa, 2002).

2.4.1.2 FINNED-TUBES

Lee *et al.* (2002:372) did an experimental study on fin-tube condensers, which had two different configurations of condenser paths and two kinds of refrigerants (R22 and R-407C) as working fluids. Different condenser capacities were obtained from both the experimental and numerical results, depending on the paths and refrigerants used. R22 performed better than R-407C for the Z-type path configuration, but no significant difference was found between results using either refrigerant in the U-type path configuration.

The objective of the study by Kim (2005:851) was to provide experimental data to be used in the optimal design of flat plate finned-tube heat exchangers with a large fin pitch. The airside heat transfer coefficient decreased with a reduction of the fin pitch and an increase of the number of tube rows. The reduction in the heat transfer coefficient of the four-row heat exchanger coil was approximately 10% as the fin pitch decreased from 15.0 to 7.5 mm over the Reynolds number range of 500–900, calculated based on the tube diameter. For all fin pitches, the heat transfer coefficient decreased as the number of tube rows increased from 1 to 4. The staggered tube alignment improved heat transfer performance more than 10% compared to the inline tube alignment. The correlation yielded good predictions of the measured data with mean deviations of 3.8% and 6.2% for the inline and staggered tube alignments, respectively.

2.4.1.3 MICROFIN TUBES

Bukasa (2002) conducted tests for the condensation of R22, R-134A and R-407C inside a smooth tube and three micro-fin tubes. These micro-fin tubes were identical to each other with only the spiral angles varied at respectively 10, 18 and 37 degrees. The experimental results showed an increase in heat transfer with the increase of spiral angle degrees. This increase of the heat transfer was due to:

(a) an increase of the heat transfer surface area,

(b) the extension of the annular flow regime due to surface drainage between the fins.

Dongsoo *et al.* (2003:1,6) examined the flow condensation heat transfer coefficients of R22, R-134A, R-407C, and R-410A inside horizontal plain and microfin tubes. The experimental work was performed at a condensation temperature of 40 °C with mass fluxes of 100, 200, and 300 $kg/(m.s^2)$ and a heat flux of 7.7–7.9 kW/m^2. For a microfin tube, the heat transfer coefficients of R-134A were similar to those of R22 while that of R-407C and R-410A were between 23% to 53% and 10% to 21% respectively, lower than those of R22. Finally, the heat transfer coefficients of a microfin tube were two to three times higher than those of a plain tube. The heat transfer enhancement factor decreased as the mass flux increased for all refrigerants tested.

Honda *et al.* (2004) did experimental work on the mass velocity and condensation temperature difference of the local heat transfer characteristics during condensation of R-407C in a horizontal microfin tube. The experiments were performed at a saturation temperature of 40°C, refrigerant mass velocities of 50, 100, 200 and 300 $kg/(m.s^2)$, and a condensation temperature difference range of 1.5, 2.5 and 4.5 K. It was found that their correlation deviates with 9.2% when the experimental heat transfer coefficients are compared to the measured values.

Kim *et al.* (2005:949) did an experimental investigation on the condensation heat transfer of R22 and R-410A in horizontal copper tubes. The local and average condensation coefficients for seven microfin tubes were presented compared to those for a smooth tube. The average condensation coefficients of R22 and R-410A for the microfin tubes were 1.7–3.19 and 1.7–2.94 times larger than those in smooth tube, respectively.

2.4.1.4 HERRINGBONE TUBES

Ebisu *et al.* (1998:1044) did an experimental study on the heat transfer coefficient and pressure drop for R-407C inside a herringbone tube. Their data showed that the evaporative heat transfer coefficient for the herringbone tube was about 90% higher than that of an inner grooved tube. But, with the increase in heat transfer an increase of 30% to 60% in pressure drop occurred.

Wellstandt *et al.* (2005) investigated in-tube evaporation of R-134A for a 4m long herringbone micro-fin tube with an outer diameter of 9.53 mm. The data from the tests were compared to the literature and available helical micro-fin correlations. With the vapour

quality less than 50% the correlations predicted the values within 30% of the experimental values. In the case where the vapour was more than 50% no correlation was able to reflect the early peak of heat transfer coefficients.

2.5 *SUMMARY*

A detailed study of the characteristics of zeotropic mixtures is necessary to correctly exploit their characteristics and improve the performance of heat exchangers. Therefore, the focus of this chapter was on the zeotropic mixture's characteristics, to explain the occurrence of temperature glide and pinch points. During phase change in the condensation process, the temperature glide of zeotropic refrigerant mixtures reduces the possibility of pinch points to occur. With the higher condensing temperature and lower pressure of zeotropic refrigerant mixtures the performance of heat exchangers can be improved.

A few studies have been done over the years on the flow patterns and characteristics of zeotropic mixtures, to improve the heat transfer of the refrigerant. The focus of this study is to use a passive technique to improve the heat transfer of R-407C, when used as the refrigerant in refrigeration systems. Fluted tubes incorporating artificially extended surfaces and spiralled walls were investigated to improve the heat transfer of R-407C used as the zeotropic refrigerant mixture. The correlation of Rousseau *et al.* (2003) was used to simulate the heat transfer and pressure drop of R-407C used inside fluted tubes.

In the next chapter the design and theory of the fluted tubes will be explained in detail.

CHAPTER 3

THEORETICAL BACKGROUND

3.1 *INTRODUCTION*

The focus of this chapter is the basic theory of the fluted tube and the correlation model of Rousseau *et al.* (2003), which predicts the characteristics of the refrigerant inside fluted tube annuli. As mentioned before, the correlation was developed for a fluted-tube condenser using R22 as the refrigerant. Their model used two enhancement factors to predict the theoretical characteristics of R22, more precise when compared to the experimental data. The drawback of the model is that it was not evaluated against zeotropic refrigerant mixtures like R-407C. As explained in Chapter 1, the objective of this study is to evaluate the model by gathering new experimental data from the test facility for R-407C.

3.2 *FLUTED TUBES*

Over the years different enhancement techniques have been applied to improve the heat transfer performance of heat exchangers. As mentioned in Paragraph 2.4.1, one such method is a passive technique. Fluted tubes are one of these passive techniques used to reduce the size of heat exchangers. Due to the surface geometry these tubes enhance convective heat transfer by introducing swirl into the bulk flow on the inside and annulus side of the tube without causing a considerable increase in the friction factor (Srinivasan, 1994:543).

3.2.1 THEORY OF FLUTED TUBES

3.2.1.1 PARAMETERS OF A FLUTED TUBE

The parameters required to define a spirally fluted geometry are the volume-based inside diameter (D_{vi}), volume-based outside diameter (D_{vo}), flute depth (e), pitch (p), and the helix angle (θ) as illustrated in Figure 3.1.

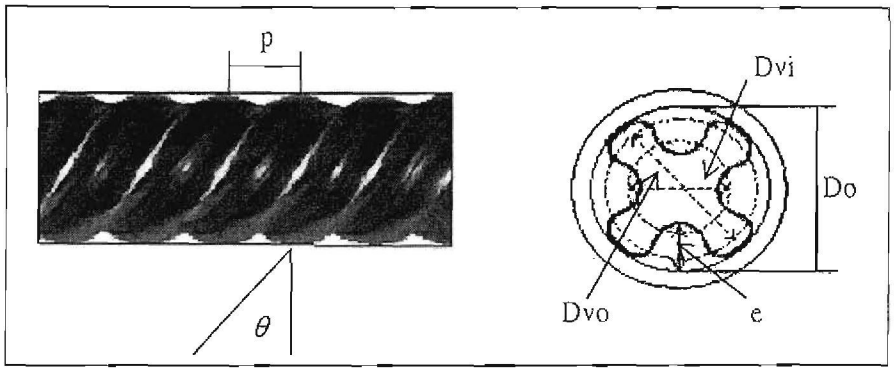


Figure 3.1: Illustration of fluted tube dimensions (Christensen *et al.*, 1993).

The profile of a fluted tube is quite complex making it difficult to determine the precise inside diameter of a fluted tube. The diameter of the fluted tube that represents the inside clear flow area (open region through the tube) is given in terms of the volume inside the tube. From the length (L) of the tube and the measured volume (Vol), the volume-based diameter (D_{vi}) is calculated as follows:

Volume-based inside diameter (D_{vi}): $$D_{vi} = \sqrt{\frac{4.Vol}{\pi.L}} \tag{3.1}$$

Due to the complex profile of a fluted tube, the same principle accounts for the calculation of the volume-based outside diameter. It is calculated by adding twice the tube wall thickness (t) to the volume-based inside diameter.

Volume-based outside diameter (D_{vo}): $$D_{vo} = D_{vi} + 2t \tag{3.2}$$

The flow area through the fluted tube (A_t): $$A_t = \frac{\pi.D_{vi}^{\ 2}}{4} \tag{3.3}$$

The flow area through the annulus (A_a): $$A_a = \frac{\pi(D_{vo}^{\ 2} - D_{vi}^{\ 2})}{4} \tag{3.4}$$

where D_{vi} = inner diameter of the outside tube

The helix angle of a fluted tube determines the swirl flow and velocity of the liquid or gas flowing through the tube and annulus. The helix angle is calculated as follows:

The helix angle (θ): $$\theta = \arctan\left(\frac{\pi . D_{vo}}{Np}\right) \tag{3.5}$$

where N = number of flute starts

p = flute pitch

These parameters are non-dimensional by dividing the flute pitch and flute depth by D_{vi} and the helix angle by $\pi/2$ to obtain p^*, e^* and θ^*.

3.3 CORRELATION OF ROUSSEAU

The method used by Rousseau *et al.* (2003) to describe the characteristics of the refrigeration fluids inside fluted tube-in-tube condensers, is based on the work done by Christensen *et al.* (1993). The next sections explain how the correlation predicts the theoretical pressure drop. Thereafter a detailed description of heat transfer follows. Firstly, the focus is on the pressure drop and heat transfer in the single-phase region inside the fluted tube and annuli. Then, the focus shifts to the pressure drop and heat transfer in the two-phase region.

3.3.1 SINGLE-PHASE REGION

Below follows the explanation of the pressure drop and heat transfer of the refrigerant in the single-phase (liquid or gas).

3.3.1.1 SINGLE-PHASE PRESSURE DROP

The aim of the correlation is to determine the pressure drop for the water flowing inside the fluted tube and the pressure drop of the refrigerant in the annulus in the single-phase region (superheated gas or liquid).

3.3.1.1.1 PRESSURE DROP IN THE INNER FLUTED TUBE

A friction factor (f), which is a function of the Reynolds number (Re_w) and geometry of the fluted tubes, is calculated to determine the pressure drop of the water inside the fluted tubes. Christensen *et al.* (1993) developed the Darcy-Weisbach friction factor to determine the

pressure drop. Re_w is based on the volumetric inside-diameter (D_{vi}) and average water velocity. The friction factor is determined as follows:

$\mathrm{Re}_w \leq 1500$

$$f = 0.554\left(\frac{64}{\mathrm{Re}_w - 45}\right).\left(e^*\right)^{0.384}.\left(\rho^*\right)^{-1.454+2.083e^*}.\left(\theta^*\right)^{-2.426} \quad (3.6\ a)$$

or

$\mathrm{Re}_w > 1500$

$$f = 1.209\left(\mathrm{Re}_w\right)^{-0.261}.\left(e^*\right)^{1.26-0.05\rho^*}.\left(\rho^*\right)^{-1.66+2.033e^*}.\left(\theta^*\right)^{-2.699+3.67e^*} \quad (3.6\ b)$$

3.3.1.1.2 PRESSURE DROP IN THE OUTER FLUTED TUBE

Rousseau *et al.* (2003:235) stated that the annulus can be effectively simulated as a number of helical coils in parallel. The single and two-phase region's pressure drops in the helical coils are determined by an enhancement ratio (r_f). This enhancement ratio is defined as the ratio of the effective friction factors when helical and straight tubes are compared.

$$r_f = \frac{f_{helical}}{f_{straight}} \quad (3.7)$$

For straight tubes, $f_{straight}$, is based on the standard single-phase correlation determined by Swamee *et al.* (1976) as follows:

$$f_{straight} = \frac{0.25}{\left\{\log\left[\left(\frac{e}{3.7xD_h}\right)+\left(\frac{5.74}{\mathrm{Re}^{0.9}}\right)\right]\right\}^2} \quad (3.8)$$

For helical coils, $f_{helical}$, described by Das (1993) in a single-phase as follows in equation (3.9):

$$f_{helical} = 4\left[0.079\mathrm{Re}^{-0.25}+0.0075\left(\frac{D_{ho}}{d_{coil}}\right)^{0.5}+17.5782\mathrm{Re}_v^{-0.3137}.\left(\frac{D_{ho}}{d_{coil}}\right)^{0.361}.\left(\frac{e_r}{D_{ho}}\right)^{0.6885}\right] \quad (3.9)$$

In the two correlations above, D_{ho} is the hydraulic diameter and e_r is the relative roughness. The unknown parameters above are given by:

$$D_{ho} = D_o - D_{vo} \quad (3.10)$$

$$d_{coil} = \frac{D_{ho}}{\sin\theta} \quad (3.11)$$

The single-phase enhancement ratio also applies to the two-phase region. Therefore, the pressure drop in the helical coils ($\Delta p_{helical}$) for both the single and two-phase regions can be calculated. This is made possible by calculating the pressure drop in the straight tubes ($\Delta p_{straight}$) and then multiplying it with the friction enhancement ratio (r_f). Equation (3.12) was used to determine the single phase pressure drop in the outer annulus.

$$\Delta p_{straight} = f_{straight}.L.\frac{V^2}{2.D_{ho}} \tag{3.12}$$

In the simulation model of Rousseau *et al.* (2003:235) an additional enhancement factor (e_f) was developed to take into account the difference between standard helical coils and the actual fluted tube annulus which is not coiled. The aim of this project is to improve this enhancement factor and thereby improve the accuracy with which the model predicts the refrigerant characteristics.

The total pressure drop was calculated as:

$$\Delta p = e_f.r_f.\Delta p_{straight} \tag{3.13}$$

The value of e_r was determined by comparing simulated results with measured data for a commercial fluted tube heat exchanger.

3.3.1.2 SINGLE-PHASE HEAT TRANSFER COEFFICIENT

Here the correlation serves to determine the heat transfer coefficient for the water flowing inside the fluted tube and the heat transfer coefficient of the refrigerant in the annulus in the single phase region.

3.3.1.2.1 HEAT TRANSFER IN THE INNER FLUTED TUBE

The condensing water flows inside the fluted tube and its heat transfer coefficient is determined by:

$$h_i = \frac{Nu.k}{D_{vi}} \tag{3.14}$$

The Nusselt number (Nu) of the water is calculated by the correlation of Christensen *et al.* (1993). The Nu_w is dependent on the Re_w as follows:

$$\text{Re}_w \leq 5000$$
$$Nu_w = 0.014\text{Re}_w^{0.842}.(e^*)^{-0.067}.(\rho^*)^{-0.293}.(\theta^*)^{-0.705}.\text{Pr}_w^{0.4} \quad (3.15\ a)$$

or

$$\text{Re}_w > 5000$$
$$Nu_w = 0.064\text{Re}_w^{0.773}.(e^*)^{-0.242}.(\rho^*)^{-0.108}.(\theta^*)^{-0.599}.\text{Pr}_w^{0.4} \quad (3.15\ b)$$

and the Prandtl number (Pr) is calculated as:

$$\text{Pr} = \frac{Cp.\mu}{k} \quad (3.16)$$

3.3.1.2.2 *HEAT TRANSFER IN THE ANNULUS*

The heat transfer of the refrigerant flowing in the annulus in the single-phase will be determined as follows:

The Nusselt number ($Nu_{straight}$) is derived from the Dittus-Boelter correlation (Incropera and Dewitt, 1996) namely:

$$Nu_{straight} = 0.023\text{Re}^{0.8}.\text{Pr}^{0.4} \quad (3.17)$$

And for fluted tubes the Nusselt number is calculated as:

$$Nu_{helical} = e_h.r_h.Nu_{straight} \quad (3.18)$$

with $r_h = r_f$

According to the Chilton-Colburn analogy (Incropera and Dewitt, 1996) the heat transfer enhancement ratio (r_h) for plain geometries is approximately equal to the friction enhancement ratio (r_f).

An additional enhancement factor (e_h) is added to Equation (4.18) for the differences in the smooth tubes and fluted tube annulus. The value of e_h was obtained by doing a comparison between the simulation and measured results. The heat transfer is then determined as indicated in Equation (3.19):

$$h_{helical} = \frac{Nu_{helical}.k}{D_{vi}} \quad (3.19)$$

3.3.2 TWO-PHASE REGION

In the next section the Rousseau correlation is applied to determine the pressure drop and heat transfer coefficient of the refrigerant in the two-phase region.

3.3.2.1 TWO-PHASE PRESSURE DROP

The two-phase pressure drop for a straight tube is dependent on the refrigerant quality and is calculated as:

$$\Delta p_{straight} = 0.09 R_{ev}^{-0.2} . x^{1.8} \left[1 + 2.85 \left(\mu_x^{-0.1} \left(\frac{1-x}{x} \right)^{0.9} . \rho_x^{0.5} \right)^{0.523} \right]^2 . \left(\frac{G^2}{\rho_v D_{ho}} \right) \tag{3.20}$$

The refrigerant properties like the quality (x), density (ρ) and viscosity (μ) play an important role in determining the pressure drop. The properties are determined at the average refrigerant temperature in the tube section which is then analysed. G is the mass flux and R_{ev} is based on the vapour properties of the refrigerant at the average temperature.

Then Equation 3.15 was used again to determine the total pressure drop for the refrigerant in the two-phase region.

3.3.2.2 TWO-PHASE HEAT TRANSFER COEFFICIENT

The technique of Shah (1979) was used to determine the heat transfer coefficient for the two-phase refrigerant in the annulus. Shah indicates that the liquid heat transfer coefficient (h_{liq}) is initially determined with the help of the Dittus-Boelter equation.

$$h_{liq} = \frac{k.Nu_{straight}}{D_h} \tag{3.21}$$

Furthermore, with the aid of the average quality of the refrigerant in the tube, the heat transfer coefficient is calculated as follows:

$$h_{tp} = h_{liq} \left[(1-x)^{0.8} + \frac{3.8.x^{0.76}(1-x)^{0.04}}{\mathrm{Pr}^{0.38}} \right] \tag{3.22}$$

where Pr is determined as:

$$\mathrm{Pr} = \frac{P_{Local_static_pressure}}{P_{Critical_pressure}} \tag{3.23}$$

3.4 THE SIMULATION MODEL OF ROUSSEAU ET AL. (2003)

The simulation models in this study are based on the model developed by Rousseau *et al.* (2003:236). The models are used to predict the heat transfer coefficient and pressure drop for R-407C and not for R22 anymore. This simulation model is developed in EES (Engineering Equation Solver) and makes use of the refrigerant property. Two models were developed for this study:

- The first model was used to process all the experimental data from the test facility to obtain new enhancement factors by comparing the theoretical data with the experimental data. The percentage error that occurred between the theoretical data and experimental data were then used to improve the enhancement factors on the pressure drop and heat transfer coefficient.
- The second model used these new improved enhancement factors to predict the heat transfer coefficient and pressure drop of R-407C under different test conditions.

3.4.1 SIMULATION MODEL NO.1

The following variables are the input values for the condenser model:

- Fluted tube geometry.
- Refrigerant mixture.
- Refrigerant mass flow rate.
- Refrigerant pressure, temperature and enthalpy where it exits the compressor.
- Refrigerant inlet pressure, temperature and enthalpy where it enters each heat exchanger in the test section.
- Refrigerant outlet pressure, temperature and enthalpy where it exits each heat exchanger in the test section.
- The water mass flow rate.
- The inlet temperature of the water at each water loop.
- The length of each condensing heat exchanger in the test section.

The basic function of the programme is: the heat exchanger area is divided up into a specific number of finite increments. Each of these increments are an indication of a section of the tubing illustrated on the left in Figure 3.2, for example in the sub-cooled region the refrigerant is a liquid, in the two-phase region the refrigerant is a mixture between a gas and liquid and in

the superheated region the refrigerant is a gas. The number of areas is adjusted so that the phase crossing point, transform exactly with the three section crossing points. This implies that the user specified number of areas is adjusted to include two extra areas as illustrated with the pressure-enthalpy diagram in Figure 3.2.

The correlation makes it possible to calculate the heat transfer coefficients and pressure drops of each section, with the given inlet and outlet temperatures and pressures. At each phase change point, the inlet and outlet temperatures can be obtained when the pressure levels at each section's crossing point are known.

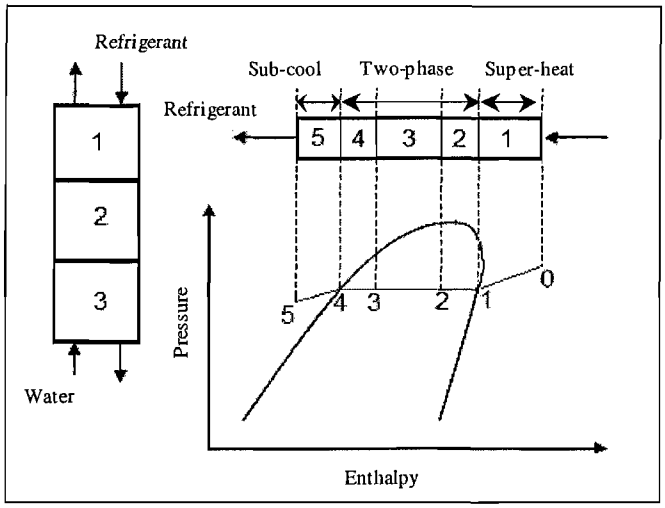


Figure 3.2: Temperature-enthalpy diagram of the test evaporator part of the refrigeration cycle Rousseau *et al.* (2003:237).

As explained by Rousseau *et al.* (2003:237), each section is then solved iteratively to achieve a heat balance between the water and the refrigerant. During this process the area of that given section is adjusted to satisfy the effectiveness (ε) – NTU equation for counter-flow given the calculated heat transfer coefficient. As this process is repeated once, new superheat and sub-cooled areas as well as a new value for the condensing temperatures are obtained. This whole procedure is then repeated until no further adjustments in areas or condensing temperatures are required.

The experimental heat transfer coefficient and pressure drop at each section, obtained from the test facility, were compared to the theoretical heat transfer coefficient and pressure drop.

By comparing the data, new enhancement factors were generated, which produced the output values of the model.

3.4.2 SIMULATION MODEL NO.2

The second model operates on the same principle, but uses the new enhancement factors to calculate the outlet temperature, pressure and enthalpy instead of the outlet temperature, pressure and enthalpy at each section. The output values of the second model are the theoretical outlet temperature, pressure and enthalpy at each section of the test facility. An average enhancement factor is gained from different test conditions through the first model. These average enhancement factors were then used in the second model to determine the theoretical heat transfer coefficient and pressure drop of R-407C under different conditions. Then the accuracy was tested for these average enhancement factors by comparing the theoretical values with the experimental values. The method that was used is fully explained in Chapter 6.

3.4.3 COUNTER-FLOW CONFIGURATION

In condensing heat exchangers a counter-flow configuration is normally used to obtain the maximum heat transfer. It is possible to achieve outlet water temperatures above the condensing temperature and approach the superheat temperature of the refrigerant gas by using a counter-flow configuration. In a counter-flow fluted tube heat exchanger the water normally flows inside the fluted tube with the refrigerant flowing in the annulus side as illustrated in Figure 3.3. According to Rousseau *et al.* (2003:239) the heat transfer is improved by two phenomena:

1. During a condensation process the condensate is drawn in the direction of the corners of the channels by surface tension, clearing the remaining surface in contact with the hot gas.
2. The liquid phase of the refrigerant experiences some micro-circulation, particularly towards the outlet side, leading to the replacement of cold liquid next to the surface with hotter liquid.

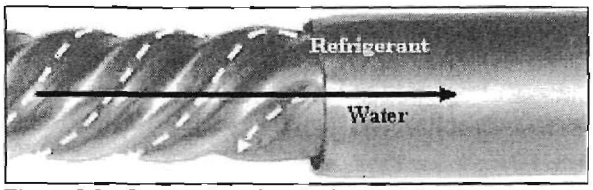


Figure 3.3: Counter-flow fluted tube geometry.

3.5 *SUMMARY*

In this chapter the design theory of a fluted tube and the correlation of Rousseau *et al.* (2003) were explained in detail to determine the heat transfer and pressure drop of R-407C when it is used as the refrigerant inside fluted tubes. The focus was to determine the characteristics of R-407C in the single-phase and two-phase region.

In the next chapter the test bench used to manufacture the fluted tubes will be described with its components. The layout of the test facility used to gather the experimental data, with its different components, measuring and acquisitioning equipment will be further discussed. To verify the accuracy of the experimental data gained from the test facility an uncertainty analysis will be performed on the measuring equipment to determine their accuracy.

CHAPTER 4

EXPERIMENTAL FACILITIES

4.1 INTRODUCTION

This chapter features the manufacturing process of the fluted tubes. It also discusses the operation of the test bench used to conduct the experimental part of this study. The existing test bench was modified from a forced convective boiling test facility to a condensation heat transfer coefficient test facility. The previous test bench configurations are briefly discussed after which a description of the test bench alterations for condensation measurements of R-407C and R 22 follows. The chapter also addresses the different components, the control of the test bench and the measuring equipment. Finally, the uncertainty analysis that was done on the measuring equipment of the test facility is discussed and explained in detail. The verification on the measuring equipment was done with R-407C and R22.

4.2 MANUFACTURING PROCESS

The fluted tubes for this study needed to be manufactured as no company in South Africa produces fluted tubes commercially. As a result, most of the fluted tubes used in the industry have to be imported, which is expensive and creates long time delays. Therefore, all the fluted tubes were manufactured by an existing workbench. But, this workbench had a few shortcomings, namely:

1. The pitch was unevenly spread out over the fluted tube, meaning that the pitch differed over the length of the fluted tube.

2. During the manufacturing process many failures occurred due to breakages on the fluted tube itself because of the feed speed of the chuck and grooving wheels.
3. Previously, the annulus was not ebb tide over the fluted tube, thus the heat transfer between the refrigerant and the water was not effective.

The fluted tubes utilised for this study were manufactured from soft drawn copper tubing for two practical reasons, namely:

- It is fairly easy to work with, meaning it is soft enough that smooth tubes can be deformed into a given flute pitch pattern using a fluted tube work bench.
- Copper have a reasonably high thermal conductivity in the region of $k = 401$ $(W/m.K)$ compared to other materials in its price category.

In the next paragraph the workbench, manufacturing and the method that was used to address the problems that occurred during the manufacturing process, will be discussed briefly.

4.2.1 WORKBENCH

In Figure 4.1 is a schematic illustration of the fluted tube test bench used to manufacture the different fluted tubes. The workbench consists of the following basic components:

- Feed frame to guide the copper tube into the chuck.
- DC motor to turn the chuck.
- Chuck with angled grooving wheels to flute the copper tube.
- Guidance car to hold, guide and stabilise the fluted tube along the I-beam.
- I-beam on which the guidance car can move.
- Winder to pull the fluted tube into the outer tube.

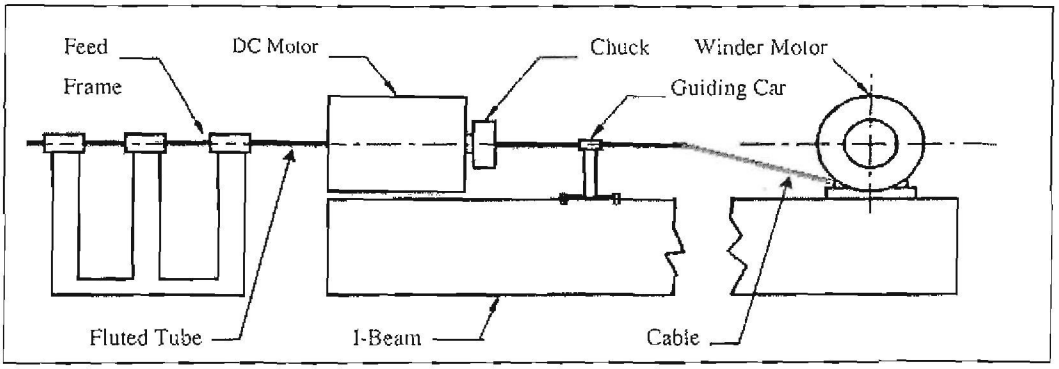


Figure 4.1: Schematic illustration of workbench.

The speed ratio of the winder motor and the DC motor controlling the rotation speed of the grooving wheels on the chuck had to be recalculated to ensure that no breakages will occur during the manufacturing process. If the ratio was incorrect the fluted tube was fed either to slow or to fast through the chuck. This resulted in the following two failures:

1. If the fluted tube was pulled to fast by the winder motor, a shear failure occurred due to shear forces by the winder motor.
2. When the winder motor was to slow the grooving wheels made a double off-set groove into the fluted tube. This normally disrupted the pitch pattern by cutting off the normal flute path that the refrigerant will follow, meaning that one flute path will overlap with another flute path.

4.2.1.1 CHUCK AND GROOVING WHEELS

The main component of the workbench is the chuck with its grooving wheels as shown in Figure 4.2. The chuck rotates around its longitudinal axis with the support of a DC motor. An adjustable speed control ensures that the tubes are fluted properly at a desirable speed. The DC motor is connected to a gearbox with the adjustable speed control and direction switch.

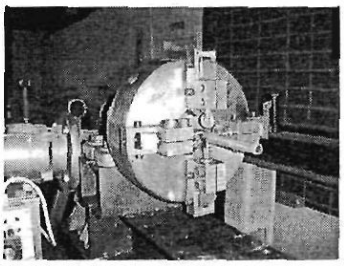


Figure 4.2: Chuck of workbench.

The rotating grooving wheels press into the tube wall, which creates the flute on the fluted tubes as illustrated in Figure 4.3. The tube is clamped at its leading end, which creates a corkscrew effect. This means that the rotational energy is converted into translation energy, which drives the tube through the chuck along the I-beam.

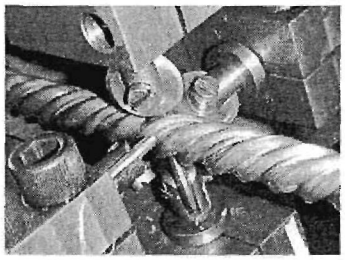


Figure 4.3: Grooving wheels of workbench.

The problem that continually occurred was fluted tubes with unequal thickness and the pitch which was unevenly spread out over the fluted tube due to the incorrect setting of the grooving wheels. The angle and flute depth of the grooving wheels was the main cause of this problem. To address this problem each wheel was individually set at a precise depth and angle with the aid of a magnetic dial gauge (Figure 4.4) on the chuck. After every setting, the gauge was recalibrated and the whole exercise was redone, to ensure the setting on the grooving wheels was correct.

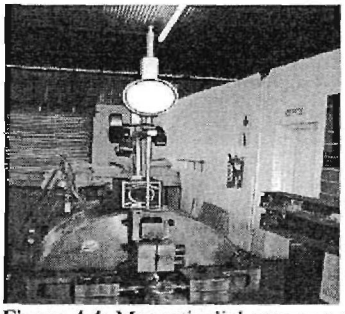


Figure 4.4: Magnetic dial gauge on chuck

4.2.1.2 BASIC MANUFACTURING PROCEDURE

As a smooth copper tube with an outside diameter (D_o) of 15.875mm is guided for the first run through the chuck, the grooving wheels, set at a certain groove angle, are simultaneously adjusted to a specified flute depth. A flute depth of e = 2.9mm was used in this study. During the manufacturing process the fluted tube passes four times through the chuck. After every cycle the flute depth was increased (increments of 0.725mm) till the desired depth was reached.

Markings on the chuck-clamps depict the angle of the grooving-wheels in degrees as illustrated in Figure 4.5. By changing the grooving-wheel angle, different sets of flute pitch configurations can be achieved. Only three different pitch angles where manufactured as

listed in Table 4.1. The minimum groove angle of 45° and maximum groove angle of 60° on the chuck restricted the manufacturing process range of pitches. The minimum and maximum angles were used to manufacture two differently pitched tubes, with a third groove angle of 55° also used. A 55° was used because this groove angle gave the least problems during the manufacturing process.

Table 4.1: Experimental fluted tube geometry results.

Geometry of the Fluted Tube	Fluted tube no.1	Fluted tube no.2	Fluted tube no.3
Fluted tube material	Copper	Copper	Copper
Fluted tube length	3 m	3 m	3 m
Flute pitch	9.5 mm	6.8 mm	11.4 mm
Flute depth	2.09 mm.	2.09 mm.	2.09 mm.
Wall thickness of fluted tube	0.73 mm	0.73 mm	0.73 mm
Number of flute starts	4	4	4
Volume inside fluted tube	0.0121 m	0.011 m	0.0135 m
Inside diameter of annulus	0.0199 m	0.0188 m	0.0213 m
Groove wheel setting [line numbers]	2	1	4
Groove angle [degrees]	55°	60°	45°

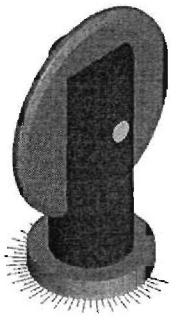


Figure 4.5: Illustration of a grooving wheel with markings.

After the manufacturing of the fluted tubes, the outer tubes are pulled and ebb tide over the fluted tube with the aid of a die to complete the process. There are three main reasons why the annulus is ebb tide over the fluted tube:

1. To ensure that the refrigerant will follow the desired path.
2. To increase the heat transfer area between the two different fluids/gasses.
3. Lessening the leak flow between the four channels on the annulus side.

4. Dividing the total mass flow of the refrigerant into four channels, improves the refrigerant's heat transfer capability during the condensation process.

4.3 *LAYOUT OF ORIGINAL TEST BENCH*

The test bench used by Venter (2000) and De Vos (2006) is a vapour-compression system as illustrated in Figure 4.6. De Vos (2006) generated data for the forced convective boiling heat transfer coefficients of R-407C in a fluted tube.

The system consists of a split evaporator design with separate expansion valves for each evaporator. The compressor described by points 1-2 delivers the refrigerant mixture to the condenser, where the hot gas is condensed to a liquid. From the condenser the refrigerant flow split into the main evaporator, described by points 6-9, and to the test evaporator, described by points 5-7-8-9.

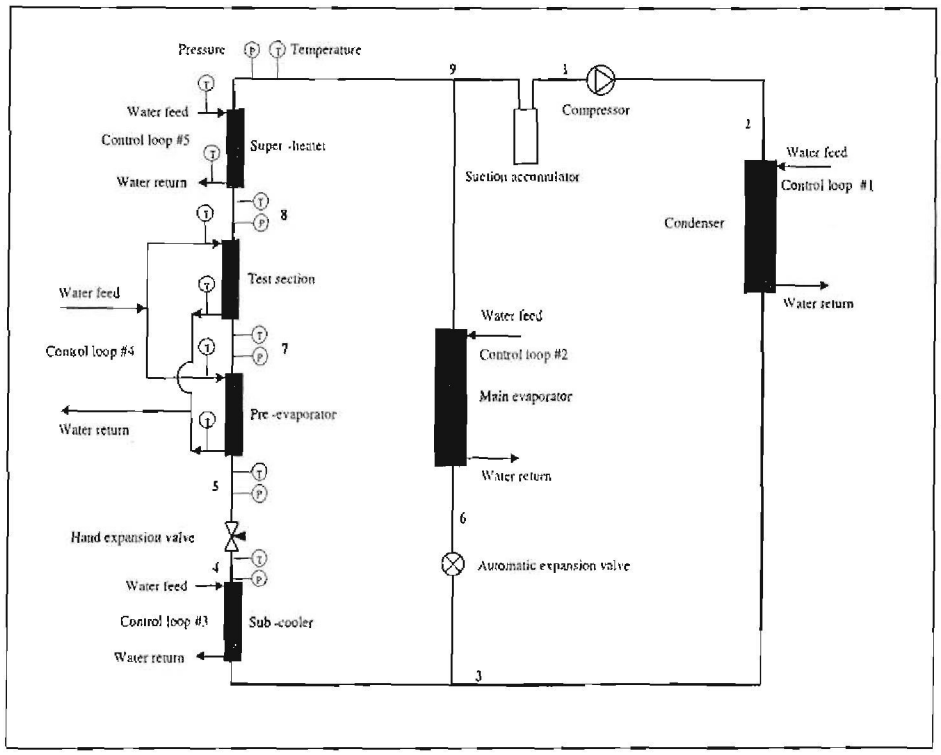


Figure 4.6: Layout of the evaporation test bench; refrigeration circuit (Venter, 2000:37).

As illustrated in Figure 4.6 the test evaporator is divided into three heat exchanger sections namely the pre-evaporator, test section and super-heater. The pre-evaporator and super-heater were smooth tube-in-tube heat exchangers, while the test section was a fluted tube in a

smooth annulus. In all three sections the refrigerant mixture flow was in the annulus and the water in the inner tube as illustrated in Figure 4.7. The pre-evaporator was used to control the dryness fraction of the refrigerant entering the test section. The test section was then used for the near complete evaporation of the refrigerant. Some liquid may still remain at the exit of the test section; the super-heater ensured that the refrigerant had completely evaporated before entering the compressor.

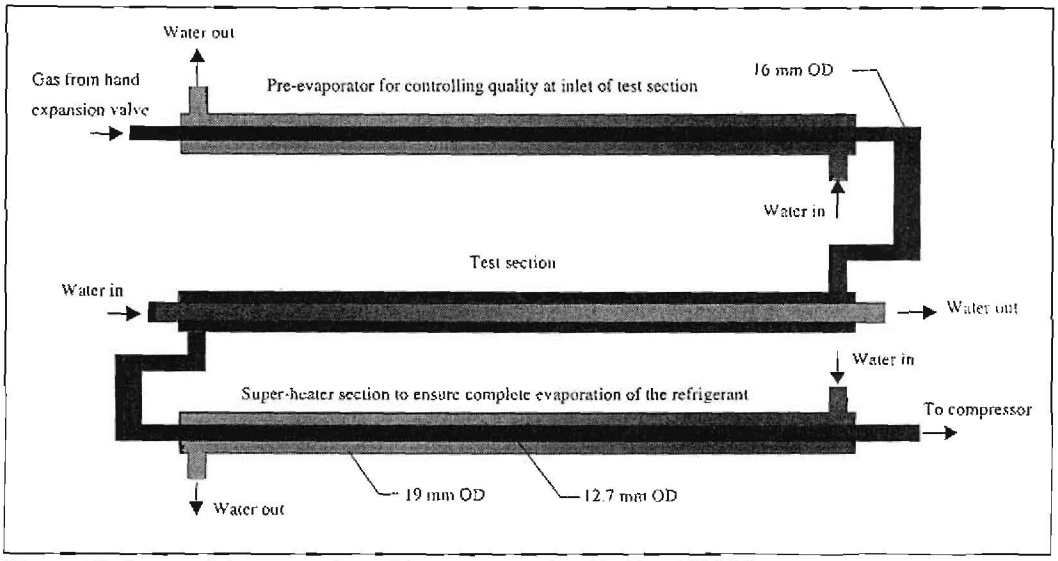


Figure 4.7: Layout of the evaopration refrigerant test section (De Vos, 2006:31).

An automatic expansion valve, described by points 3-6 in Figure 4.6, controls the condensation and evaporation pressure. The automatic expansion valve was adjusted by a setting screw to change the evaporator pressure. The refrigerant mass flow through the two evaporator lines were controlled by a hand expansion valve as described by points 4-5 in Figure 4.6.

Before the refrigerant enters the test evaporator it passes through the sub-cooler as described by points 3-4 in Figure 4.6. The sub-cooler controls the dryness fraction at point 5, just before the refrigerant enters the test evaporator. Varying the water mass flow rate and temperature entering the heat exchanger, does this.

All the heat exchangers are supplied with water through external water loops. Each of these water loops is capable of controlling the water temperature and the water mass flow at the inlet of the heat exchangers.

4.4 TEST BENCH ALTERATIONS

4.4.1 NEW TESTING CONFIGURATION

The existing test facility used by Venter (2000) and De Vos (2006) was designed and built to determine the boiling characteristics of R22/R-407C. In order to determine the condensation characteristics of R-407C, a few main alterations on the test facility had to be made. During the condensation process of R-407C the test facility is exposed to pressures in the region of 1400kPa to 2200kPa. Therefore the range of the pressure sensors had to be altered and re-calibrated. Furthermore, the test section layout on the test bench was for evaporation testing, which had to be changed into a condensing test facility.

The layout of the condensation system is shown in Figure 4.8. The compressor, described by points 1-2 delivers the hot refrigerant gas to both the main condenser, described by points 2-3, and the test condenser, indicated by points 2-4-5-6. The main condenser and test condenser is in a parallel system, so that the excess refrigerant, not used by the test condenser can flow through the main condenser. The test condenser is divided into three heat exchanger sections namely the pre-cooler, the test section and the sub-cooler. Point 2 indicates that the system is of a split condenser design with separate expansion valves for each condenser. The blue and red arrows in Figure 4.8 indicate the flow directions of the refrigerant. The red arrows indicate where the refrigerant is in gas phase and the blue arrow where the refrigerant is in liquid phase.

The hand expansion valve, described by points 7-8, controls the refrigerant mass flow rate through the test bench. As the compressor delivers a constant refrigerant mass flow at a given temperature and pressure, the remaining refrigerant that does not flow through the test section will flow through the main condenser.

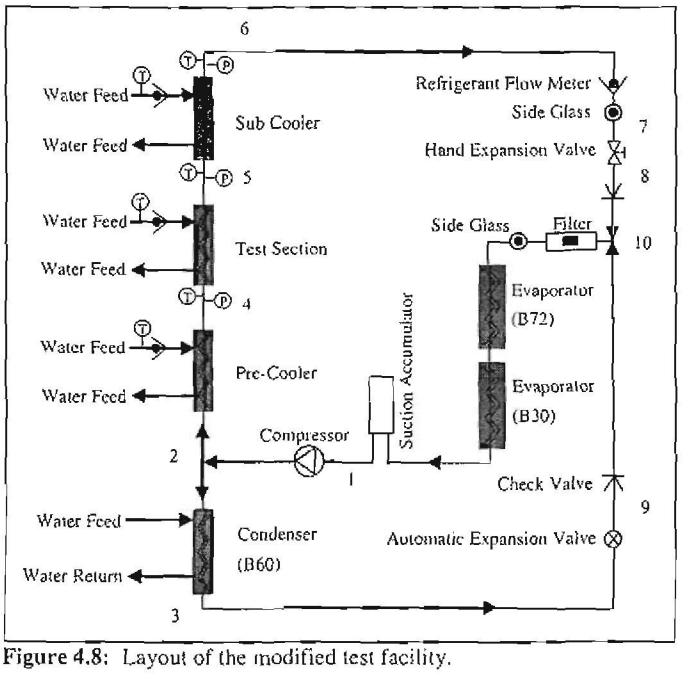


Figure 4.8: Layout of the modified test facility.

An automatic expansion valve, described by points 3-9, provides a constant evaporation pressure in both the test condenser and main condenser. The automatic expansion valve can be adjusted by a setting screw to change the condensing pressure.

The two evaporators on the return cycle to the compressor, evaporates the refrigerant mixture into gas. If the first evaporator's capacity is not sufficient, the second evaporator will ensure that only gas is supplied to the compressor. Each of the evaporators has its own water supply to evaporate the refrigerant.

Figure 4.8 shows that all the heat exchangers are supplied with separate external water loops. Each of these water loops is capable of controlling the water temperature and the water mass flow rate at the inlet of the heat exchanger. The condensers are supplied with cold water (10°C to 20°C) from the cold-water tank and the evaporators with warm water (50°C).

In Figure 4.9 the refrigerant cycle of the test bench is illustrated on a temperature-entropy diagram. The numerical indexing and measurement sensor positions on Figure 4.9 match those of Figure 4.8. The quality of the refrigerant at points 2, 4, 5 and 6 can be calculated from the water-side heat transfer, since the refrigerant conditions, at point 1 and 6 can be measured along with the conditions of the feed water. To evaluate the overall measurement

accuracy of the test bench, a heat balance is carried out between points 2 and 6 and then compared to the sum of the heat balances of points 2-4, 4-5 and 5-6. In Figure 4.8 the T indicates a temperature measuring point and the P indicates a pressure measuring point on the test facility.

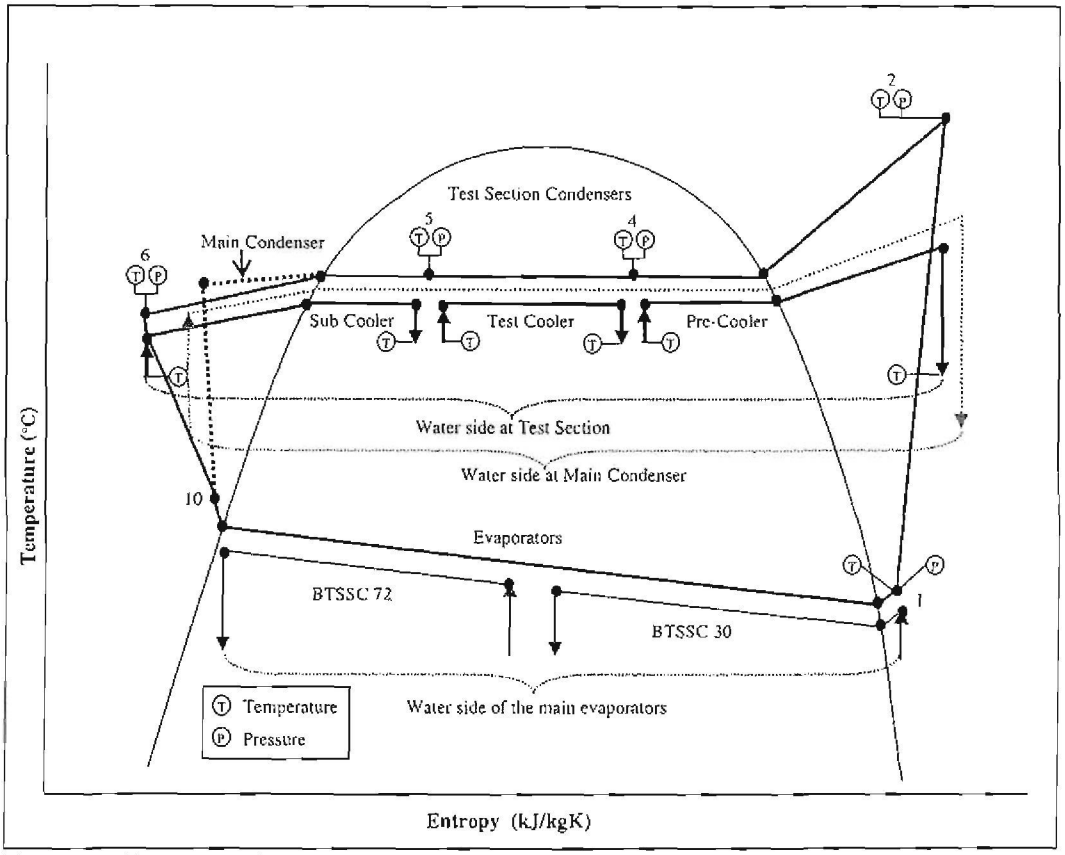


Figure 4.9: Temperature-Entropy diagram of the cycle.

Before the uncertainty analysis can be discussed, it is necessary to discuss the measuring equipment in more detail. The next section gives detailed information of the measuring equipment.

4.4.2 TEST BENCH COMPONENTS

4.4.2.1 COMPRESSOR

The compressor used in the test bench is a three-phase Copeland ZR72KC-TFD-523 scroll compressor. The lubrication oil used in the compressor is synthetic polyol refrigerant lubricant (Emkarate RL 32H), which is suitable for both R22 and R-407C.

4.4.2.2 *SUCTION ACCUMULATOR*

The suction accumulator accumulates all the excess liquid of the refrigerant to ensure that only gas enters the compressor. The accumulator has a porous opening of 0.5 mm for the oil, which serves as an oil pick-up. This porous opening is suitable for refrigerants like R22 and R-407C.

4.4.2.3 *EXPANSION VALVES*

Automatic expansion valve *(Egelhof AEK 4)*: Is used in the main condenser loop of the test bench to manually control the condensing pressure in the condensers.

Hand expansion valve *(Danfoss 6F0009)*: Is used in the test section of the test bench to vary the mass flow rate of the refrigerant manually.

4.4.2.4 *HEAT EXCHANGERS*

The main condenser and the main evaporators on the test bench, excluding the three heat exchangers in the test section, are all Turbotec fluted coils. A counter-flow configuration was applied to all heat exchangers to enhance the heat transfer. For all the heat exchangers the water flowed in the fluted tube and the refrigerant in the annulus. The following models were used:

- Main condenser: Turbotec BTSSC 48 (11 kW maximum condensing capacity)
- Main evaporator: Turbotec BTSSC 72 (26 kW maximum evaporating capacity)
- Second evaporator: Turbotec BTSSC 30 (8 kW maximum evaporating capacity)

4.4.2.5 *TEST SECTION HEAT EXCHANGERS*

The test condenser consists of three water cooled fluted tube heat exchangers, connected in series on the refrigerant side as illustrated in Figure 4.10. The pre-cooler, test-cooler and sub-cooler are the three components of the test condenser and their dimensions are listed in Table 4.1. Inside the fluted tube the refrigerant's temperature and pressure are measured at every inlet and outlet of each section of the test condenser. Only the temperature of the refrigerant in the annulus side is measured. In the fluted tube the water is exposed to an open cycle and the pressure drop is negligible.

The refrigerant delivered from the compressor enters the pre-cooler as a superheated gas. The pre-cooler is required to control the dryness fraction of the refrigerant entering the test section and is also used to gather data on the refrigerant in the superheated conditions. Based on the condensation conditions the refrigerant should exit the pre-cooler as a two-phase mixture. The test-cooler is required to gather the data of the refrigerant in its two-mixture phase during the condensation process. The sub-cooler is used to gather the data of the refrigerant in the liquid phase.

Heat loss from the system, especially through the three heat exchangers, must be prevented. Therefore, the heat exchanger tubes were insulated with 37mm thick polyethylene insulation foam, to minimize the heat loss. This is to ensure that the data gathered during the condensation process is more accurate.

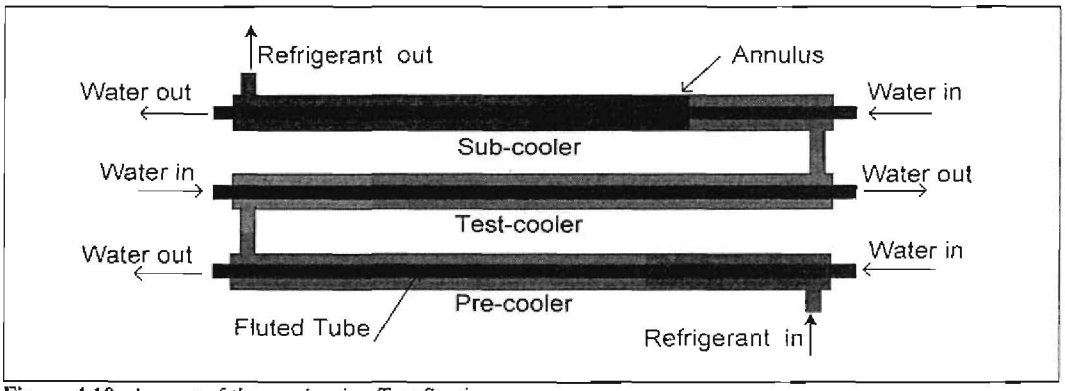


Figure 4.10: Layout of the condensing Test Section.

4.4.2.6 WATER SUPPLY TO THE HEAT EXCHANGERS

Two 10 000 *l* tanks, one with warm water (temperature was kept at 30°C) and the other with cold water (temperature was altered between 10°C and 20°C) respectively supplied water to the two evaporators, the test-condenser and the main condenser. The water temperature to the different heat exchangers are regulated and controlled by Johnson (VG7822LT) mixing valves and the mass flow is measured by Burkert (8035) mass flow meters.

The water temperature and mass flow to the heat exchangers needed to be controlled by a system, to ensure accurate measuring at different test conditions. The measuring equipment, like temperature sensors and mass flow meters, are coupled to a PID control device. The PID control device is then connected to a computer control system, which accurately controls the water temperature with mixing valves (mixing the cold and warm water together) and the

mass flow of the water with a regulating valve. Pretorius (1999) thoroughly described the water loops with its mixing valves, mass flow meters and regulating valves supplying the different heat exchangers.

The water loop supplying the test condenser with water is similar to the system supplying the evaporators and main condenser. One main cold-water loop is divided into three sections, each with its own water pump supplying the pre-cooler, test-cooler and sub-cooler. The mass flow of the water through the test section is altered manually by a needle valve. The mass flow meters (Endress & Houser Promass 63F) indicate the water mass flow through each section. As the needle valves are adjusted, the water mass flow meters indicate the mass flow rate visually on the computer with the aid of the data acquisition system

4.5. MEASUREMENT AND DATA ACQUISITION SYSTEM

The temperature, pressure and mass flow data from the test bench, as illustrated in Figure 4.8 were gained with the help of two data acquisition systems. The PREMA sub-system reads and stores the temperatures of the refrigerant and water at different points in the test condenser.

The VisiDAQ sub-system has a multiple function on the test bench. Firstly, it reads and stores the refrigerant pressure and mass flow rate through the test section. Secondly, it measures the temperature and flow rate of the water loops supplying the evaporators, main condenser and test condenser. These inputs from the water data are used to control mixing valves via a PID controller to obtain the required water temperatures entering the heat exchangers. The following sections briefly discuss the measurement and acquisition equipment.

4.5.1 MEASURING EQUIPMENT

4.5.1.1 TEMPERATURE MEASUREMENT

Two types of temperature sensors are used to measure the temperature of the refrigerant and the water.

- Grade A three-wire Pt 100: This sensor (Figure 4.11) inside a thermowell probe measures the temperature of the water loops supplying the evaporators and

condensers. The temperature readings from these sensors were used to control the mixing valves in order to obtain the correct supply temperature.

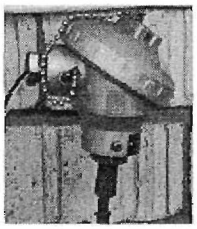


Figure 4.11: Pt 100 grade A three-wire with thermowell probe.

- Grade A four-wire Pt 100: This sensor (Figure 4.12) was used to measure the temperature of the refrigerant and water on the test bench at the different positions illustrated in Figure 4.11 by **T** (temperature) and **P** (pressure). At these positions the sensors together with thermal paste were placed into stainless steel thermowells, which were soldered into the refrigerant and water pipe lines. The four-wire Pt 100 was connected via shielded 4-wire extensions to a PREMA 3040 electronic temperature scanner and logger as shown in Figure 4.13.

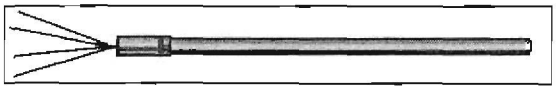


Figure 4.12: Pt 100 grade A four-wire.

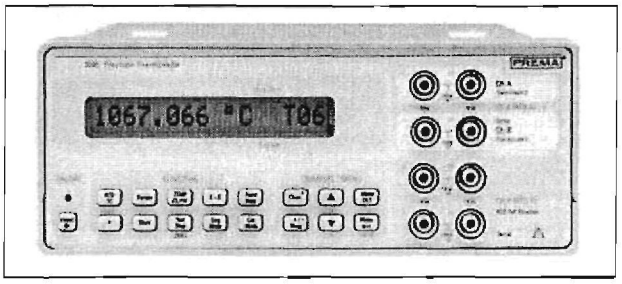


Figure 4.13: PREMA 3040 scanner and logger (3040 Precision Thermometer, 1998).

4.5.1.2 PRESSURE MEASUREMENT

The refrigerant pressure is measured at the five points as illustrated in Figure 4.8. The pressure at each inlet and outlet of the test-cooler are measured to gain the necessary information about the condensation characteristics of the refrigerant. On the test bench the outlet pressure of the pre-cooler is also the inlet pressure of the test-cooler and the same

applies to the outlet of the test-cooler, which is also the inlet of the sub-cooler. All the pressure sensors are Endress & Hauser PMC731 sensors (Figure 4.14) with a pressure range of 0 – 20 bar.

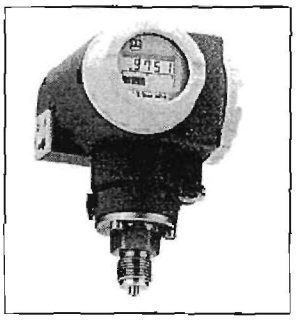


Figure 4.14: Endress + Hauser PMC731 pressure sensor (Endress + Hauser, 2006).

4.5.1.3 MASS FLOW MEASUREMENT

The water mass flow rate supplying the pre-cooler, test-cooler and sub-cooler are measured with Coriolis flow meters (Endress & Hauser Promass 63F). Figure 4.15 is a photo of one of these flow meters. The span in which the flow rate meter can operate is 0 to 0.1204 kg/s.

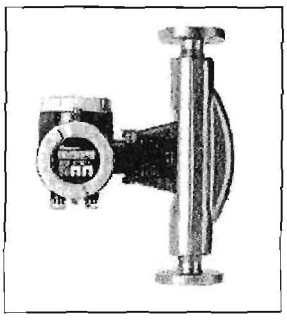


Figure 4.15: Endress + Hauser Promass 63F flow meter (Endress + Hauser, 2005).

The refrigerant mass flow rate is measured with a Coriolis flow meter (Micromotion RFT9739) with a span of 0 to $0.5 kg/s$. This flow meter (Figure 4.16) is installed between the sub-cooler and the hand-expansion valve to avoid measurement errors as a result of two-phase flow.

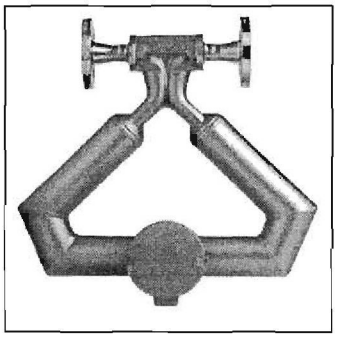


Figure 4.16: Micromotion RTF9739 flow meter.

4.5.2 ACQUISITIONING EQUIPMENT

4.5.2.1 TEMPERATURE ACQUISITIONING

The temperatures measured from the test section, with the Grade A four-wire Pt 100 sensors, are directly connected to the PREMA 3040 (Figure 4.13) temperature scanner and logger. The temperatures are sequentially read by the PREMA 3040 scanner and is then logged in its memory buffer and transferred via a RS232 connection cable to a personal computer, where the information is stored as an ASCII file. The ASCII file is then copied from the PREMA software program and pasted into a Microsoft Excel spread sheet for further calculations. The accuracy of the scanner is accepted as thorough at 0.06% (Venter, 2000).

4.5.2.2 PRESSURE AND FLOW DATA ACQUISITIONING

The 4-20mA analogue signals outputs generated by the flow and pressure sensors are sent to the analogue input modules (ADAM 4018 modules) where it is converted to digital signals. The data is then transferred via a RS232 to the VisiDAQ software where the signals are converted to kPa for the pressure and kg/s for mass flow. The manufacturer guarantees an accuracy of more than 0.1% of the measured value in the signal conversion process.

In the next section the uncertainty analysis that was done on the measuring equipment will be discussed to determine the accuracy of the measurement of the equipment used on the facility.

4.6 UNCERTAINTY ANALYSIS

The method stipulated in the ISO (1993) standard was used to calculate the uncertainty in the experimental results. The method is based on a careful specification of the uncertainties in the various primary experimental measurements. To carry out this method, a random

selection was done on various experimental results of R-407C against water. An uncertainty analysis was done on the heat transfer of the refrigerant and the water. In Table 4.2 all the uncertainties of the measuring equipment used are listed to determine the characteristics of the refrigerant and the water. The measuring equipment was calibrated before it was installed on the test bench. The pressure sensors and mass flow meters were calibrated by the manufactures (Endress and Houser), while the temperature sensors were calibrated with the aid of a temperature bath. In Appendix F the uncertainty on the calculation of the heat transfer on the water and the refrigerant is illustrated.

Table 4.2: Uncertainty of measuring equipment.

no.	Measurement	Equipment	Range	Uncertainty
1	Temperature sensors on the test section	Grade A four-wire Pt 100	(-20 °C) - (150 °C)	± 0.1°C
2	Temperature sensors on the water loops	Grade A three-wire Pt 100	(-27 °C) - (105 °C)	± 0.1°C
3	Pressure	Endress & Houser PMC731	0 - 20 Bar	± 0.5%
4	Mass flow rate: Water	Endress & Houser Promass 63F	0 - 0.1204 kg/s	± 0.5%
5	Mass flow rate: Refrigerant	Micromotion RFT9739	0 - 0.5 kg/s	± 0.1%
6	Tube length	Tape measure	0 - 3m	± 1.11mm
7	Volume of flute	Volumetric tube	100 ml^3	± 0.1ml^3
8	Data acquisitioning	VisiDAQ & PREMA	4 - 20 mA inputs	± 0.1%

The uncertainty calculation of the nominal heat transfer on the water side is calculated by multiplying the mass flow rate of the water through a given test section with the temperature difference between the inlet and outlet of the test section:

$$Q_w = \dot{m} \cdot c_p (T_{out} - T_{in}) \tag{4.1}$$

The primary experimental measurements that played a role in the calculation of the uncertainty analysis of the water heat transfer are indicated by the following parameters:

- Mass flow rate (m)
- Inlet temperature (T_{in})
- Outlet temperature (T_{out})
- Specific heat capacity (c_p)

The uncertainty heat transfer waterside is calculated as follows:

$$u(q_w) = \sqrt{\left(u(\dot{m}).\frac{\partial Q_w}{\partial \dot{m}}\right)^2 + \left(u(c_p).\frac{\partial Q_w}{\partial C_p}\right)^2 + \left(u(T_{in}).\frac{\partial Q_w}{\partial T_{in}}\right)^2 + \left(u(T_{out}).\frac{\partial Q_w}{\partial T_{out}}\right)^2} \quad (4.2)$$

The percentage error ($w_{error\,w}$) is obtained through Equation 4.3:

$$w_{error\,w} = \left(\frac{u(q_w)}{Q_w}\right) \quad (4.3)$$

The calculated uncertainty on the experimental data set on the fluted tubes resulted in the following maximum and average uncertainties as illustrated in Table 4.3.

Table 4.3: Average and maximum uncertainty of the heat transfer (Q_w) on the water side.

All three fluted tubes combined	Maximum Uncertainty	1.721%
	Average Uncertainty	1.124%
Fluted Tube no.1	Maximum Uncertainty	2.012%
	Average Uncertainty	1.173%
Fluted Tube no.2	Maximum Uncertainty	1.182%
	Average Uncertainty	1.144%
Fluted Tube no.3	Maximum Uncertainty	1.860%
	Average Uncertainty	1.054%

The uncertainty analysis on the refrigerant's heat transfer was done as described below. The nominal heat transfer on the refrigerant side is calculated based on the same principle as the waterside:

$$Q_r = m_r(h_{out} - h_{in}) \quad (4.4)$$

The primary experimental measurements that played a role in the calculation of the uncertainty analysis of the refrigerant heat transfer are as follows:

- Mass flow rate ($\dot{m}$)
- Outlet temperature (T_{out})
- Inlet pressure (P_{in})
- Outlet pressure (P_{out})
- The inlet enthalpy (h_{in}) is a function of the inlet pressure and temperature

  $h_{in} = f(T_{in}, P_{in})$
- The outlet enthalpy (h_{out}) is a function of the outlet pressure and temperature

  $h_{out} = f(T_{out}, P_{out})$

The uncertainty heat transfer of the refrigerant is calculated as shown in Equation 4.5:

$$u(q_r) = \sqrt{\left(u(\dot{m}).\frac{\partial Q_r}{\partial \dot{m}}\right)^2 + \left(u(h_{in}).\frac{\partial Q_r}{\partial h_{in}}\right)^2 + \left(u(h_{out}).\frac{\partial Q_r}{\partial h_{out}}\right)^2} \quad (4.5)$$

The percentage error ($w_{error\,r}$) is obtained through Equation 4.6:

$$w_{error\,r} = \left(\frac{u(q_r)}{Q_r}\right) \quad (4.6)$$

The calculated uncertainty on the experimental data set on the fluted tubes resulted in the following maximum and average uncertainties as illustrated in Table 4.4.

Table 4.4: Average and maximum uncertainty of the Heat transfer (Q_r) on the refrigerant side.

All three fluted tubes combined	Maximum Uncertainty	1.490%
	Average Uncertainty	1.074%
Fluted Tube no.1	Maximum Uncertainty	1.482%
	Average Uncertainty	1.191%
Fluted Tube no.2	Maximum Uncertainty	1.483%
	Average Uncertainty	1.091%
Fluted Tube no.3	Maximum Uncertainty	1.481%
	Average Uncertainty	0.941%

More detail regarding the uncertainty analysis is available in Appendix F.

4.7 *CALIBRATION OF THE INSTRUMENTATION WITH R22*

Refrigerant R22 was used to calibrate and determine the accuracy of the measuring equipment on the test facility. The main reason why R22 was used to calibrate the instrumentation was that no temperature glide occurs in the two-phase region during the condensation process as happens with zeotropic mixtures. By comparing the refrigerant's heat transfer (Q_r) to the water's heat transfer (Q_w) the accuracy of the measuring equipment could be determined by calculating the percentage error.

The following values from the measuring equipment were taken to determine the heat transfer of the refrigerant:

(1) Mass flow rate from the Coriolis (Micromation RTF9739) flow meter.

(2) Temperature from the PT100 temperature sensors.

(3) Pressure from the Endress & Hauser PMC731 pressure sensors.

The following values from the measuring equipment were taken to determine the heat transfer of the water:

(1) Mass flow rate from the Endress & Hauser Promass 63F flow meter.

(2) Temperature from the PT100 temperature sensors.

The pressure of the water was taken as atmospheric pressure, because the secondary side (water side) of the heat exchanger was an open cycle.

Test results from fluted tube no.1 were taken to determine the accuracy of the measuring equipment. Only the refrigerant's mass flow rate was kept constant at m_r = 0.05 kg/s, while the other conditions were altered:

(1) The water mass flow rate (m_w = 0.05 kg/s, 0.07 kg/s and 0.09 kg/s).

(2) Water temperature (T = 10°C, 15°C and 20°C).

The results of the accuracy of the measuring equipment are listed in Table 4.5. The average percentage error between the heat transfers calculated from the refrigerant side compared to that calculated from the water is 0.96%, while the maximum error is 1.94%. With this kind of accuracy the calibration of the measuring equipment on the test bench is considered to be sufficient for use during the R-407C experiments.

Table 4.5: Determining the accuracy of the measuring equipment with R22

Mass flow rate (kg/s)	Temperature (°C)	Q_r (kJ.kg/K)	Q_w (kJ.kg/K)	Error (%)
0.05	10	14.69	14.24	1.07
0.05	15	11.99	11.87	1.00
0.05	20	10.62	10.53	0.85
0.07	10	14.15	14.08	0.47
0.07	15	11.88	11.65	1.94
0.07	20	10.98	10.87	1.04
0.09	10	13.57	13.52	0.38
0.09	15	11.45	11.39	0.53
0.09	20	11.36	11.21	1.31
Average percentage error (%)				0.96
Maximum percentage error (%)				1.94

The experimental results of the condensing characteristics of R22 are shown in Appendix B (Part2).

4.8 SUMMARY

In this chapter the work bench and the manufacturing process of fluted tubes were explained in detail. These, are all part of the passive technique to reduce heat exchanger size and to improve the overall heat transfer in refrigeration systems.

Furthermore, the layout of the existing test facility with its different components, measuring and acquisitioning equipment were discussed in detail. This was done to explain the working of the test facility more thoroughly.

Lastly, the chapter focused on the calculation method, used to determine the uncertainty analysis of the experimental data. This was done to determine the validity of the data that represented the condensing characteristics of R-407C. The results proved that the experimental data were acquired with a maximum uncertainty of 2.02% on the waterside and 1.49% on the refrigerant side.

The next chapter focuses on the experimental method used to gain the experimental test data from the test bench.

CHAPTER 5

EXPERIMENTAL INVESTIGATION

5.1. *INTRODUCTION*

This chapter describes the method used to gather the experimental data of the refrigerant and water from the fluted tube heat exchangers of the test facility. The test conditions were varied over a range of condensing conditions, to determine the accuracy of the simulation model in order to predict the theoretical data over a larger spectrum.

In the first section the test facility with its experimental set-up of the measuring equipment and controlled variables are discussed. Then the procedure of how the data reduction was carried out through a test matrix is explained in detail. The focus then shifts to the experimental data obtained and the factors influencing the experimental pressure drop and the heat transfer.

5.2 *TEST FACILITY*

5.2.1 *EXPERIMENTAL SET-UP*

Figure 4.7 gave the layout of the experimental test system indicating the positions of the temperature sensors, pressure sensors and mass flow meters. The eleven temperature probes (T), five pressure sensors (P) and four mass flow meters (M) are positioned on the test condenser as indicated in Figure 5.1.

The temperature and pressure of the refrigerant is measured at the inlet and outlet conditions of the pre-cooler, test cooler and sub-cooler of the test section. The refrigerant conditions are measured by the first five temperature and pressure sensors as indicated in Figure 5.1. The temperature and pressure at these points make it possible to calculate the enthalpy and quality at each point on the test condenser.

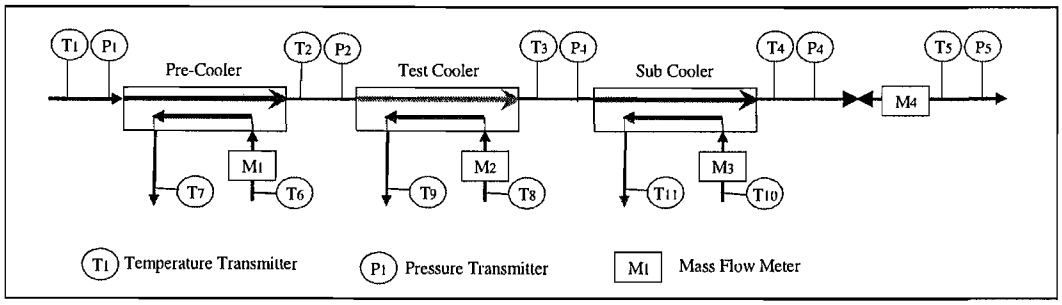


Figure 5.1: Positioning of measuring equipment on the test condenser.

It is possible to calculate the refrigerant heat transfer through each condenser and the test condenser with Equation 5.1.

$$Q_r = m_r(h_{r,out} - h_{r,in}) \tag{5.1}$$

The same method is used to calculate the water heat transfer with the aid of Equation 5.2. The water heat transfer is calculated with the aid of the temperature sensors (number six to eleven situated on the test facility at the inlet and outlet of each condenser), the mass flow meter (on each water cycle) and the atmospheric pressure.

$$Q_w = m_w(h_{w,in} - h_{w,out}) \tag{5.2}$$

The conservation of energy stipulates that the heat loss of the refrigerant must equal the heat gained by the water. So, if the heat transfer of the refrigerant (Equation 5.1) and of the water (Equation 5.2) match up to each other ($Q_r = Q_w$), it means that the heat transfer is calculated correctly from the test facility. The total refrigerant heat transfer of the three condensers is compared to the total heat transfer of the three water loops. Therefore, the heat transfer of the water can then be used to determine the outlet conditions of the refrigerant.

In the next section the controlled variables that were varied over a range of conditions are briefly discussed. The test conditions were varied to ensure the experimental data is an accurate representation of the condensation characteristics of the refrigerant used in fluted tube heat exchangers.

5.2.2 *CONTROLLED VARIABLES*

During the condensation process of R-407C the experimental data was varied over a range of different conditions. This was done to obtain an accurate representation of the heat transfer coefficient and pressure drop of the refrigerant through fluted tubes over a larger spectrum. The heat transfer coefficient and pressure drop of the refrigerant are greatly influenced by the following variables that were adjusted:

(1) The refrigerant mass flux.

(2) The refrigerant inlet temperature to the test condenser.

(3) The refrigerant heat flux.

Due to limitations on the instrumentation side and the test bench itself, it was difficult to control the quality of the flow entering and exiting the test section. The following method was followed to determine in which phase the refrigerant is flowing through the test section: The pressure and temperature at the inlet and outlet of the Test Section were measured. The values of the pressure and temperature were entered into EES to calculate the enthalpy (h). With the aid of the inlet and outlet enthalpy and pressure, the quality (x) of the refrigerant was determined through the test section as illustrated with the simulation programme in Appendix A. The quality of the refrigerant determined which phase the refrigerant is in:

(1) $x = 0$: Refrigerant in the liquid phase region

(2) $x = 1$: Refrigerant in the gas phase region

(3) $x > 0$ but $x < 1$: Refrigerant in the two-phase (mixture) region

To determine exactly where the phase change happens, each section of the Test Bench was broken up into smaller pieces theoretically in the EES simulation program. Through repetitive iterations running through the simulation program the theoretical area was determined where the condensation happens.

5.2.2.1 *THE REFRIGERANT MASS FLUX*

The hand expansion valve altered the mass flow rate of the refrigerant, until the required mass flow was achieved. But, this adjustment also changed the condensing pressure and inlet temperature of the refrigerant. An attempt was made to keep the pressure and temperature at a specific value with the aid of the automatic expansion valve. By adjusting the automatic expansion valve the mass flow rate changed again. The hand expansion valve had to be

altered again to achieve the desired mass flow rate. This procedure had to be repeated at least three times to achieve the desired test conditions.

5.2.2.2 *THE REFRIGERANT INLET CONDITIONS TO THE TEST CONDENSER*

By adjusting the automatic expansion valve the refrigerant inlet temperature and pressure were altered through the test condenser. Once again this brought a variation in the refrigerant mass flow rate. Then the hand expansion valve was altered to the desired mass flow rate, which changed the inlet temperature/pressure again and the entire procedure had to be repeated. The main focus was to keep the refrigerant inlet temperature constant, but there was a slight change in the refrigerant condensing inlet pressure. This is due to the set-up of the test facility, which made it very difficult to keep the pressure precise at a certain value. The reason is that the existing expansion valve cannot be adjusted subtly enough as required to control the test conditions, which are operating under higher pressure.

5.2.2.3 *THE REFRIGERANT HEAT FLUX*

The variation of the water inlet temperature to the test condenser and the variation of the water mass flow rate through the test condenser had an effect on the refrigerant heat flux. The water mass flow rate through the test condenser was controlled and varied with the aid of needle valves in the water loops. The water temperature was fixed at a certain value with the support of a heat pump connected to a water tank, which supplied water to the test facility. The water temperature was also regulated via three mixing valves in the water loops supplying the water to the test facility.

5.2.2.4 *DATA REDUCTION PROCEDURE*

Basically the same method as described by De Vos (2006: paragraph 4.2.3) was used to start up the test bench and to change the conditions to a required setting. The five main differences are set out below:

1. There was a waiting period of an hour after start-up before any data was gathered from the test bench. This was done to ensure that the system had stabilised and the water temperature oscillations had minimised.
2. After an expansion valve set point was altered, a ten-minute period was required for the test bench to stabilise.
3. A 15-minute period was required for the water temperatures to stabilise at a new set point via the PID control system and the mixing valves.

4. The temperature of the two water tanks was kept at the following conditions:
   - The warm water tank: 25°C
   - The cold water tank: 10°C, 15°C and 20°C.
5. Precaution should be taken to make sure the condensing temperature in the main condenser is not higher than the thermal overload of the compressor (120°C), when the system is started up or during operations. When the refrigerant temperature is too high, the compressor will trip internally in thermal overload, which reduces the life expectancy of the compressor. Increasing the water mass flow rate on the secondary side of the main condenser can prevent this. It also ensures that the refrigerant's temperature is not too high for the system to manage.

In the next section the test matrix and the data sampling from the test facility will be explained in detail.

5.2.3. *TEST MATRIX*

As indicated in Table 5.1 the refrigerant mass flow rate was controlled at 0.02kg/s, 0.03kg/s and 0.05kg/s and the water mass flow rates were controlled at 0.05kg/s, 0.07kg/s and 0.09kg/s. Then, for each refrigerant and water mass flow rate combination the water inlet temperature to the test section was varied for 10°C, 15°C and 20°C. As illustrated in Table 5.1 the water mass flow rate was kept constant as the water temperature varied from 10°C to 20°C. The restrictions of the test facility played an important role in the decision making process at which mass flow rates and temperatures the experimental tests will be carried out.

Table 5.1: Test Matrix.

Mass Flow Rates		Range of Water Inlet Temperatures
Gas	Water	
0.02 kg/s	0.05 kg/s	10°C, 15°C and 20°C
	0.07 kg/s	10°C, 15°C and 20°C
	0.09 kg/s	10°C, 15°C and 20°C
0.03 kg/s	0.05 kg/s	10°C, 15°C and 20°C
	0.07 kg/s	10°C, 15°C and 20°C
	0.09 kg/s	10°C, 15°C and 20°C
0.05 kg/s	0.05 kg/s	10°C, 15°C and 20°C
	0.07 kg/s	10°C, 15°C and 20°C
	0.09 kg/s	10°C, 15°C and 20°C

The following factors influenced the selection of the mass flow rates on the refrigerant and watersides as well as the temperature of the water:

a. If the mass flow rate of the refrigerant was below 0.02kg/s, the main evaporator had a tendency to freeze up. The reason being that the evaporation taking place was not sufficient any longer under the specific test conditions. This factor determined the lower limit of the refrigerant mass flow rate at 0.02kg/s. In the main condenser the upper limit of the water mass flow rate must not be higher than 0.09kg/s and the lower limit of the water temperature must not be lower than 10°C, otherwise the water would cool the refrigerant down below freeze point. This was only applicable when the refrigerant mass flow rate was set at 0.02kg/s.

b. If the mass flow rate of the refrigerant is too high, the compressor has the tendency to trip in thermal overload. This happens because of the following reasons: from the evaporator the refrigerant's temperature entering the compressor was too high (20°C), the water had not cooled the refrigerant down sufficiently and the compressor is operating under higher temperature (superheated region of the refrigerant) than the test facility was originally designed for. This factor also determined the upper limit of the refrigerant mass flow rate, which should not be higher than 0.05 kg/s. Therefore, the water must not reach a mass flow rate lower than 0.05 kg/s and a temperature of 20°C either, otherwise the water will not cool the refrigerant down sufficiently and the compressor will trip in thermal overload.

A total of three tests were performed at each test condition resulting in a total of twenty-seven tests performed per fluted tube as illustrated in Table 5.1. This method was carried out for all three fluted tubes, which resulted in a total of eighty one tests performed.

A drawback of the test facility, mainly due to the expansion valves, is the difficulty involved with maintaining the inlet condensation pressure within 15% for all tests performed at a given pressure condition. In contrast the temperatures and mass flow rates of the refrigerant and water were controlled within 3% for all tests performed at a given condition. With this in mind, several preliminary tests were performed from which it was noticed that the inlet pressure affected the pressure drop in the single– and two-phase regions. Also, to be illustrated in a later section, the total effect of the inlet pressure on the accuracy of the simulation model was negligible.

In the next section the method used for data sampling is explained in more detail.

5.2.4 *DATA SAMPLING*

The data logging routine of the acquisition system only recorded experimental data once the refrigerant mass flow rate, water mass flow rate and water temperature became stable. As stated earlier, after every adjustment a waiting period of 10 – 20 minutes was required for the test facility to stabilise again. The data gathered was then plotted to identify a period of stability as illustrated in Figure 5.2. The average deviation in the data selected was 0.99% and the maximum were 0.97% for the entire test performed at the test facility. The red block in Figure 5.2 illustrates the recorded data with the least deviation used to calculate the heat transfer.

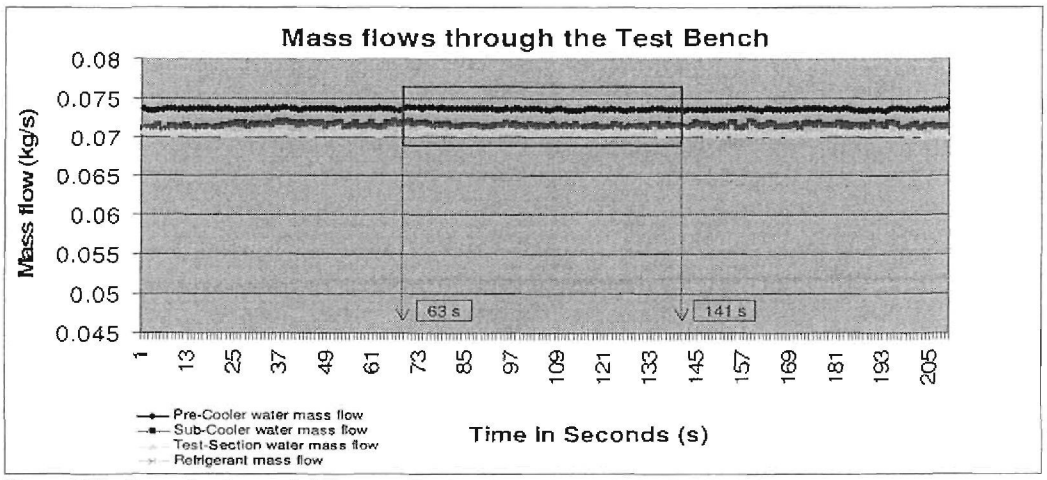


Figure 5.2: Example of recorded data set.

These values of the maximum deviation and average deviation were added together to the Uncertainty Analysis of the Test Bench mentioned in Chapter 4 in section 4.6.

5.3 *EXPERIMENTAL RESULTS*

In this section the effects that played a role on the experimental pressure drop and heat transfer of R-407C on fluted tubes are fully discussed.

The detailed results of the experimental data, including the temperature decrease of the refrigerant, temperature increase of the water, and refrigerant pressure drop and heat transfer during the condensation process are listed in Appendix B. An example of these results is given in Table 5.2. The results are for fluted tube no.1 with a fixed refrigerant mass flow rate of 0.05 kg/s.

Table 5.2: Experimental results from Fluted Tube no.1 with refrigerant mass flow = 0.05 kg/s.

Water mass flow rate (kg/s)		T1 (°C)	P1 (kPa)	T2 (°C)	P2 (kPa)	T3 (°C)	P3 (kPa)	T4 (°C)	P4 (kPa)		Water Temperature (°C)
	0.05	66.05	1827	38.24	1523	29.9	1369	15	1357	10	
		67.32	1919	40.64	1622	32.05	1446	18.73	1434	15	
		64.46	1919	40.87	1639	34.25	1437	27.09	1389	20	
	0.07	72.41	1942	40.43	1679	13.93	1645	11.83	1633	10	
		68	1900	39.57	1611	20.7	1543	16.85	1532	15	
		63.53	1807	37.61	1510	31.53	1342	21.6	1332	20	
	0.09	72.9	1801	35.08	1535	11.5	1512	10.63	1501	10	
		69.39	1801	39.76	1542	17.47	1512	16.33	1501	15	
		70.13	1996	41.85	1747	21.62	1708	20.06	1698	20	

Indication of symbols:

T1 -Temperature: Inlet at Pre-cooler (refrigerant)

T2 -Temperature: Outlet Pre-cooler / Inlet Test-cooler (refrigerant)

T3 -Temperature: Outlet Test-cooler / Inlet Sub-cooler (refrigerant)

T4 -Temperature: Outlet Sub-cooler (refrigerant)

P1 - Pressure: Inlet at Pre-cooler (refrigerant)

P2 - Pressure: Outlet Pre-cooler / Inlet Test-cooler (refrigerant)

P3 - Pressure: Outlet Test-cooler / Inlet Sub-cooler (refrigerant)

P4 - Pressure: Outlet Sub-cooler (refrigerant)

In the following section, the impact that the five main factors had on the condensation process, is discussed.

5.3.1 PRESSURE LOSS

In this section only those factors that had the most observable effect on the pressure loss are explained.

5.3.1.1 REFRIGERANT PRESSURE LOSS IN THE SINGLE-PHASE REGION

During the R-407C condensation process a trend was noticed from the results of all three fluted tubes. For higher superheated inlet condensation pressures, the pressure loss would increase in both the superheated and sub-cooled regions. The reason that the pressure loss is higher is due to the fact that the density (ρ) and the viscosity (μ) increase as the condensing pressure increases. But, the density increases more than the viscosity. When the density and viscosity increase, the Reynolds (Re) value of the refrigerant will increase as explained in Equation 5.3. With a higher Reynolds value, the friction factor (f) will also increase as explained in Equations 3.8 and 3.9. With the increase in friction factor the pressure drop will increase as explained in Equation 3.12. For this application the mass flow rate of the refrigerant was kept at certain values (0.02 kg/s, 0.03 kg/s and 0.05 kg/s) and the hydraulic diameter (D_h) was kept constant, while the inlet condensing pressure was altered.

$$\mathrm{Re} = \frac{\rho.V.D_h}{\mu} \tag{5.3}$$

5.3.1.2 *REFRIGERANT PRESSURE LOSS IN THE TWO-PHASE REGION*

Figure 5.3 illustrates the pressure loss characteristic in the two-phase region for a fixed refrigerant mass flow rate. If a comparison is made between a refrigerant entering the two-phase region at a high condensing pressure (P_1) and at a lower condensing pressure (P_2) the following effect was noticed:

When a refrigerant enters the two-phase region at a high condensing pressure (P_1), the pressure drop (ΔP_1) would be lower. The reason is that the heat transfer area according to the length of the heat exchanger (L_1) is smaller. If the length of the heat transfer area were smaller, then the pressure drop would be smaller as explained by Equation 3.12. The friction factor is higher, but the length of the heat transfer area has a bigger effect on the pressure drop as indicated through the experimental data.

The opposite also applies for this statement, that the pressure loss would be higher when the condensing pressure is low as indicated by the second line (L_2) on Figure 5.3.

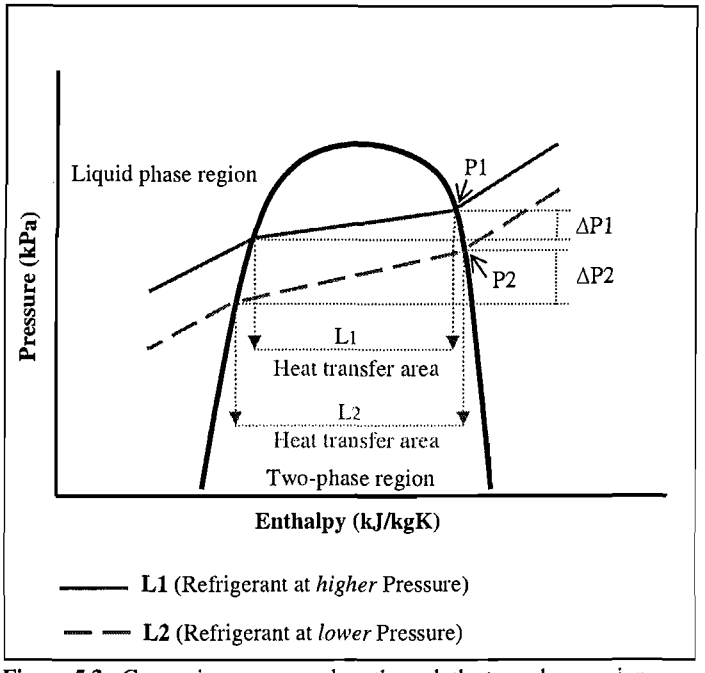


Figure 5.3: Comparison pressure drop through the two-phase region.

5.3.1.3. *EFFECT OF REFRIGERANT MASS FLOW RATE ON THE PRESSURE LOSS*

There is a clear pattern as illustrated in Table 5.3, indicating that when there is an increase in the refrigerant mass flow rate the velocity (V) will also increase. As the velocity increases the Reynolds number (Re) will increase as explained by Equation 5.3 and then the friction factor (f) will also increase. Due to the higher friction factor the pressure drop will increase.

Table 5.3: Refrigerant pressure drop on flute no.2 for different mass flow rates.

Refrigerant mass flow rate (kg/s) = **0.02** kg/s

Water mass flow (kg/s)	P_1	$P_{in,tp}$	$P_{out,tp}$	P_4	ΔP_{gas}	ΔP_{tp}	ΔP_{liq}	ΔP_{total} (kPa)	Water Temperature (°C)
0.05	2085	2080	2069	2048	5	11	21	37	10°C
	1393	1387	1349	1337	6	38	12	56	15°C
	1735	1731	1708	1685	4	23	23	50	20°C
0.07	2110	2107	2097	2077	3	10	20	33	10°C
	1488	1481	1448	1434	7	33	14	54	15°C
	1678	1672	1644	1631	6	28	13	47	20°C
0.09	2126	2124	2114	2098	2	10	16	28	10°C
	1509	1504	1476	1461	5	28	15	48	15°C
			Average ΔP =		5	23	17	**44**	(kPa)

Refrigerant mass flow rate (kg/s) = **0.03** kg/s

Water mass flow (kg/s)	P_1	$P_{in,tp}$	$P_{out,tp}$	P_4	ΔP_{gas}	ΔP_{tp}	ΔP_{liq}	ΔP_{total} (kPa)	Water Temperature (°C)
0.05	1931	1918	1883	1857	13	35	26	74	10°C
	1820	1810	1740	1734	10	70	6	86	15°C
	1661	1649	1548	1522	12	101	26	139	20°C
0.07	1903	1894	1870	1839	9	24	31	64	10°C
	1755	1741	1699	1684	14	42	15	71	15°C
	1647	1639	1539	1534	8	100	5	113	20°C
0.09	1882	1876	1854	1824	6	22	30	58	10°C
	1717	1708	1659	1648	9	49	11	69	15°C
	1656	1648	1585	1556	8	63	29	100	20°C
			Average ΔP =		10	56	20	**86**	**kPa**

Refrigerant mass flow rate (kg/s) = **0.05** kg/s

Water mass flow (kg/s)	P_1	$P_{in,tp}$	$P_{out,tp}$	P_4	ΔP_{gas}	ΔP_{tp}	ΔP_{liq}	ΔP_{total} (kPa)	Water Temperature (°C)
0.05	1962	1922	1685	1641	40	237	44	321	10°C
	1923	1883	1594	1572	40	289	22	351	15°C
	2115	2079	1814	1794	36	265	20	321	20°C
0.07	1931	1917	1702	1657	14	215	45	274	10°C
	1906	1891	1637	1609	15	254	28	297	15°C
	2046	2033	1796	1772	13	237	24	273	20°C
0.09	1909	1865	1740	1669	44	125	71	240	10°C
	1939	1929	1782	1702	10	147	80	237	15°C
	1995	1985	1785	1761	10	200	24	235	20°C
			Average ΔP =		25	219	40	**283**	kPa

Indication of symbols:

- P_1 - Pressure: Inlet at Pre-cooler
- P_4 - Pressure: Outlet at Sub-cooler
- ΔP_{gas} - Pressure Drop: Gas region
- ΔP_{tp} - Pressure Drop: Two-phase region
- ΔP_{liq} - Pressure Drop: Liquid region
- ΔP_{total} - Total Pressure Drop from P_1 to P_4

5.3.1.4 *EFFECT OF FLUTE PITCH ON THE PRESSURE DROP*

From Table 5.4 it can be seen that the pitch of the fluted tube has a major effect on the pressure drop of the refrigerant. There is an obvious indication from the results that the fluted tube with a fine pitch has the largest pressure drop due to the geometry. If the mass flow rate were the same through a fluted tube with a fine or larger pitch, the velocity of the refrigerant would be the highest through the fluted tube with a finer pitch. The fluted tube with a finer pitch has a smaller area through which the refrigerant must flow. Thus, the velocity will increase. With the increase in velocity the Reynolds number will increase and then the friction factor will also increase. As a result, the higher the friction factor the higher the pressure drop would be.

Tables 5.4: The effect of pitch on the pressure drop for a refrigerant mass flow rate = 0.02 kg/s.

Flute no.1: p = **9.5** mm

P_1 (kPa)	P_2 (kPa)	P_3 (kPa)	P_4 (kPa)	ΔP
1632	1597	1588	1579	53
1749	1723	1714	1706	43
1815	1796	1788	1779	36
1642	1612	1602	1597	45
1773	1748	1739	1730	43
1804	1789	1780	1772	32
1657	1633	1624	1615	42
1738	1716	1707	1698	40
1811	1800	1792	1783	28
		Average ΔP (kPa) =		40

Flute no.2: p = **6.8** mm

P_1 (kPa)	P_2 (kPa)	P_3 (kPa)	P_4 (kPa)	ΔP
2085	2066	2059	2048	37
1393	1341	1338	1337	56
1735	1691	1698	1684	51
2110	2095	2088	2077	33
1488	1447	1440	1434	54
1678	1644	1637	1631	47
2126	2112	2105	2098	28
1509	1475	1468	1461	48
		Average ΔP (kPa) =		44

Flute no.3: p = **11.4** mm

P_1 (kPa)	P_2 (kPa)	P_3 (kPa)	P_4 (kPa)	ΔP
1797	1774	1768	1758	39
1810	1788	1780	1771	39
2061	2038	2030	2019	42
1590	1561	1553	1543	47
1860	1844	1834	1824	36
2076	2058	2049	2039	37
1464	1441	1434	1424	40
1966	1951	1942	1937	29
1768	1749.5	1742	1735	33
		Average ΔP (kPa) =		38

5.3.2 *HEAT TRANSFER*

During the condensation process heat transfer takes place between the refrigerant and the cooling water. A few factors that have an effect on this heat transfer will be discussed in this section.

Table 5.5: Heat transfer on the three fluted tubes with a fixed refrigeration mass flow = 0.05 kg/s.

		Flute no.1 (p = 9.5)				
Water Flow Rate (kg/s)		Q (kW)	Q (kW)	Q (kW)		Water Temperature (°C)
	0.05	1.580	9.432	0.697	10	
		1.200	9.371	0.598	15	
		1.101	9.217	0.501	20	
	0.07	1.363	9.310	0.830	10	
		1.240	9.299	0.590	15	
		1.210	9.107	0.470	20	
	0.09	1.510	9.276	1.000	10	
		1.313	9.258	0.740	15	
		1.168	8.924	0.650	20	

	Flute no.2 (p = 6.8)				
Water Flow Rate (kg/s)		Q (kW)	Q (kW)	Q (kW)	Water Temperature (°C)
	0.05	1.690	9.915	0.780	10
		1.540	8.956	0.690	15
		1.340	8.662	0.580	20
	0.07	1.450	9.980	0.900	10
		1.260	8.991	0.740	15
		1.240	9.740	0.620	20
	0.09	1.890	11.450	1.300	10
		1.450	10.450	0.880	15
		1.270	10.108	0.700	20

	Flute no.3 (p = 11.4)				
Water Flow Rate (kg/s)		Q (kW)	Q (kW)	Q (kW)	Water Temperature (°C)
	0.05	1.442	6.559	0.305	10
		1.123	5.493	0.215	15
		1.015	5.355	0.207	20
	0.07	1.577	8.336	0.410	10
		1.194	7.032	0.305	15
		1.118	6.478	0.271	20
	0.09	1.498	8.400	0.510	10
		1.269	8.057	0.470	15
		1.181	7.289	0.400	20
Phases:		Liquid	Two	Gas	

5.3.2.1 *EFFECT OF REFRIGERANT MASS FLOW RATE*

As the refrigerant mass flow rate increases, for all three fluted tubes, the heat transfer also increases as illustrated in Table 5.3. The following parameters were kept constant: the condensing pressure of the refrigerant, cooling water's temperature and mass flow rate of the water. This means that the heat transfer coefficient also increases as the mass flow rate increases. The heat transfer ($Q_{refrigerant(1)}$) increases as the refrigerant mass flow rate increases, which also increase the heat transfer coefficient ($h_{heat_transfer_coefficient}$) as illustrated in Equation 5.5 and 5.6.

$$Q_{refrigerant(1)} = m_{refrigerant} . \Delta h_{refrigerant} \tag{5.5}$$

$$Q_{refrigerant(1)} = Q_{refrigerant(2)}$$

$$Q_{refrigerant(2)} = h_{heat_transfer_coefficient} . A . \Delta T_{LMTD} \tag{5.6}$$

5.3.2.2 *EFFECT OF WATER MASS FLOW RATE*

Table 5.3 shows that when the water mass flow rate increases the heat transfer also increases when the inlet water temperature and refrigerant mass flow rate is kept constant. This results in the heat transfer coefficient of the refrigerant also increasing as the water mass flow rate increases. The reason is that the water can transfer more energy to and from the refrigerant as

the water mass flow rate increases and ΔT_{water} is kept constant as illustrated in Equation 5.7. The refrigerant mass flow rate and inlet conditions are kept constant while the outlet conditions change. This will have an effect on the refrigerant heat transfer as illustrated in Equations 5.8.

$$Q_{water} = m_{water}.Cp_{water}.\Delta T_{water} \quad (5.7)$$

$$Q_{water} = Q_{refrigerant}$$

$$Q_{refrigerant} = m_{refrigerant}.\Delta h_{refrigerant} \quad (5.8)$$

5.3.2.3 EFFECT OF THE COOLING WATER INLET TEMPERATURE

The refrigerant heat transfer increased as the cooling water inlet temperature decreased and if all the other parameters are kept constant. The explanation for the heat transfer increase can be seen in Equations 5.6. A larger heat transfer will be achieved if the temperature difference between the inlet water temperature and inlet refrigerant temperature is larger, while it is attempted to keep the mass flow rates and the outlet conditions constant. A larger water temperature difference can be achieved trough colder inlet water temperature flowing to the heat exchanger as illustrated in Table 5.3.

5.3.2.4 EFFECT OF THE CONDENSING PROCESS IN THE TWO-PHASE REGION

The condensing pressure also has an effect on the heat transfer coefficient as seen in Table 5.2 and as described in Paragraph 5.3.1.2. If the pressure increases the heat transfer also increases.

5.3.2.5 EFFECT OF FLUTED PITCH

In Table 5.2 the fluted tube with the finer pitch (flute tube no.2) has the larger heat transfer compared to the other tubes. Fluted tube no.2 has in the region of 20% larger heat transfer than fluted tubes no.1 and 30% larger than fluted tube no.3. Furthermore, flute no.2 has a better contact area between the refrigerant and the tube wall due to the geometry of the tube and therefore the heat transfer and pressure drop is larger than that of the other tubes.

5.4 SUMMARY

The following conclusions can be made from the experimental pressure drop and heat transfer for the three fluted tubes:

1. The fluted tube with a finer pitch has a larger heat transfer coefficient, but also the larger pressure drop.
2. Each fluted tube has to be chosen for a specific application. In the heat pump application the fluted tube with the finer pitch will be the most suitable. This is because the fluted tubes with finer pitches will have a larger heat transfer contact area between the refrigerant and tube wall, due to the geometry of the fluted tube. Thus, the heat exchanger can be more compact, resulting in saving material, money and manufacturing cost.

In the next chapter the new enhancement factor derived from the experimental results is implemented in the correlation of Rousseau *et al.* (2003) to predict the theoretical pressure drop and heat transfer. The method used to implement the new enhancement factors is thoroughly discussed and explained. The results gained from the theoretical correlation are compared to the experimental results to determine the accuracy of the correlation of Rousseau *et al.* (2003) with the new improved enhancement factors.

CHAPTER 6

SIMULATION MODEL VERIFICATION

6.1 INTRODUCTION

In the previous chapter the factors that had an effect on the pressure drop and heat transfer coefficients were fully discussed. The main focus of this chapter is to improve the accuracy of the correlation of Rousseau *et al.* (2003). This is done by comparing the simulation results against the experimental data. Based on this, new enhancement factors are derived for the pressure drop (e_f) and heat transfer coefficient (e_h). The aim is to use these new derived enhancement factors in the simulation model to predict the total pressure drop and total heat transfer of R-407C during a condensation process with a higher degree of accuracy.

6.2 MODEL ACCURACY

6.2.1 ACCURACY OF EXISTING CORRELATION

When the original enhancement factors are used in the correlation of Rousseau *et al.* (2003), the model accuracy can be determined by comparing the theoretical data to the experimental data. The original pressure drop enhancement factor is $e_f = 4.409$ and for the heat transfer coefficient it is $e_h = 0.867$. These enhancement factors were used in the model to simulate the pressure drop and heat transfer for Fluted Tube no.1. as illustrated in Table 6.1. The following conditions were kept constant: the refrigerant mass flow rate at $m_r = 0.02$kg/s, the water mass flow rate at $m_w = 0.09$kg/s and the cooling water temperature at T = 20°C.

These enhancement factors indicate that the correlation under predicts the pressure drop and requires to be increased with a factor of 4.409 and the correlation over predicts the heat transfer and requires to be decreased by a factor of 0.867.

The accuracy of the model (using the existing enhancement factors obtain from the correlation of Rousseau *et al.* (2003)) to predict the refrigerant's theoretical pressure drop, enthalpy decrease, heat transfer and the Log Mean Temperature Difference (LMTD) over the heat exchanger are listed in Table 6.1. The LMTD (ΔT_{lm}) for a counterflow heat exchanger is calculated as shown in Equation 6.1.

$$\Delta T_{lm} = \frac{\Delta T_1 - \Delta T_2}{\ln(\Delta T_1 / \Delta T_2)} \qquad 6.1$$

where $\Delta T_1 = T_{h,i} - T_{c,o}$

$\Delta T_2 = T_{h,o} - T_{c,i}$

$T_{h,i}$ = refrigerant entering the heat exchanger

$T_{h,o}$ = refrigerant exiting the heat exchanger

$T_{c,i}$ = water entering the heat exchanger

$T_{c,o}$ = water exiting the heat exchanger

Table 6.1: Accuracy of existing enhancement factors.

Experimental data		**Theoretical data**	
Pressure (kPa)			
$P_{1(exp)}$	1811	$P_{1(theo)}$	1811
$P_{4(exp)}$	1792	$P_{4(theo)}$	1782
$\Delta P_{Total\ (exp)}$	19	$\Delta P_{Total\ (theo)}$	29
Percentage Error		52 %	
Enthalpy (kJ/kg.K)			
$H_{1(exp)}$	315.1	$H_{1(theo)}$	315.1
$H_{4(exp)}$	87.15	$H_{4(theo)}$	98.63
$\Delta H_{Total\ (exp)}$	227.95	$\Delta H_{Total\ (theo)}$	216.47
Percentage Error		5.04 %	
LMTD (°C)			
$LMTD_{(exp)}$	10.72	$LMTD_{(theo)}$	19.28
Percentage Error		44.39 %	
Heat Transfer (kW)			
$Q_{Total\ (exp)}$	4.559	$Q_{Total\ (theo)}$	4.3294
Percentage Error		5.04 %	

From the table it is evident that the accuracy of the existing enhancement factors is such that it cannot be used effectively to predict the pressure drop and temperature decrease of R-407C during the condensation process inside fluted tube annuli. The maximum pressure drop error is 52%, with an average error of 44.42%. The highest accuracy is for the calculation of the

heat transfer where the maximum error is 8.82% with an average error of 3.75%. Therefore, new enhancement factors needs to be generated, to create a more accurate simulation model.

6.2.2 *DERIVED NEW ENHANCEMENT FACTORS*

In this section the method used to derive the newly obtained enhancement factors will be thoroughly explained.

From the three fluted tubes used in the test facility a total of 81 experimental data sets were gathered. The same methodology was followed for a *specific* fluted tube (e.g. fluted tube no.1) where a total of 27 experimental data sets were obtained over all the test conditions. But, for one specific fluted tube with a fixed refrigerant mass flow rate, while the other conditions were altered as explained in Chapter 3, a total of 9 experimental data sets were gathered as illustrated in Table 6.2. The experimental data listed in Appendix B were used as input data for the correlation of Rousseau *et al.* (2003). From the experimental data new pressure drop (e_f) enhancement factors were generated with Equations 3.13 and 3.20 and new heat transfer coefficient (e_h) enhancement factors from Equations 3.19 and 3.22. For each of the 81 data sets, enhancement factors were derived, which are illustrated in Appendix C. From this average, enhancement factors were derived for each fluted tube to determine the accuracy thereof. The accuracy is determined by comparing the theoretical results with the experimental data.

Table 6.2: Enhancement factors and heat transfer on the three fluted tubes with a fixed refrigeration mass flow of 0.05 kg/s.

Water Flow Rate (kg/s)		Flute no. 1 (p = 9.5)														Water Temperature (°C)
		P_{exp_out} (kPa)	ef	eh	Q (kW)	P_{theo_out} (kPa)	ef	eh	Q (kW)	P_{theo_in} (kPa)	ef	eh	Q (kW)	P_{exp_in} (kPa)		
	0.05	**1357**	5.053	1.146	1.580	**1381**	9.600	2.180	9.432	**1792**	5.053	3.210	0.697	**1827**	**10**	
		1434	4.981	0.990	1.200	**1453**	9.500	2.650	9.371	**1884**	4.981	3.920	0.598	**1919**	**15**	
		1389	4.781	0.91	1.101	**1409**	9.435	2.73	9.217	**1880**	4.729	3.830	0.501	**1919**	**20**	
	0.07	**1633**	4.784	1.684	1.363	**1658**	7.083	2.420	9.310	**1917**	4.784	3.290	0.830	**1942**	**10**	
		1532	4.431	1.210	1.240	**1552**	7.200	3.050	9.299	**1877**	4.431	3.160	0.590	**1900**	**15**	
		1332	4.372	1.065	1.210	**1346**	9.100	3.910	9.107	**1787**	4.372	2.780	0.470	**1807**	**20**	
	0.09	**1501**	4.463	1.744	1.510	**1522**	7.300	3.120	9.276	**1781**	4.463	4.350	1.000	**1801**	**10**	
		1501	4.482	1.267	1.313	**1530**	7.860	3.420	9.258	**1779**	4.482	4.090	0.740	**1801**	**15**	
		1698	4.160	1.032	1.168	**1716**	7.590	4.180	8.924	**1980**	4.160	4.360	0.650	**1996**	**20**	
		Liquid-Phase					**Liquid-Phase**				**Gas-Phase**					

Water Flow Rate (kg/s)	Flute no. 2 (p = 6.8)														Water Temperature (°C)
	P_{exp} (kPa)	ef	eh	Q (kW)	P_{theo} (kPa)	ef	eh	Q (kW)	P_{theo} (kPa)	ef	eh	Q (kW)	P_{exp} (kPa)		
0.05	1641	6.038	1.702	1.690	1685	13.15	4.870	9.915	1922	6.038	5.840	0.780	1962	10	
	1572	6.376	1.663	1.540	1594	13.50	4.190	8.956	1883	6.376	5.800	0.690	1923	15	
	1794	6.073	1.253	1.340	1814	11.80	4.050	8.662	2079	6.073	4.620	0.580	2115	20	
0.07	1656	6.029	1.996	1.450	1702	13.00	5.490	9.980	1917	6.029	6.960	0.900	1931	10	
	1609	6.708	1.783	1.260	1637	13.22	5.390	8.991	1891	6.708	6.020	0.740	1906	15	
	1773	6.027	1.457	1.240	1796	12.62	5.220	9.740	2033	6.027	5.110	0.620	2046	20	
0.09	1669	6.307	2.174	1.890	1740	12.80	6.120	11.450	1865	6.307	6.520	1.300	1909	10	
	1702	6.088	1.936	1.450	1728	13.01	6.020	10.450	1929	6.088	6.390	0.880	1939	15	
	1761	6.614	1.749	1.270	1785	12.70	5.320	10.108	1985	6.614	5.740	0.700	1995	20	
	Liquid-Phase					Two-Phase				Gas-Phase					

Water Flow Rate (kg/s)	Flute no. 3 (p = 11.4)														Water Temperature (°C)
	P_{exp} (kPa)	ef	eh	Q (kW)	P_{theo} (kPa)	ef	eh	Q (kW)	P_{theo} (kPa)	ef	eh	Q (kW)	P_{exp} (kPa)		
0.05	1715	2.246	0.761	1.442	1812	3.547	1.793	6.559	1877	2.246	1.890	0.305	2013	10	
	1438	2.229	0.638	1.123	1633	4.300	1.532	5.493	1704	2.229	1.880	0.215	1844	15	
	1524	2.390	0.584	1.015	1615	4.890	1.481	5.355	1806	2.390	1.690	0.207	1939	20	
0.07	1691	2.299	1.031	1.577	1764	4.440	2.700	8.336	1842	2.299	2.160	0.410	1929	10	
	1414	2.258	0.884	1.194	1505	4.430	2.160	7.032	1665	2.258	2.129	0.305	1765	15	
	1511	2.219	0.813	1.118	1564	4.230	2.130	6.478	1777	2.219	2.030	0.271	1873	20	
0.09	1288	2.248	1.248	1.498	1354	4.460	3.801	8.400	1505	2.248	2.562	0.510	1593	10	
	1418	2.290	1.048	1.269	1486	4.190	3.273	8.057	1646	2.290	2.450	0.470	1726	15	
	1506	2.260	0.909	1.181	1568	4.069	3.669	7.289	1748	2.260	2.440	0.400	1825	20	
	Liquid-Phase					Two-Phase				Gas-Phase					

From Table 6.2 the following trends were noticed when the correlation of Rousseau *et al.* (2003) is used to describe the characteristics of R-407C during the condensation process:

Pressure drop enhancement factors (e_f) of the refrigerant:

- The e_f increases with an increase in pressure. This means that the correlation of Rousseau *et al.* (2003) becomes less accurate at higher condensing pressures and under predicts the pressure drop as illustrated in Table 6.2.
- As the refrigerant mass flow increases the e_f also increase by 3.5% from 0.02kg/s to 0.05kg/s. This means that the correlation becomes less accurate for higher refrigerant mass flow rates.
- Furthermore, as the pitch becomes finer the correlation becomes less accurate, resulting in an increase in the e_f to correct the accuracy. This means as the pressure drop increases the e_f increases. The refrigerant pressure drop for fluted tube no.2 (pitch = 6.8mm) is 26% higher than for fluted tube no.1 (pitch = 9.5mm) and 64% higher for fluted tube no.3 (pitch = 11.4mm).

Heat transfer coefficient enhancement factors (e_h) of the refrigerant.

- The e_h increases as the refrigerant mass flow rate increases. This means that the correlation of Rousseau *et al.* (2003) under predicts the heat transfer coefficient and is less accurate as the refrigerant mass flow rate increases from 0.02kg/s to 0.05kg/s. Therefore, the enhancement factors needs to be increased on average with 0.47%.
- The e_h of the refrigerant also increases as the water mass flow rate increases. Furthermore, the correlation also under predicts the heat transfer and is less accurate with an average of 0.1%.
- As the inlet water temperature decrease, the e_h also increases. This indicates that the correlation is less accurate with an average of 0.86% as the water temperature decreases.
- The correlation of Rousseau *et al.* (2003) under predicts the heat transfer in the two-phase region with an average of 3.38%, for the liquid phase region with 1.25% and for the gas phase region with 3.803%.
- The e_h also increase as the fluted tube pitch decreases. For a fluted tube with a fine pitch the correlation of Rousseau *et al.* (2003) under predicts the heat transfer and is less accurate with an average of 4.5% compared to that of a flute tube with a larger pitch.

6.2.2 *DERIVING AVERAGE ENHANCEMENT FACTORS*

A set of enhancement factors were needed in the correlation of Rousseau *et al.* (2003), to predict the theoretical pressure drop and heat transfer coefficient under different test conditions. This set of enhancement factors for a *specific* fluted tube was generated from the 27 test results, by obtaining the average value from each enhancement factor's value as illustrated in Table 6.3. In Table 6.3 this "set", which is known as the "First Set" of enhancement factors are that of fluted tube no.1. All the simulated results of the enhancement factors generated through the correlation of Rousseau *et al.* (2003) are in Appendix C.

The "First Set" of enhancement factors for fluted tube no.1 is listed in Table 6.3 and the same methodology was followed to generate the enhancement factors for the other fluted tubes.

Table 6.3: Generating "First Set" of enhancement factors.

Fluted tube no1: Refrigerant mass flow rate = 0.02 kg/s									
Water mass flow rate	(kg/s)	$e_{f(Liq)}$	$e_{h(Liq)}$	$e_{f(2)}$	$e_{h(2)}$	$e_{f(Gas)}$	$e_{h(Gas)}$	°C	Water inlet Temperature
	0.05	3.90	0.88	6.68	1.77	3.90	2.18	10	
		4.10	0.87	4.91	1.45	4.10	2.13	15	
		4.11	0.54	3.39	2.58	4.11	2.06	20	
	0.07	4.26	1.17	6.02	1.92	4.26	2.40	10	
		4.16	0.94	5.48	1.74	4.16	2.28	15	
		4.14	0.62	3.57	1.83	4.14	2.24	20	
	0.09	4.11	1.31	5.76	1.25	4.11	2.89	10	
		4.15	0.94	5.38	1.28	4.15	2.77	15	
		4.14	0.76	2.50	1.59	4.14	2.69	20	
	Average	**4.12**	**0.89**	**4.85**	**1.71**	**4.12**	**2.40**		

Fluted tube no1: Refrigerant mass flow rate = 0.03 kg/s									
Water mass flow rate	(kg/s)	$e_{f(Liq)}$	$e_{h(Liq)}$	$e_{f(2)}$	$e_{h(2)}$	$e_{f(Gas)}$	$e_{h(Gas)}$	°C	Water inlet Temperature
	0.05	4.02	0.94	7.51	1.87	4.02	2.26	10	
		4.11	0.92	4.90	2.15	4.11	2.24	15	
		4.26	0.84	4.08	2.29	4.26	2.21	20	
	0.07	4.14	1.31	7.10	1.84	4.14	2.42	10	
		4.15	1.13	4.70	3.03	4.15	2.38	15	
		4.46	0.79	3.08	3.48	4.46	2.34	20	
	0.09	4.16	1.42	4.84	1.19	4.16	2.98	10	
		4.17	1.16	4.11	3.19	4.17	2.81	15	
		4.16	0.90	3.80	3.86	4.16	2.75	20	
	Average	**4.18**	**1.05**	**4.90**	**2.55**	**4.18**	**2.49**		

Fluted tube no1: Refrigerant mass flow rate = 0.05 kg/s									
Water mass flow rate	(kg/s)	$e_{f(Liq)}$	$e_{h(Liq)}$	$e_{f(2)}$	$e_{h(2)}$	$e_{f(Gas)}$	$e_{h(Gas)}$	°C	Water inlet Temperature
	0.05	5.05	1.15	9.60	2.18	5.05	3.21	10	
		4.98	0.99	9.50	2.65	4.98	3.92	15	
		/	/	/	/	/	/	20	
	0.07	4.78	1.68	7.08	2.42	4.78	3.29	10	
		4.43	1.21	7.20	3.05	4.43	3.16	15	
		4.37	1.07	9.10	3.91	4.37	2.78	20	
	0.09	4.46	1.74	7.30	3.12	4.46	4.35	10	
		4.48	1.27	7.86	3.42	4.48	4.09	15	
		4.16	1.03	7.59	4.18	4.16	4.36	20	
	Average	**4.59**	**1.27**	**8.15**	**3.12**	**4.59**	**3.65**		

Fluted no.1: "First Set" of enhancement factors							
Average	$e_{f(Liq)}$	$e_{h(Liq)}$	$e_{f(2)}$	$e_{h(2)}$	$e_{f(Gas)}$	$e_{h(Gas)}$	
	4.30	**1.07**	**5.97**	**2.46**	**4.30**	**2.85**	

The "Second Set" of enhancement factors were generated from the "First Set" as illustrated in Table 6.4. The same methodology, as described above, were followed to obtain the "Second Set" of enhancement factors by obtaining the average of each fluted tube's "First Set" of enhancement factors. The "Second Set" was applied in the correlation of Rousseau *et al.*

(2003) to predict the theoretical pressure drop and heat transfer coefficient. But, the "Second Set" of enhancement factors was applied on all three fluted tubes and not to a specific fluted tube as with the "First Set" of enhancement factors.

The "Third Set" of enhancement factors was obtained through the three phases (gas-, two- and liquid phase) of the "Second Set" of enhancement factors. Obtaining the arithmetic average of the three phases resulted in this. The enhancement factors for the pressure drop and heat transfer coefficient is the same value for all three phases as illustrated in Table 6.4 for the "Third Set" of enhancement factors. The logic about the "Third Set" of enhancement factors is to obtain a quick value, within a certain amount of error, for the pressure drop and heat transfer in the practical field, if you do not have Table 6.4 to obtain the precise value of the different enhancement factors in each section.

Table 6.4: The three sets of enhancement factors.

	Liquid-phase		Two-phase		Gas-phase	
First set	ef	eh	ef	eh	ef	eh
Fluted tube no.1	4.30	1.07	5.97	2.46	4.30	2.85
Fluted tube no.2	4.04	1.04	6.26	2.62	4.04	2.93
Fluted tube no.3	4.78	2.19	3.84	1.95	4.78	2.19

	Liquid-phase		Two-phase		Gas-phase	
Second set	ef	eh	ef	eh	ef	eh
All fluted Tubes	4.37	1.43	5.36	2.34	4.37	2.66

	All three phases	
Third set	ef	eh
All fluted Tubes	4.70	2.14

In the next section the simulation results will be discussed for each fluted tube, when the different enhancement factors are used in the correlation of Rousseau *et al.* (2003).

6.3. *ACCURACY OF CORRELATION WITH NEW ENHANCEMENT FACTORS*

6.3.1 *RESULTS FOR FLUTED TUBE NO.1*

In this section the new improved enhancement factors, which are obtained from Table 6.4, are used in the correlation of Rousseau *et al.* (2003) to predict the refrigerant's theoretical pressure drop, heat transfer and enthalpy drop during the condensation process over the heat exchanger. The log mean temperature difference (LMTD) of the heat exchanger is also calculated during the condensation process of the refrigerant. These theoretical results are then compared to the experimental data to determine the accuracy of the correlation with the

new improved enhancement factors. All the data gained from the experimental results are in Appendix B and the data of the theoretical results are in Appendix D.

By comparing the theoretical results with the experimental data, as illustrated in the graphs to follow and those in Appendix E, the accuracy of the correlation with the new improved enhancement factors is evaluated. As illustrated on the graphs the Red dots (•) indicate the theoretical results of the simulation when the "First Set" of enhancement factors is used in the correlation. The result of the "Second Set" is indicated with blue stripes (—) and the results of the "Third Set" with green stars (+).

6.3.1.1 FLUTED TUBE NO.1: PRESSURE DROP RESULTS

In Figure 6.1 the "First Set" of enhancement factors is used in the correlation to predict the pressure drop and the average percentage error difference between the experimental values and the theoretical values is 7.18% and the maximum difference is 31.58%. In general, it can be seen that 88% of the results with the "First Set" of enhancement factors are all within a 10% error from the experimental values. With the "Second Set" of enhancement factors the average percentage error is 9.48%, the maximum percentage error is 36.84% and 78% of the theoretical data points are inside the 10% error deviation lines. Then, with the "Third Set" of enhancement factors the average percentage error is 9.97%, the maximum percentage error is 25% and 78% of the data points are in the 10% error deviation lines.

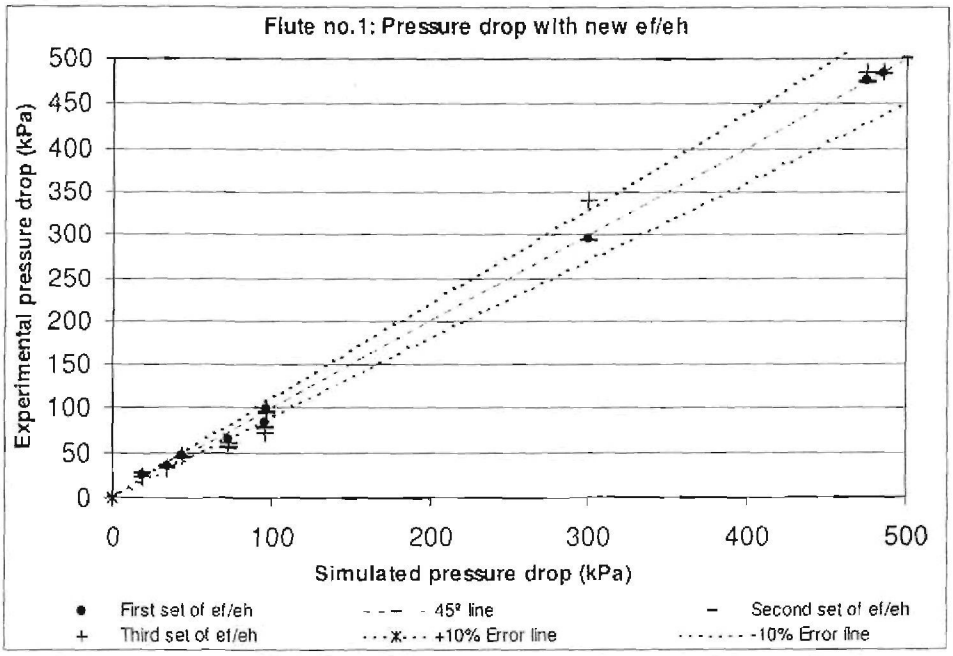


Figure 6.1: Simulation of the pressure drop by using the new enhancement factors on fluted tube no.1.

6.3.1.2 *FLUTED TUBE NO.1: ENTHALPY DROP RESULTS*

With the "First Set" of enhancement factors used in the correlation to predict the enthalpy drop, the average percentage error difference between the experimental values and the theoretical values is 0.22% and the maximum difference is 0.64% as illustrated in Figure 6.2. The "Second Set" of enhancement factors had an average percentage error of 0.34%, and maximum percentage error of 0.80%. Then, with the "Third Set" of enhancement factors the average percentage error is 0.78% and the maximum percentage error is 1.31%. In general, it can be seen that 100% of the enhancement factors used to calculate the theoretical pressures are all within a 2% error deviation from the experimental values.

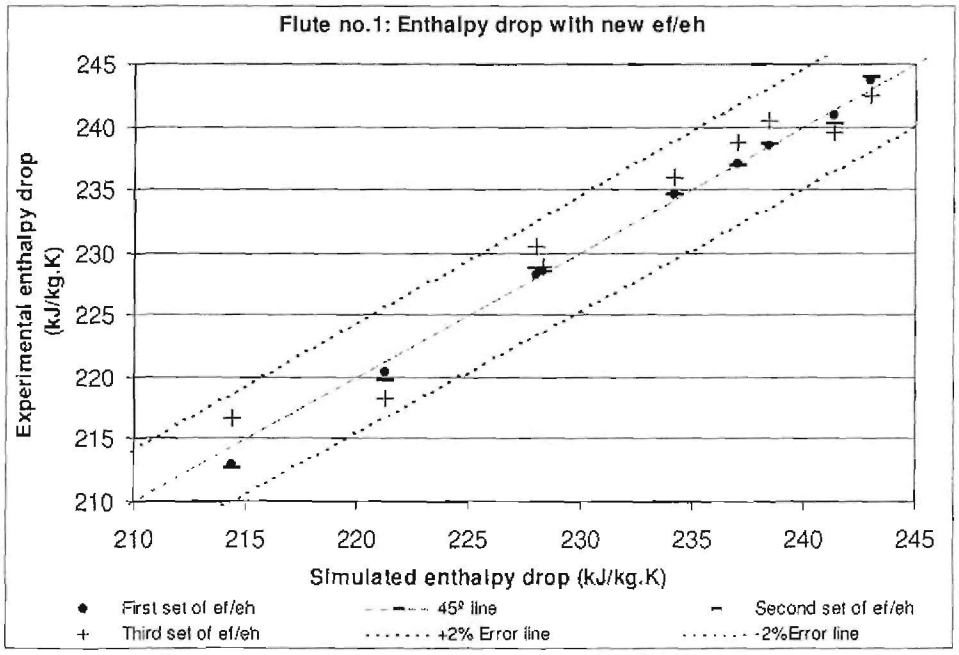


Figure 6.2: Simulation of the enthalpy drop by using the new enhancement factors on fluted tube no.1.

6.3.1.3 *FLUTED TUBE NO.1: HEAT TRANSFER RESULTS*

With the "First Set" of enhancement factors used in the correlation to predict the heat transfer the average percentage error difference between the experimental values and the theoretical values is 0.22% and the maximum difference is 0.63%. The "Second Set" of enhancement factors had an average percentage error of 0.34%, and the maximum percentage error of 0.79%. Then, with the "Third Set" of enhancement factors the average percentage error is 0.77% and the maximum percentage error is 1.30%. In general, it can be seen in Figure 6.3 that 100% of the enhancement factors used to calculate the theoretical pressures are all within a 5% error deviation from the experimental values.

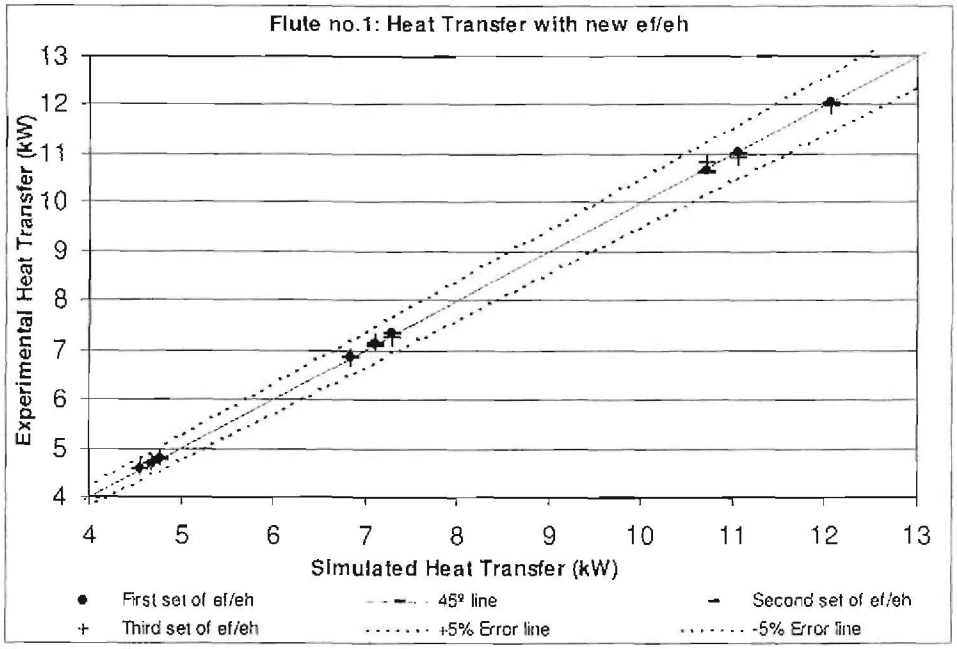


Figure 6.3: Simulation of the heat transfer by using the new enhancement factors on fluted tube no.1.

6.3.1.4 FLUTED TUBE NO.1: LMTD RESULTS

In Figure 6.4 the "First Set" of enhancement factors used in the correlation to predict the LMTD the average percentage error difference between the experimental values and the theoretical values is 2.25% and the maximum difference is 7.04%. In general, it can be seen that 100% of the results with the "First Set" of enhancement factors are all within a 5% error deviation from the experimental values. The "Second Set" of enhancement factors had an average percentage error of 2.50%, a maximum percentage error of 37.91% and 100% of the theoretical data points are inside the 5% error deviation lines. Then, with the "Third Set" of enhancement factors the average percentage error is 4.80%, the maximum percentage error is 10.56% and 77% of the data points are in the 5% error deviation lines.

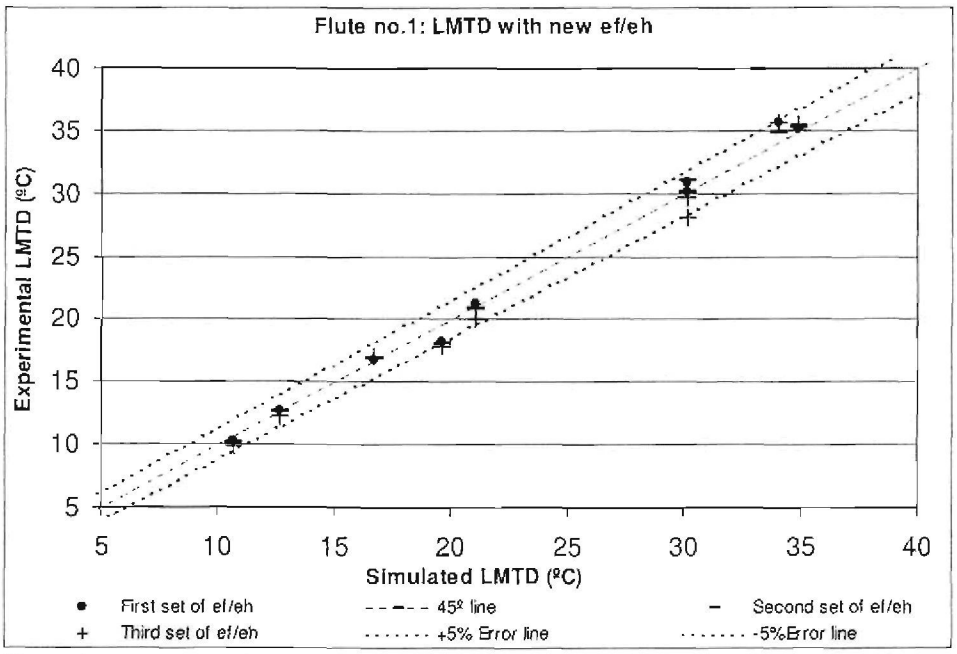


Figure 6.4: Simulation of the LMTD by using the new enhancement factors on fluted tube no.1.

Table 6.5 is a summary of all the data gathered from the figures by comparing the theoretical and experimental data. In the next section the results of Fluted Tube no.2 are discussed in table format and not as a figure, in order to compare the theoretical and experimental results in this section.

In Table 6.5, 6.6 and 6.7 the following information are listed:

- Average error: The average percentage error difference between the experimental data and the simulated values.
- Maximum error: The maximum percentage error difference between the experimental data and the simulated values.
- Regression line: The regression line through the deviation of the theoretical data points resulted in a coefficient of determination.
- First Set: The "First Set" of enhancement factors is used from Table 6.4 in the correlation.
- Second Set: The "Second Set" of enhancement factors is used from Table 6.4 in the correlation.
- Third Set: The "Third Set" of enhancement factors is used from Table 6.4 in the correlation.

Table 6.5: The theoretical results compared to the experimental results for Fluted tube no.1.

Set of enhancement factors used		First Set	Second Set	Third Set
ΔP (kPa)	Average Error =	7.18%	9.48%	9.97%
	Maximum Error =	31.58%	36.84%	25.10%
	Regression line =		0.9928	
ΔH (kJ/kg.K)	Average Error =	0.22%	0.34%	0.78%
	Maximum Error =	0.64%	0.80%	1.31%
	Regression line =		0.9836	
Q (kW)	Average Error =	0.22%	0.34%	0.77%
	Maximum Error =	0.63%	0.79%	1.30%
	Regression line =		0.9994	
LMTD (°C)	Average Error =	2.25%	2.50%	4.80%
	Maximum Error =	7.04%	7.91%	10.56%
	Regression line =		0.9912	

6.3.2 *Results for Fluted Tube no.2*

6.3.2.1 *Fluted Tube no.2: Pressure drop results*

In Figure 6.5 the "First Set" of enhancement factors is used in the correlation to predict the pressure drop and the average percentage error difference between the experimental values and the theoretical values is 9.47% and the maximum difference is 22.46%. In general, it can be seen that 77% of the results with the "First Set" of enhancement factors are all within a 10% error from the experimental values. With the "Second Set" of enhancement factors the average percentage error is 9.93%, the maximum percentage error is 23.53% and 77% of the theoretical data points are inside the 10% error deviation lines. Then, with the "Third Set" of enhancement factors the average percentage error is 13.23%, the maximum percentage error is 27.81% and 56% of the data points are in the 10% error deviation lines.

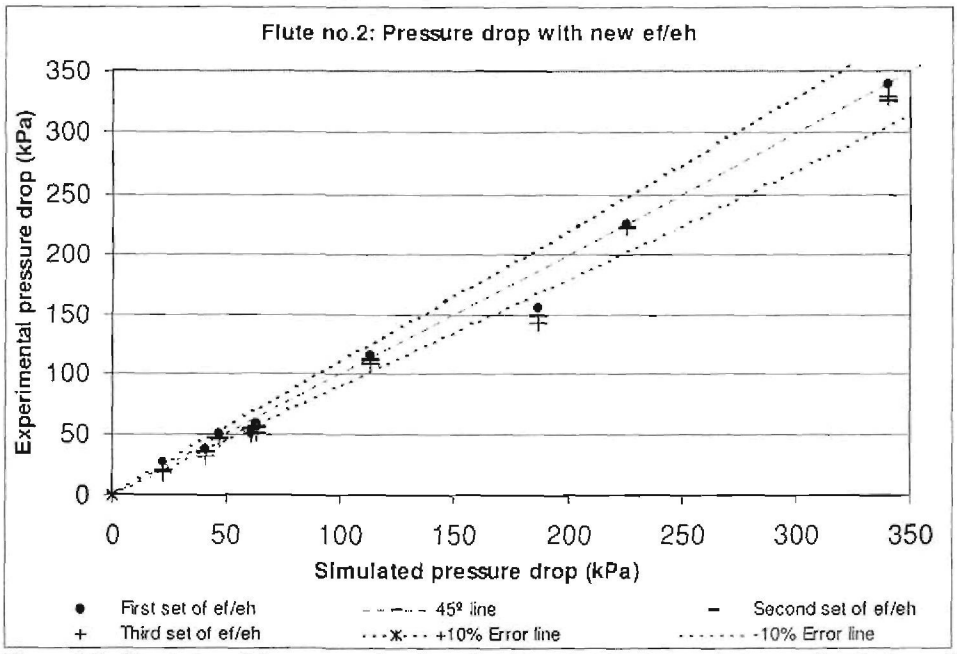


Figure 6.5: Simulation of the pressure drop by using the new enhancement factors on fluted tube no.2.

6.3.2.2 *FLUTED TUBE NO.2: ENTHALPY DROP RESULTS*

With the "First Set" of enhancement factors used in the correlation to predict the enthalpy drop the average percentage error difference between the experimental values and the theoretical values is 0.26% and the maximum difference is 0.56% as illustrated in Figure 6.6. The "Second Set" of enhancement factors had an average percentage error of 0.70%, and maximum percentage error of 1.12%. Then, with the "Third Set" of enhancement factors the average percentage error is 1.21% and the maximum percentage error is 1.89%. In general, it can be seen that 100% of the enhancement factors used to calculate the theoretical pressures are all within a 2% error deviation from the experimental values.

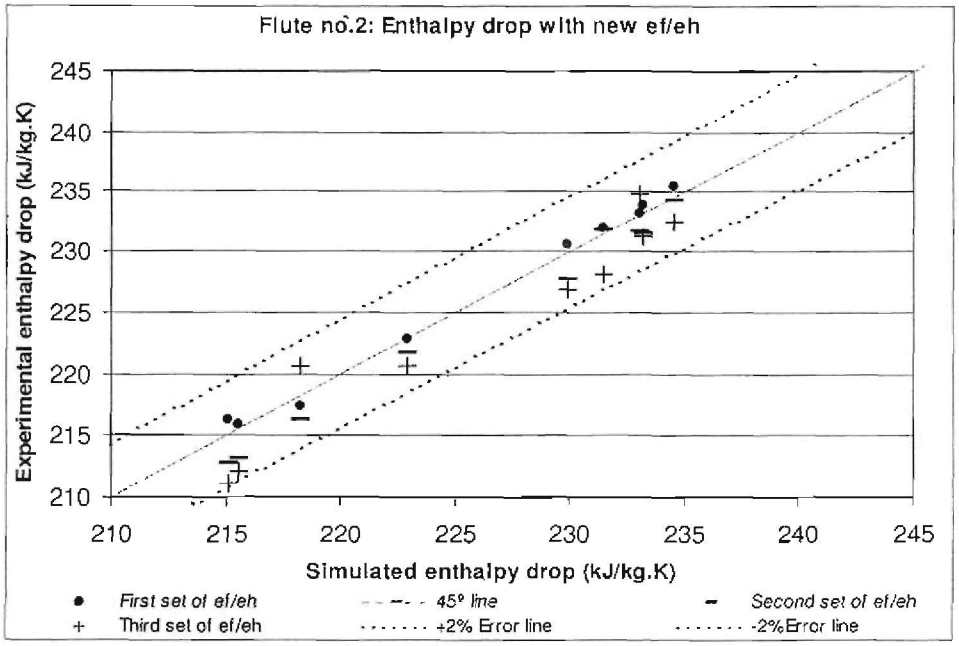


Figure 6.6: Simulation of the enthalpy drop by using the new enhancement factors on fluted tube no.2.

6.3.2.3 FLUTED TUBE NO.2: HEAT TRANSFER RESULTS

With the "First Set" of enhancement factors used in the correlation to predict the heat transfer the average percentage error difference between the experimental values and the theoretical values is 0.25% and the maximum difference is 0.55%. The "Second Set" of enhancement factors had an average percentage error of 0.69%, and the maximum percentage error of 1.12%. Then, with the "Third Set" of enhancement factors the average percentage error is 1.20% and the maximum percentage error is 1.89%. In general, it can be seen in Figure 6.7 that 100% of the enhancement factors used to calculate the theoretical pressures are all within a 5% error deviation from the experimental values.

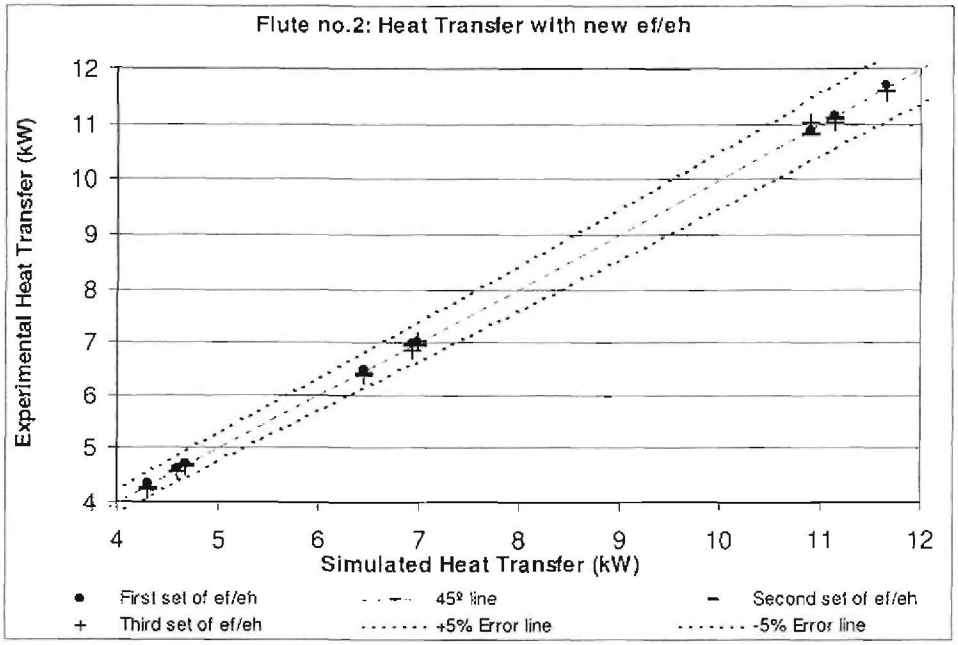


Figure 6.7: Simulation of the heat transfer by using the new enhancement factors on fluted tube no.2.

6.3.2.4 FLUTED TUBE NO.2: LMTD RESULTS

In Figure 6.8 the "First Set" of enhancement factors used in the correlation to predict the LMTD the average percentage error difference between the experimental values and the theoretical values is 1.47% and the maximum difference is 4.77%. It can largely be seen that 100% of the results with the "First Set" of enhancement factors used are all within a 5% error deviation from the experimental values. The "Second Set" of enhancement factors had an average percentage error of 5.46%, the maximum percentage error of 11.45% and 100% of the theoretical data points are inside the 5% error deviation lines. Then, with the "Third Set" of enhancement factors the average percentage error is 7.21%, the maximum percentage error is 13.46% and 77% of the data points are all within a 5% error deviation.

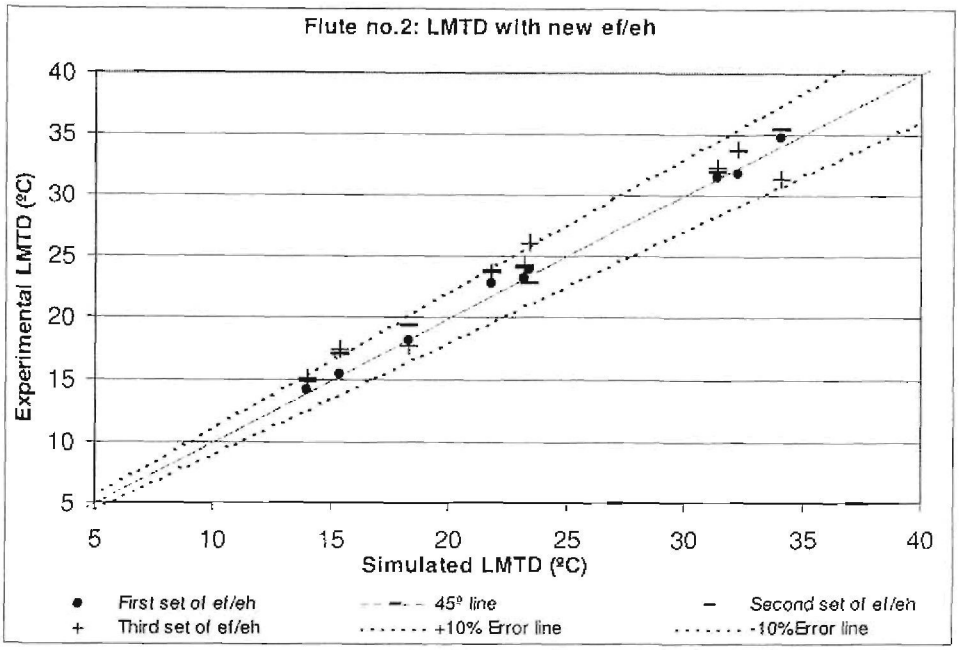


Figure 6.8: Simulation of the LMTD by using the new enhancement factors on fluted tube no.2.

Table 6.6 is a summary of all the data gathered from the figures by comparing the theoretical and experimental data. In the next section the results of Fluted Tube no.3 are discussed in table format and not as a figure in order to compare the theoretical and experimental results in this section.

Table 6.6: The theoretical results compared to the experimental results for Fluted tube no.2.

Set of enhancement factors used		First Set	Second Set	Third Set
ΔP (kPa)	Average Error =	9.47%	9.93%	13.23%
	Maximum Error =	22.46%	23.53%	27.81%
	Regression line =	0.9808		
ΔH (kJ/kg.K)	Average Error =	0.26%	0.70%	1.21%
	Maximum Error =	0.56%	1.12 %	1.89%
	Regression line =	0.9725		
Q (kW)	Average Error =	0.25%	0.69%	1.20%
	Maximum Error =	0.55%	1.12%	1.89%
	Regression line =	0.9997		
LMTD (°C)	Average Error =	1.47%	5.46%	7.21%
	Maximum Error =	4.77%	11.45%	13.46%
	Regression line =	0.9797		

6.3.3 *RESULTS FOR FLUTED TUBE NO.3*

6.3.2.1 *FLUTED TUBE NO.3: PRESSURE DROP RESULTS*

In Figure 6.9 the "First Set" of enhancement factors is used in the correlation to predict the pressure drop and the average percentage error difference between the experimental values and the theoretical values is 5.59% and the maximum difference is 14.82%. Overall, it can be seen that 88% of the results with the "First Set" of enhancement factors all within a 10% error from the experimental values. With the "Second Set" of enhancement factors the average percentage error is 9.98%, the maximum percentage error is 26.67% and 88% of the theoretical data points are inside the 10% error deviation lines. Subsequently, with the "Third Set" of enhancement factors the average percentage error is 10.86%, the maximum percentage error is 26.67% and 77% of the data points are within a 10% error deviation.

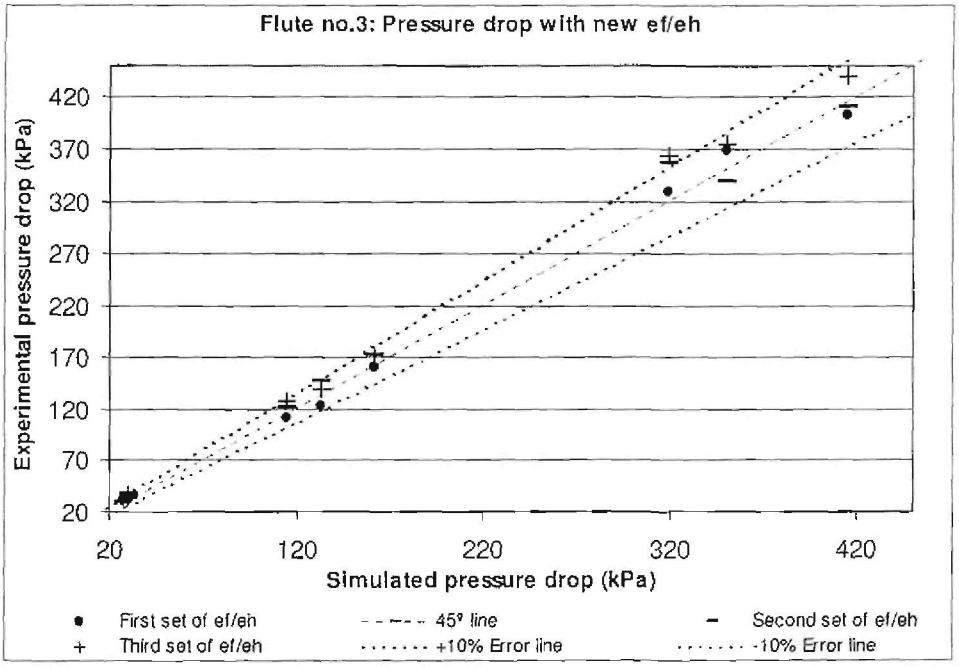


Figure 6.9: Simulation of the pressure drop by using the new enhancement factors on fluted tube no.3.

6.3.2.2 *FLUTED TUBE NO.3: ENTHALPY DROP RESULTS*

With the "First Set" of enhancement factors used in the correlation to predict the enthalpy drop the average percentage error difference between the experimental values and the theoretical values is 0.22% and the maximum difference is 0.66% as illustrated in Figure 6.10. The "Second Set" of enhancement factors had an average percentage error of 0.36%, and a

maximum percentage error of 0.96%. Then, with the "Third Set" of enhancement factors the average percentage error is 0.54% and the maximum percentage error is 1.10%. In general, it can be seen that 100% of the enhancement factors used to calculate the theoretical pressures are all within a 2% error deviation from the experimental values.

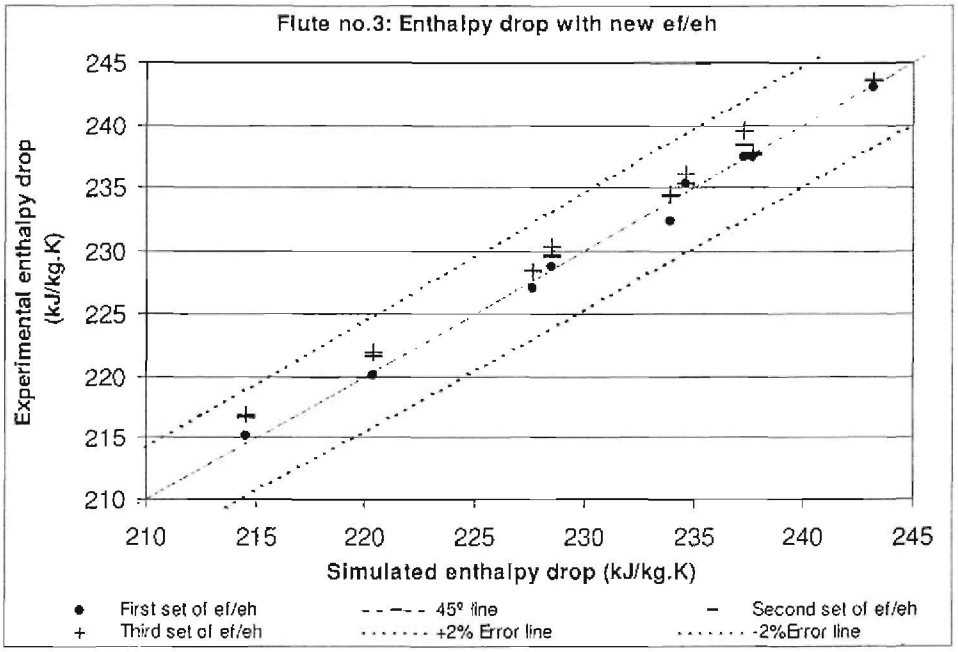


Figure 6.10: Simulation of the enthalpy drop by using the new enhancement factors on fluted tube no.3.

6.3.2.3 FLUTED TUBE NO.3: HEAT TRANSFER RESULTS

With the "First Set" of enhancement factors used in the correlation to predict the heat transfer the average percentage error difference between the experimental values and the theoretical values is 0.22% and the maximum difference is 0.64%. The "Second Set" of enhancement factors had an average percentage error of 0.47%, and the maximum percentage error of 0.96%. The "Third Set" of enhancement factors then have an average percentage error of 0.53% and the maximum percentage error is 1.06%. Generally, Figure 6.11 shows that 100% of the enhancement factors used to calculate the theoretical pressures are all within a 5% error deviation from the experimental values.

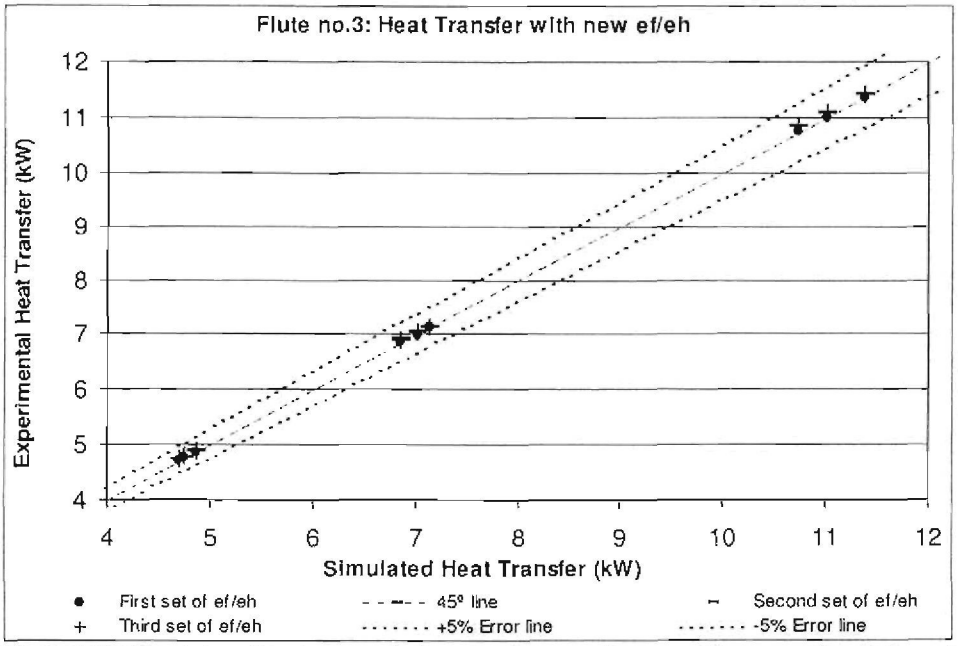


Figure 6.11: Simulation of the heat transfer by using the new enhancement factors on fluted tube no.3.

6.3.2.4 FLUTED TUBE NO.3: LMTD RESULTS

In Figure 6.12 the "First Set" of enhancement factors used in the correlation to predict the LMTD the average percentage error difference between the experimental values and the theoretical values is 1.47% and the maximum difference is 6.47%. The "Second Set" of enhancement factors had an average percentage error of 1.60% and the maximum percentage error of 5.13%. Following this, the "Third Set" of enhancement factors have an average percentage error of 2.75%, the maximum percentage error is 6.69%. On the whole, this indicates that 100% of the enhancement factors used to calculate the theoretical pressures are all within a 5% error deviation from the experimental values.

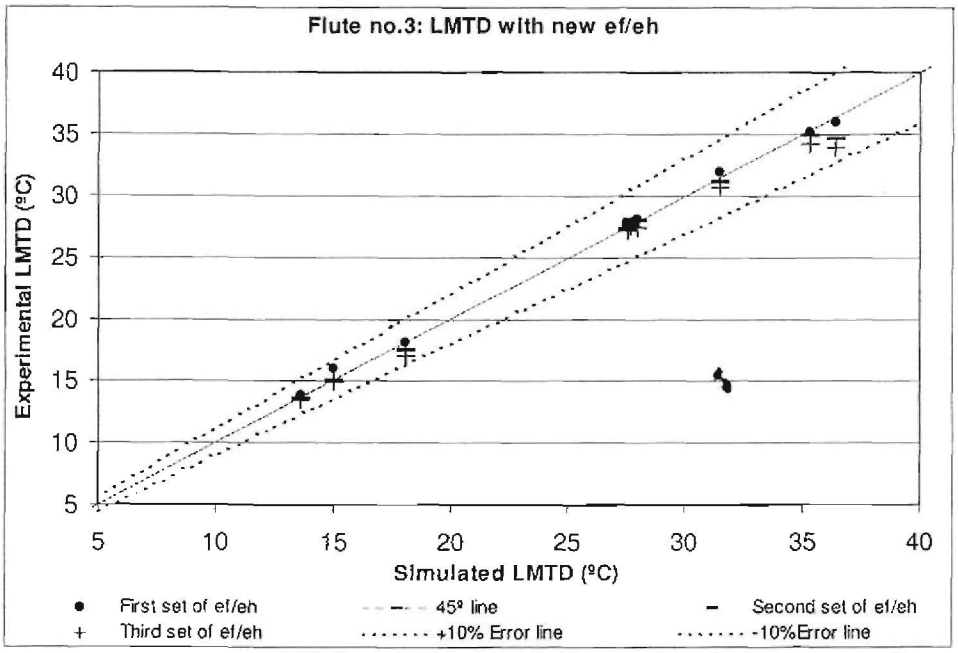


Figure 6.12: Simulation of the LMTD by using the new enhancement factors on fluted tube no.3.

Table 6.7 is a summary of all the data gathered from the figures by comparing the theoretical and experimental data.

Table 6.7: The theoretical results compared to the experimental results for Fluted tube no.3.

Set of enhancement factors used		First Set	Second Set	Third Set
ΔP (kPa)	Average Error =	5.59%	9.98%	10.86%
	Maximum Error =	14.82%	26.67%	26.67%
	Regression line =	0.9937		
ΔH (kJ/kg.K)	Average Error =	0.22%	0.36%	0.54%
	Maximum Error =	0.66%	0.96%	1.10%
	Regression line =	0.9955		
Q (kW)	Average Error =	0.22%	0.47%	0.53%
	Maximum Error =	0.64%	0.96%	1.06%
	Regression line =	0.9999		
LMTD (°C)	Average Error =	1.47%	1.60%	2.75%
	Maximum Error =	6.47%	5.13%	6.69%
	Regression line =	0.9959		

6.4 *COMPARISON OF ENHANCEMENT FACTORS*

From Tables 6.5, 6.6 and 6.7 it is evident that the correlation of Rousseau *et al.* (2003) predicts the total theoretical pressure drop, enthalpy change, heat transfer and LMTD over the entire heat exchanger more accurate with the newly generated enhancement factors from Table 6.4. In Table 6.8 a comparison is made between the correlation with the new enhancement factors, the correlation with the original enhancement factors, and the experimental data. The same input data from Table 6.1 were used in the correlation. Furthermore, the following conditions were also kept constant on Fluted Tube no.1: the refrigerant mass flow rate m_r = 0.02kg/s, water mass flow rate m_w = 0.09kg/s and the cooling water temperature at T = 20°C.

Table 6.8: Theoretical results of the correlation with each set of enhancement factors

Experimental data		Theoretical data							
		Original Set (ef/eh)		First Set (ef/eh)		Second Set (ef/eh)		Third Set (ef/eh)	
Pressure (kPa)									
$P_{1\,(exp)}$	1811	$P_{1\,(theo)}$	1811	$P_{1\,(theo)}$	1811	$P_{1\,(theo)}$	1811	$P_{1\,(theo)}$	1811
$P_{4\,(exp)}$	1792	$P_{4\,(theo)}$	1782	$P_{4\,(theo)}$	1789	$P_{4\,(theo)}$	1785	$P_{4\,(theo)}$	1788
$\Delta P_{Total\,(exp)}$	19	$\Delta P_{Total\,(theo)}$	29	$\Delta P_{Total\,(theo)}$	22	$\Delta P_{Total\,(theo)}$	26	$\Delta P_{Total\,(theo)}$	23
Percentage Error		52 %		15 %		36.84 %		21.05 %	
Enthalpy (kJ/kg.K)									
$H_{1\,(exp)}$	315.1	$H_{1\,(theo)}$	315.1	$H_{1\,(theo)}$	315.1	$H_{1\,(theo)}$	315.1	$H_{1\,(theo)}$	315.1
$H_{4\,(exp)}$	87.15	$H_{4\,(theo)}$	98.63	$H_{4\,(theo)}$	86.82	$H_{4\,(theo)}$	86.36	$H_{4\,(theo)}$	84.62
$\Delta H_{Total\,(exp)}$	227.95	$\Delta H_{Total\,(theo)}$	216.47	$\Delta H_{Total\,(theo)}$	228.28	$\Delta H_{Total\,(theo)}$	228.74	$\Delta H_{Total\,(theo)}$	230.48
Percentage Error		5.04 %		0.16 %		0.35 %		1.11 %	
LMTD (°C)									
$LMTD_{(exp)}$	10.72	$LMTD_{(theo)}$	19.28	$LMTD_{(theo)}$	10.3	$LMTD_{(theo)}$	10.1	$LMTD_{(theo)}$	9.83
Percentage Error		44.39 %		3.92 %		5.78 %		8.30 %	
Heat Transfer (kW)									
$Q_{Total\,(exp)}$	4.559	$Q_{Total\,(theo)}$	4.329	$Q_{Total\,(theo)}$	4.566	$Q_{Total\,(theo)}$	4.574	$Q_{Total\,(theo)}$	4.610
Percentage Error		5.04 %		0.15 %		0.33 %		1.11 %	

Pressure	**(kPa)**		**Enthalpy**		**(kJ/kg.K)**
$P_{x\,(exp)}$ =	Experimental Pressure		$H_{x\,(exp)}$ =		Experimental Enthalpy
$P_{x\,(theo)}$ =	Theoretical Pressure		$H_{x\,(theo)}$ =		Theoretical Enthalpy
Heat Transfer	**(kW)**		**LMTD**		**(°C)**
$Q_{Total\,(exp)}$ =	Experimental Heat Transfer		$LMTD_{(exp)}$ =		Experimental LMTD
$Q_{Total\,(theo)}$ =	Theoretical Heat Transfer		$LMTD_{(theo)}$ =		Theoretical LMTD

It is evident from the example in Table 6.8 that there is an improvement on all the theoretical results obtained with the newly generated enhancement factors. The main improvement of the correlation is in predicting the theoretical pressure drop which improved (from 52% error to a maximum error of 36.84%) and LMTD (from 44.39% error to a maximum of 3.92%

error). Thus, all the theoretical results in Table 6.8, which was obtained with the new enhancement factors, are within 63.16% accuracy compared to the experimental results.

6.5 *SUMMARY*

The main purpose of this chapter was to determine the accuracy of the Rousseau *et al.* (2003) correlation by comparing simulated results with experimental data. The previous enhancement factors from the correlation of Rousseau *et el.* (2003) for the pressure drop was $e_f = 4.409$ and for the heat transfer coefficient $e_h = 0.867$. But, the average percentage error of the correlation was 52% for the pressure drop, 5.04% for the heat transfer and 44.39% for the LMTD during the condensation process of R-407C. Based on this, new enhancement factors were derived for the pressure drop (e_f) and heat transfer coefficient (e_h).

The new improved enhancements, listed in Table 6.4, were implemented in the correlation. The average error for predicting the theoretical pressure drop is 9.52%, 0.51% for the heat transfer and 3.28% for the LMTD during the condensation process. While the maximum error for pressure drop is 36.84%, 1.89% for heat transfer and 13.46% for the LMTD during the condensation process. This is an improvement on the average accuracy compared to the existing enhancement factors of 42.48% on the pressure drop, 4.53% on the heat transfer and 41.11% on the LMTD.

The next chapter is a summary of all the previous chapters and results. Then, all the important factors gained from the study are discussed and some recommendations for further research in this field are given.

CHAPTER 7

CONCLUSION AND RECOMMENDATIONS

7.1 INTRODUCTION

This chapter sets out the most important results gained from the study. The chapter also summarises the conclusions from the experimental and theoretical data about the characteristics of R-407C used inside fluted annuli. It concludes with a few recommendations for future studies in this field.

7.2 SUMMARY OF THE STUDY

Chapter 1 focused on the technical implications when non-ozone depleting refrigerants replace refrigeration systems operating on ozone depleting refrigerants. Through the years several studies on different refrigerant mixtures and methods of passive schemes were developed to improve the heat transfer of refrigeration systems. The problem statement indicated that there are limited information and data available on the condensation characteristics of R-407C when used inside fluted tubes. The main focus of this study was to gain experimental data from the test facility and to determine the accuracy of the correlation of Rousseau *et al.* (2003).

In Chapter 2 an extensive literature survey was done focusing on the characteristics of zeotropic mixtures. Several studies were done over the years on the zeotropic mixture's flow patterns during the condensation process. During the condensation process phase change occurred, therefore the refrigerant mixture's temperature glide and pinch point must be taken

into consideration. Studies have shown if these characteristics are exploited correctly it will improve the performance of refrigeration systems.

The basic theory of the fluted tube and the correlation of Rousseau *et al.* (2003) were thoroughly discussed in Chapter 3. The simulation model used in the study is also based on the model developed by Rousseau *et al.* (2003).

The manufacturing process of the test sections was discussed in Chapter 4 along with the modifications to the test facility, including the components and measuring equipment. The accuracy of the measuring equipment was verified with R22 and the average percentage error was 0.96%. The chapter finally focused on an uncertainty analysis of the experimental data. The maximum uncertainty on the waterside was 2.02% and on the refrigerant side 1.49%.

Chapter 5 featured the methodology that was used during the experimental phase. The experimental data obtained from the test facility was used to determine the factors that had an influence on the pressure drop and the heat transfer coefficient of R-407C during the condensation process.

In Chapter 6 the enhancement factors derived from a comparison between the correlation of Rousseau *et al.* (2003) and the experimental data were discussed. The enhancement factors derived by Rousseau *et al.* (2003) had an average error of 52% to determine the pressure drop, 5.04% on the heat transfer and 44.59% on the LMTD when compared to the experimental results. This inaccuracy resulted in the calculation of three sets of newly improved enhancement factors from the available test data. These enhancement factors were used to predict the pressure drop and heat transfer of the refrigerant and the LMTD for the heat exchanger. The theoretical data was compared to the experimental data to determine the accuracy of the correlation when used with the different enhancement sets. For all three sets of enhancement factors it was determined that the average theoretical results had an accuracy of 90% compared to the experimental results. The newly generated enhancement factors had an average error of 9.52% on the pressure drop, 0.51% on the heat transfer and 3.28% on the LMTD. Thus, there is an improvement of 38.48% in the prediction of the pressure drop, 3.53% on the heat transfer and 41.11% on the LMTD. Based on these results, it is advisable to use the newly generated enhancement factors to predict the heat transfer characteristics of R-407C during the condensation process.

7.3 CONTRIBUTION OF THIS STUDY

The contributions made by this study can be summarised as follows:

1. A wide range of experimental data has been produced on the condensation heat transfer and pressure drop characteristics of R-407C inside fluted tubes.
2. The method and process to manufacture fluted tubes were improved.
3. Newly improved enhancement factors (listed in Table 7.1) were generated, which can be used in simulation models to predict the pressure drop and heat transfer more precise than the original enhancement factors of Rousseau *et al.* (2003).

Table 7.1: The newly generated enhancement factors.

	Liquid-phase		Two-phase		Gas-phase	
First set	ef	eh	ef	eh	ef	eh
Fluted tube no.1	4.30	1.07	5.97	2.46	4.30	2.85
Fluted tube no.2	4.04	1.04	6.26	2.62	4.04	2.93
Fluted tube no.3	4.78	2.19	3.84	1.95	4.78	2.19

	Liquid-phase		Two-phase		Gas-phase	
Second set	ef	eh	ef	eh	ef	eh
All fluted Tubes	4.37	1.43	5.36	2.34	4.37	2.66

	All three phases	
Third set	ef	eh
All fluted Tubes	4.70	2.14

7.4 RECOMMENDATIONS FOR FURTHER WORK

During the study the following limitations were identified and the following recommendations were made for further work in this field:

- The condensation pressure of the refrigerant (the pressure at which the refrigerant enters the Pre-Cooler) must be kept constant at a certain value. In this study it varied and was not kept exact at a certain value for each test that was performed. The condensing pressure must also be altered over a larger spectrum to determine the total effect on the heat transfer and pressure drop on fluted tubes during the condensation process.
- More detailed experimental measurements should be obtained over a larger test spectrum for the refrigerant mass flow rate to validate the cycle simulation. The mass flow rate of the refrigerant was altered from 0.02kg/s to 0.05kg/s, but in the future an attempt should be made to alter the mass flow rate from 0.01kg/s to 0.1kg/s. This will lead to a better understanding of how the refrigerant mass flow rate influence the heat transfer and pressure drop.

- The correlation of Rousseau *et al.* (2003) with the newly derived enhancement factors should be validated against commercially available heat pump results.
- Only one refrigerant mixture has been evaluated during this study. Other mixtures should also be tested to determine their ability to replace refrigerants being phased-out or provide improved system performance for heat pumps equipped with fluted tubes. Furthermore, this must also be carried out to determine the accuracy of the Rousseau *et al.* (2003) correlation with other refrigerant fluids.
- To improve the accuracy of the correlation of Rousseau *et al.* (2003) furthermore, rather change the coefficient "to the power of" in the equations, than change or improve the enhancement factors on the equations.

REFERENCES

ALBRECHT, R. 1996. Investigation of a refrigerant metamorphosis on refrigerator performance. Johannesburg: WITS. (Dissertation - M.Sc. Eng.)

ALLCHEM. 2002. Alternative one-component refrigerants.
[Web:] http://www.allchemi.com/eng/refregerants/alternative.html
[Date of use: 23 May 2006]

BUKASA, J.M. 2002. Heat transfer performance during condensation inside spiralled micro-fin tubes. Johannesburg: RAU. (Thesis - D. Eng.)

CAVALLINI, G., CENSI, D., DEL COL, L., DORETTI, G.A. LONGO. & ROSSETTO, L. 2001. Experimental investigation on condensation heat transfer and pressure drop of new HFC refrigerants(R134a, R125, R32, R410A, R236ea)in a horizontal smooth tube. International Journal of Refrigeration, Vol. 24, pp 73-87.

CAVALLINI, A., CENSI, G., DEL COL, D., DORETTI, L., LONGO., G.A., ROSSETTO, L. & ZILIO, C. 2003. Condensation inside and outside smooth and enhanced tubes – a review of recent research. International journal of refrigeration, Vol. 26, pp. 373-392.

CHEN, J. & KRUSE, H. 1997. Concentration shift for the mixed refrigerant R-404A, R32/134a and R-407C in an air conditioning system. HVAC&R RESEARCH, Vol. 3, No. 2, pp. 149-157.

CHRISTENSEN, R.N., ARNOLD, J.A. & GARIMELLA, S. 1993. Fluted tube heat exchanger design manual. Date. 9-29-93.

CHOI, T.Y., KIM, Y.J., KIM, M.S. & RO, S.T. 2000. Evaporation heat transfer of R-32, R-134a, R-32/134a and R-32/125/134a inside a horizontal smooth tube. International Journal of Heat and Mass Transfer, Vol. 43, pp. 3651 – 3660.

DAS, S.K. 1993. Water flow through helical coils in turbulent condition. The Canadian Journal of Chemical Engineering Vol.71, pp. 971 – 973.

DE BOS, W.P. 2006. Experimental determination of the forced convective boiling heat transfer coefficients of R407C in fluted-tubes. Northwest University, Potchefstroom campus. (Dissertation - M. Eng.)

DE MONTE, F. 2002. Calculation of thermodynamic properties of R-407C and R410A by Martin-Hou equation of state – part II: technical interpretation. International journal of refrigeration, Vol. 25, pp. 314-329.

DE VOS, P.W. 2006. Experimental determination of the forced convective boiling heat transfer coefficients of R407C in Fluted-tubes. North-West University (Dissertation - M. Eng.)

DEPARTMENT OF ENVIRONMENTAL AFFAIRS AND TOURISM, 2006. Montreal protocol: The ozone depletion story and measures taken towards the protection of the ozone layer in south Africa. ISBN 0-621-29272-9.

DONGSOO, J., CHONG-BO, K., SOO-MIN, H., KYANG-KI, K. 2003. Condensation heat transfer coefficient of R22, R-407C and R410A on a horizontal plain, low fin, and turbo-fin tubes. International Journal of Refrigeration. Vol. 26, pp. 1-7.

DOUGLAS, J.D., BRAUN, J.E., GROLL, E.A. & TREE, D.R. 1999. A cost-based method for comparing alternative refrigerants applied to R-22 systems. International Journal of Refrigeration 22 (1999) 107–125.

EBISU, T. & TORIKOSHI, K. 1998. Experimental study on evaporation and condensation heat transfer enhancement factors for R-407C using herringbone heat transfer tube. ASHRAE Transactions: Symposia, Vol. 104, PART 2, pp. 1044-1052.

ELKINS, J.M. 1997. Chlorofluorocarbons CFCs.
[Web:] http://www.cmdl.noaa.gov/noah/publictn/elkins/cfcs.html
[Date of use: 23 May 2006]

ENDRESS + HAUSER, 2006. Pressure transmitter cerebar S PMC731, PMP731 user manual.
[Web:] http://www.za.endress.com/
[Date of use: 23 May 2006]

ENDRESS + HAUSER, 2005. Coriolis sass slow seasurement system promass 63
Pressure transmitter cerebar S PMC731, PMP731 user manual.
[Web:] http://www.za.endress.com/
[Date of use: 23 May 2006]

GABRIELII, C. & LENNART, V. 1997. Replacement of R22 in tube and shell condensers: experimnetla and simulation. Int. Journal of refrigeration. Vol. 20, No.3 pp. 165-178.

GABRIELLII, C. & VAMBLING, L. 1998. Changes in optimal distribution of heat exchanger area between the evaporator and suction gas heat exchanger when replacing R22 with R-407C. International Journal of Refrigeration, Vol. 21, No.7, pp. 518-534.

GUNGOR, K.E. & WINTERTON, R.H.S. 1987. Simplified general correlation for saturated flow boiling and comparisons of correlations with data, Chemical Engineering Research, Vol. 65, pp. 148 – 156.

HONDA, H. 1987. A theoretical model of film condensation in a bubble horizontal flow finned tubes. SDME-HTD-85, pp. 789-85.

HONDA, H. WIJAYANTA, A.T. & TAKATA, N. 2004. Condensation of R407C in a horizontal microfin tube. Accepted 22 July 2004 and Available online 16 December 2004.

HWANG, Y., JUDGE, J. & RADERMACHER, R. 1997. Experience with refrigerant mixtures, ASHRAE Transactions. 1031 pp. 765 – 776.

INCROPERA, F.P. & DE WITT, D.P. 1996. Fundamentals of Heat and mass transfer, 4th edition Canada: John Wiley & Sons.

ISO. 1993. guide to the expression of uncertainty in measurement. Geneva, Switzerland.

JOHANNSEN, A. 1992. Potential of non-azeotropic refrigerant mixtures for water heating heat pumps in South Africa, National Energy Council. Prepared for the National Energy Council by the Division of Production Technology, CSIR.

JENG, T. CHANG, C & WANG, C. 2001. Vapor pressure of R-410A/oil and R-407C/oil mixtures. Applied thermal engineering, Vol. 21, pp. 863-870.

JUNG, D. & RADERMACHER R. 1993. Prediction oOf evaporation heat transfer coefficient and pressure drop of refrigeration mixtures in horizontal tubes. Rev. Int. Froid, Vol. 16, No. 3, pp. 201-209.

KANG, Y.T., STOUT, R. & CHRISTENSEN, R.N. 1997. The effects of inclination angle on flooding in a helically fluted tube with a twisted insert. International Journal of Multiphase Flow, Vol. 23, No. 6, pp. 1111-1129.

KARLSSON, T & VAMLING, L. 2004. Reasons for drop in shell-and-tube condenser performance when replacing R22 with zeotropic mixtures.Part 2: investigation of mass transfer resistance effects. International Journal of Refrigeration. Vol.27, pp. 561–566.

KIM, M & SHIN, J. 2005. Condensation heat transfer of R22 and R410A in horizontal smooth and microfin tubes. International Journal of Refrigeration. Vol.28, pp. 949–957.

KLINE, S.J., MCCLINTOCK F.A., 1953. Descrining uncertainties in single sample experiments. Mechanical engineering. Vol. 75, pp. 3-8.

KUSAKA, M., NAKATANI, K. & TAKATANI, T. 2000. The development of the energy-saving technology by the composition control of R-407C. Eight international refrigeration conference at Purdue University, USA – July 25-28, pp. 55-62.

LEE, J.H., BAE, S.W., BANG, K.H & KIM, M.H. 2002. Experimental and numerical research on condenser performance for R-22 and R-407C refrigerants. International Journal of Refrigeration. Vol.25, pp. 372–382.

MACBAIN, S.M., BERGLES, A.E. & RAINA, S. 1997. Heat Transfer and Pressure Drop Characteristics of Flow in a Horizontal Deep Spirally Fluted Tube, HVAC&R Research, Vol. 3 Part I, pp.65 – 80.

MICROMOTION, 2004. Micro Motion® ELITE® Mass Flow and Density Meters. Product Data sheet. [Web:] www.micromotion.com [Date of use: 23 May 2006]

MILLS, A.F. 1995. Heat and Mass Transfer, Chicago: Irwin. pp. 647 - 654.

PRETORIUS, C.A. 1999. Simulation of non-azeotropic heat pump performance, Potchefstroom. Potchefstroom University for Christian Higher Education. (Dissertation - M. Eng.)

ROUSSEAU, P.G., VAN ELDIK, M. & GREYVENSTEIN, G.P. 2003. Detailed simulation of fluted tube water heating condensers, International Journal of Heat and Mass Transfer, Vol. 26, pp. 232 – 239.

SAMI, S.M. & SCHNOLATE, J. 1992. Comparative study of two phase flow boiling of refrigerant mixtures and pure refrigerant inside enhanced surface tubing. International communications in heat and mass transfer, Vol. 19, pp. 137-148.

SAMI, S.M., TULEJ, P.J. & SONG, B. 1994. Heat transfer characteristics of ternary blends inside enhanced surface tubing. International communications in heat and mass transfer, Vol. 21, No. 4, pp. 489-498.

SAMI, S.M., & MALTAIS, H. 2000. Experimental investigation of two phase flow condensation of alternatives to HCF-22 inside enhanced surface tubing. Applied thermal engineering, Vol. 20, pp. 1113-1126.

SHAH, M.M., 1979. A correlation for heat transfer during film condensation inside pipes, Int. J. Heat and mass transfer, Vol. 93, Part 1, pp. 392-416.

SRINIVASAN, V., CHRISTENSEN, R.N., 1992. Experimnetal investigation of heat transfer and pressure drop characteristics of flow through spirally fluted tubes. Experimental thermal and fluid science. Vol.5, pp. 820-827.

SRINIVASAN, V., VAFAI, K. & CHRISTENSEN, R.N. 1994. Analysis of heat transfer and fluid flow through a spirally fluted tube using a porous substance approach. Journal of heat transfer, Vol. 116, pp. 543-551.

SWAMEE, P.K., JAIN, A.K. 1976. Explicit equations for pipe-flow problems. J hydraulic Div Proc., ASCE, pp. 657-664.

THOME, J.R. & HAJAL, J. 2002. Two-phase flow patter map for evaporation in horizontal tubes: latest version. HEFAT: 1st International conference on heat transfer, fluid mechanics and thermodynamics, 8-9 April 2002, pp. 182-188.

TRAVISS, D.P., ROHSENOW, W.M. BARON, A.B. 1972. Forced convection condensation inside tubes: a heat transfer equation for condenser design. ASHRAE Transaction, Vol. 79, No.1, pp. 157-165.

THOME, J.R. 2002. On the recent advances in modeling of two-phase flow and heat transfer. HEFAT, 1st International Conference on Heat Transfer, Fluid Mechanics and Thermodynamics.

VENKATARATHNAM, G., MOKASHI, G. & MURTHY, S.S. 1996. Occurrence of pinch points in condensers and evaporators for zeotropic refrigerant mixtures. International Journal of Refrigeration, Vol. 19, No. 6, pp. 361-368.

VENKATARATHNAM, G. & MURTHY, S.S. 1999. Effect of mixture composition on the formation of pinch points in condensers and evaporators for zeotropic refrigerant mixtures. International Journal of Refrigeration, Vol. 22, pp. 205-215.

VENTER, J.M. 2000. Experimental Determination of the heat transfer coefficients of R407C. Potchefstroom: PU for CHE. (Dissertation - M. Eng.)

VIJAYARAGHAM, S., KAMBIZ, V. & CHRISTENSEN, R.N. 1994. Analysis of heat transfer and fluid through a spirally fluted tube using a porous substrate approach. Journal of Heat Transfer, Vol. 116, pp. 543-551.

UNEP. 2000. Montreal Protocol on substances that deplete the ozone layer. Beijing: United Nations Environmental Programme.

WANG, C., CHIANG, C. & LU, D. 1997. Visual observation of two-phase flow pattern of R-22, R-134A and R-407C in a 6.5mm smooth tube. Experimental Thermal and fluid science, Vol. 15, pp. 395-405.

WANG, L., SUN, D., LIANG, P., ZHUANG, L. & TAN, Y. 2000. Heat transfer characteristics of carbon steel spirally fluted tube for high pressure preheaters. Energy Conversion & Management 41 (2000) 993±1005.

WELLSTANDT, S. & VAMLING, L. 2005. Evaporation of R134a in a horizontal herringbone micro-fin tube: heat transfer and pressure drop., International Journal of Refrigeration, Vol. 28.

YANA MOTTA, S.F. & DOMANSKI, P.A. 2000. Performance of R22 and its alternatives working at high outdoor temperatures. Eight international refrigeration conference at Purdue University, USA – July 25-28, pp. 47-54.

Y.Y, KIM. 2005. Heat transfer characteristics of flat plate finned-tube heat exchangers with large fin pitch. International Journal of Refrigeration 28 (2005) 851–858.

3040 Precision Thermometer, 1998. 3040 Precision Thermometer datasheet.
[Web:] http://www.google.co.za/search?hl=en&q=PREMA+3040+&meta=
[Date of use: 23 May 2006]

APPENDIX A

EES program

```
FUNCTION Nusselt_w_1(Re_w_T[1],elstar,plstar,thetalstar,Pr_w_T[1])

        IF (Re_w_T[1]<=5000)        Then
        Nusselt_w_1 = 0.014*(Re_w_T[1]^0.842)*(elstar^(-0.067))*(plstar^(-0.293))*(thetalstar^(-0.705))*Pr_w_T[1]^0.4
        else
        Nusselt_w_1= 0.064*(Re_w_T[1]^0.773)*(elstar^(-0.242))*(plstar^(-0.108))*(thetalstar^(0.599))*Pr_w_T[1]^0.4
        endif
end

FUNCTION Nusselt_w_gas_1(Re_w_1_phase[1],elstar,plstar,thetalstar,Pr_w_1_phase[1])

        IF (Re_w_1_phase[1]<=5000)    Then

        Nusselt_w_gas_1=0.014*(Re_w_1_phase[1]^0.842)*(elstar^(-0.067))*(plstar^(0.293))*(thetalstar^(0.705))*Pr_w_1_phase[1]^0.4
        else
        Nusselt_w_gas_1=0.064*(Re_w_1_phase[1]^0.773)*(elstar^(-0.242))*(plstar^(0.108))*(thetalstar^(0.599))*Pr_w_1_phase[1]^0.4
        endif
end

FUNCTION Nusselt_w_gas_2(Re_w_1_phase[2],elstar,plstar,thetalstar,Pr_w_1_phase[2])

        IF (Re_w_1_phase[2]<=5000)    Then
        Nusselt_w_gas_2=0.014*(Re_w_1_phase[2]^0.842)*(elstar^(-0.067))*(plstar^(0.293))*(thetalstar^(0.705))*Pr_w_1_phase[2]^0.4
        else
        Nusselt_w_gas_2=0.064*(Re_w_1_phase[2]^0.773)*(elstar^(-0.242))*(plstar^(0.108))*(thetalstar^(0.599))*Pr_w_1_phase[2]^0.4
        endif
end

FUNCTION Nusselt_g_gas_1(Re_g_1_phase[1],elstar,plstar,thetalstar,r_f_g[1],e_h_1,Pr_g_1_phase[1])

        Nusselt_g_gas_straight=0.023*(Re_g_1_phase[1]^0.8)*(Pr_g_1_phase[1]^0.4)
        {e_h={1.8}0.867}
        r_h=r_f_g[1]
        Nusselt_g_gas_1=Nusselt_g_gas_straight*e_h_1*r_h
end

FUNCTION Nusselt_g_gas_2(Re_gL_2_phase[1],elstar,plstar,thetalstar,r_f_g_pre[2],e_h_pre,Pr_g_2phase_out[1],x_ave_2phase[1],pr1)

        Nusselt_g_gas_straight1=0.023*((Re_gL_2_phase[1]^0.8)*Pr_g_2phase_out[1]^0.4)
        Nusselt_g_gas_helical1=Nusselt_g_gas_straight1*((1x_ave_2phase[1])^(0.8)+3.8*x_ave_2phase[1]^(0.76)*(1x_ave_2phase[1])^
        (0.04)/pr1^(0.38))
        r_h=r_f_g_pre[2]
        Nusselt_g_gas_2=Nusselt_g_gas_helical1*e_h_pre*r_h
end

FUNCTION Nusselt_g_gas_3(Re_g_1_phase[2],elstar,plstar,thetalstar,r_f_g[3],e_h_3,Pr_g_1_phase[2])

        Nusselt_g_gas_straight3=0.023*(Re_g_1_phase[2]^0.8)*(Pr_g_1_phase[2]^0.4)
        {e_h={1.8}0.867}
```

```
        r_h_3=r_f_g[3]
        Nusselt_g_gas_3=Nusselt_g_gas_straight3*e_h_3*r_h_3
end

FUNCTION Nusselt_g_gas_4(Re_g_l_phase[3],elstar,plstar,thetalstar,r_f_g[4],e_h_4,Pr_g_l_phase[3])

        Nusselt_g_gas_straight4=0.023*(Re_g_l_phase[3]^0.8)*(Pr_g_l_phase[3]^0.4)
        {e_h=(1.8)0.867}
        r_h_4=r_f_g[4]
        Nusselt_g_gas_4=Nusselt_g_gas_straight4*e_h_4*r_h_4
end

FUNCTION Nusselt_g_gas_5(Re_g_l_phase[4],elstar,plstar,thetalstar,r_f_g[5],e_h_5,Pr_g_l_phase[4])

        Nusselt_g_gas_straight5=0.023*(Re_g_l_phase[4]^0.8)*(Pr_g_l_phase[4]^0.4)
        {e_h=(1.8)0.867}
        r_h_5=r_f_g[5]
        Nusselt_g_gas_5=Nusselt_g_gas_straight5*e_h_5*r_h_5
end

"Single phase pressure drop in the annulus"

FUNCTION SPPD(m_R22,Area_g, Dh_g,L_pre_gas,rho_ref_in,rho_ref_out,mu_ref_in,mu_ref_out,f_straight[1],r_f_g[1],e_f_g[1])

    mu_ref_ave=(mu_ref_in+mu_ref_out)/2
    rho_ref_ave=(rho_ref_in+rho_ref_out)/2
    G_ref=m_R22/Area_g
    V_ref=G_ref/rho_ref_ave
    SPPD=e_f_g[1]*r_f_g[1]*f_straight[1]*L_pre_gas*rho_ref_ave*V_ref^(2)/(2*Dh_g)/1000
end

FUNCTION SPPD_2(m_R22,Area_g, Dh_g,L_sub_1Liq,rho_ref_in,rho_ref_out,mu_ref_in,mu_ref_out,f_straight[3],r_f_g[3],e_f_g[3])

    mu_ref_ave=(mu_ref_in+mu_ref_out)/2
    rho_ref_ave=(rho_ref_in+rho_ref_out)/2
    G_ref=m_R22/Area_g
    V_ref=G_ref/rho_ref_ave
    SPPD_2=e_f_g[3]*r_f_g[3]*f_straight[3]*L_sub_1Liq*rho_ref_ave*V_ref^(2)/(2*Dh_g)/1000
end

FUNCTION SPPD_3(m_R22,Area_g, Dh_g,L_test,rho_ref_in,rho_ref_out,mu_ref_in,mu_ref_out,f_straight[4],r_f_g[4],e_f_g[4])

    mu_ref_ave=(mu_ref_in+mu_ref_out)/2
    rho_ref_ave=(rho_ref_in+rho_ref_out)/2
    G_ref=m_R22/Area_g
    V_ref=G_ref/rho_ref_ave
    SPPD_3=e_f_g[4]*r_f_g[4]*f_straight[4]*L_test*rho_ref_ave*V_ref^(2)/(2*Dh_g)/1000
end
```

```
FUNCTION SPPD_4(m_R22,Area_g, Dh_g,L_sub,rho_ref_in,rho_ref_out,mu_ref_in,mu_ref_out,f_straight[5],r_f_g[5],e_f_g[5])

    mu_ref_ave=(mu_ref_in+mu_ref_out)/2
    rho_ref_ave=(rho_ref_in+rho_ref_out)/2
    G_ref=m_R22/Area_g
    V_ref=G_ref/rho_ref_ave
    SPPD_4=e_f_g[5]*r_f_g[5]*f_straight[5]*L_sub*rho_ref_ave*V_ref^(2)/(2*Dh_g)/1000
end

"Two-phase pressure drop in the annulus"

FUNCTION TPPD(m_dot_ref,A_cr,d_coil_T,D_h_o,L_test_1gas,x_in,x_out,rho_ref_l,rho_ref_v,mu_ref_l,mu_ref_v,e_f)
    x_ave=(x_in+x_out)/2
    mu_ref_x=mu_ref_v/mu_ref_l
    rho_ref_x=rho_ref_v/rho_ref_l
    G_ref=m_dot_ref/A_cr
    Re_ref_l=G_ref*D_h_o/mu_ref_l
    Re_ref_v=G_ref*D_h_o/mu_ref_v
    Re_ref_x=Re_ref_l+mu_ref_x*((1/rho_ref_x)^(0.5))*Re_ref_v
    p_ref_Traviss=0.09*Re_ref_v^(0.2)*x_ave^(1.8)*(1+2.85*(mu_ref_x^(0.1)*((1x_ave)/x_ave)^(0.9)*rho_ref_x^(0.5))^(0.523))^
    (2)*G_ref^2/(rho_ref_v*D_h_o)*L_test_1gas
    f_helical=4*(0.079*Re_ref_v^(0.25)+0.0075*(D_h_o/d_coil_T)^(0.5)+17.5782*Re_ref_v^(0.3137)*(D_h_o/d_coil_T)^(0.362)
    *(0.0015/D_h_o)^(0.6885))
    f_straight=0.25/((log10(0.0015/(3.7*D_h_o)+(5.74/Re_ref_x^(0.9))))^(2))
    r_f=f_helical/f_straight
    TPPD=e_f*r_f*p_ref_Traviss/1000
end

"----------FIXED PARAMETERS----------"

"----------GAS LINE----------"

"Temperature"
T_g[1] = Lookup('Lookup 1',1,1)          "Pre-Cooler Inlet"
T_g[2] = Lookup('Lookup 1',1,2)          "Pre-Cooler Outlet / Test Inlet"
T_g[3] = Lookup('Lookup 1',1,3)          "Test Outlet / Sub-Cooler Inlet"
T_g[4] = Lookup('Lookup 1',1,4)          "Sub-Cooler Outlet"

"Pressure"
P[1] = Lookup('Lookup 1',1,16)           "Pre-Cooler Inlet"
P[2] = Lookup('Lookup 1',1,17)           "Pre-Cooler Outlet / Test Inlet"
P[3] = Lookup('Lookup 1',1,18)           "Test Outlet / Sub-Cooler Inlet"
P[4] = Lookup('Lookup 1',1,19)           "Sub-Cooler Outlet"

"Refrigerant Mass flow"
m_R407C = Lookup('Lookup 1',1,15)        "Gas mass flow rate = kg/s"

"Enthalpy"
h_g[1] = ENTHALPY(R407C,T=T_g[1],P=P[1])
h_g[4] = ENTHALPY(R407C,T=T_g[4],P=P[4])
```

```
h_g[3] = h_g[4] - Q_w_sub_total[3]/m_R407C
h_g[2] = h_g[3] - Q_w_test_total[2]/m_R407C

"Quality"
x[1] = QUALITY(R407C,h=h_g[1],P=P[1])
x[2] = QUALITY(R407C,h=h_g[2],P=P[2])
x[3] = QUALITY(R407C,h=h_g[3],P=P[3])
x[4] = QUALITY(R407C,h=h_g[4],P=P[4])

"----------WATER LINE ----------"

"Temperature"
T_w[1] = Lookup('Lookup 1',1,6)          "Pre-Cooler water in"
T_w[2] = Lookup('Lookup 1',1,7)          "Pre-Cooler water out"
T_w[3] = Lookup('Lookup 1',1,8)          "Test water in"
T_w[4] = Lookup('Lookup 1',1,9)          "Test water out"
T_w[5] = Lookup('Lookup 1',1,10)         "Sub-Cooler in"
T_w[6] = Lookup('Lookup 1',1,11)         "Super-Cooler out"

"Water Mass flow"
m_dot_w_pre[1] = Lookup('Lookup 1',1,12)     "Pre-Cooler = kg/s"
m_dot_w_test[2] = Lookup('Lookup 1',1,13)    "Test Cooler = kg/s"
m_dot_w_sub[3] = Lookup('Lookup 1',1,14)     "Sub Cooler = kg/s"

"Heat Transfer"
Q_w_pre_total[1] = m_dot_w_pre[1]*CP_w_pre*(T_w[1]-T_w[2])
Q_w_test_total[2] = m_dot_w_test[2]*CP_w_test*(T_w[3]-T_w[4])
Q_w_sub_total[3] = m_dot_w_sub[3]*CP_w_sub*(T_w[5]-T_w[6])

"Specific Heat Capacity"
CP_w_pre = CP(Water,T=((T_w[1] + T_w[2])/2),P=85)
CP_w_test= CP(Water,T=((T_w[3] + T_w[4])/2),P=85)
CP_w_sub = CP(Water,T=((T_w[5] + T_w[6])/2),P=85)

"---------- ACCURACY TEST ----------"

Q_total_gas = m_R407C* (h_g[1] - h_g[4])
Q_total_w = -Q_w_sub_total[3]-Q_w_pre_total[1] -Q_w_test_total[2]
DELTAQ=Q_total_gas-Q_total_w
Persentage_error=(DELTAQ/Q_total_gas)*100

"---------- GEOMETRY OF FLUTED TUBES ----------"

"Fixed parameters"

    "Flute depth"
    e=0.00209 [m]

    "Flute pitch"
    p=0.0095  [m]
```

```
"Inside Volume Diameter"
D_vi=0.01177        [m]
r_i=D_vi/2

"Outside Volume Diameter"
r_o=D_vo/2

"Helix angle of flute"
theta=55            [Degrees]

"Number of flute starts"
N=4

"t-Flute thickness"
D_vo=D_vi+2*t
t=0.73/1000

"Non-Dimensional Parameters"
elstar=e/D_vi
plstar=p/D_vi
thetalstar=theta/90

"Lentgh"
L_pre=2.87          [m]
L_test=2.93         [m]
L_sub=2.91          [m]

"Annulus inside diameter"
D_o=0.01667

"Heat Transfer Area through the water"
A_w_hta_pre=PI*D_vi*L_pre
A_w_hta_test=PI*D_vi*L_test
A_w_hta_sub=PI*D_vi*L_sub

"Heat Transfer Area through the gas"
A_g_hta=PI*D_vo*L_pre

"Area flow of the water"
Area_w=PI*(D_vi/2)^2

"Area flow of the gas"
Area_g=PI*(D_o/2)^2-PI*(D_vo/2)^2

"Hydroulic diameter of the Annulus-gas"
Dh_g=D_o-D_vo

"Hydroulic diamater of Annulus tube-through which heat transfer takes place"
Dh_heat=(4*((PI*(D_o/2)^2)-PI*r_o^2))/(2*PI*r_o)
```

"Diameter of the coiled fluted tube"
d_coil_T=D_vo/sin(thetalstar*(PI/2))

"Heat Flux"
Heatflux[1]=-Q_w_pre_total[1]/A_g_hta

"Mass Flux"
Massflux[1]=m_R407C/Area_g

"Pressure Parameters"
d_coil_P=Dh_g/(sin(theta))

"---------- PRE-COOLER ----------"

" ----------One-Phase (Gas) region (GAS) ---------- "
"----------Water side----------"

"Heat Transfer of Water over Pre-Cooler"

"Average water temperature over pre-cooler"
T_w_ave_T[1]=(T_w[1]+T_w[2])/2

"Density of water"
rho_w_T[1]=DENSITY(Water,T=T_w_ave_T[1],P=85)

"Conductivity of the water"
k_w_T[1]=CONDUCTIVITY(Water,T=T_w_ave_T[1],P=85)/1000

"Water Velocity"
m_dot_w_pre[1]= rho_w_T[1]*V_water_T[1]*Area_w

"Viscocity"
mu_w_T[1]=VISCOSITY(Water,T=T_w_ave_T[1],P=85)

"Reynolds number"
Re_w_T[1]=(rho_w_T[1]*V_water_T[1]*D_vi)/mu_w_T[1]

"Prandtl number"
Pr_w_T[1]=PRANDTL(Water,T=T_w_ave_T[1],P=85)

"Heat Transfer Coefficient of the water"
hw_heat_transfer_T [1]=(Nusselt_w_T[1]*k_w_T[1])/D_vi
Nusselt_w_T[1]=Nusselt_w_1(Re_w_T[1],elstar,plstar,thetalstar,Pr_w_T[1])

"LMTD-method"
DELTAT_1[1]=(T_g[1]-T_w[2])
DELTAT_2[1]=(T_g[2]-T_w[1])
DELTAT_lm[1]=(DELTAT_1[1]-DELTAT_2[1])/(ln(DELTAT_1[1]/DELTAT_2[1]))

```
"U_water"
-Q_w_pre_total[1]=U_water[1]*A_w_hta_pre*DELTAT_lm[1]
U_water[1]*A_w_hta_pre=UA_T[1]


"------------------------Heat Transfer-------------------------------"
"----------------Determine Refrigerant Temperature-------------"

"Point of entering the 2phase region"
x_g=1
T_gg[1]=TEMPERATURE(R407C,h=H,P=P_g[3])
H=ENTHALPY(R407C,x=x_g,P=P_g[3])

"Enthalpy"
h_g_1_phase[1]=ENTHALPY(R407C,x=x_g,P=P_g[3])

"Heat transfer of R-407C in the gas-one phase"
Q_g_1_phase[1]=m_R407C*(h_g[1]-h_g_1_phase[1])

"Heat transfer on each side and effectiveness"
Q_W_T[1]=m_dot_w_pre[1]*CP_w_pre*(T_w[1]-T_w[2])
Q_G_T[1]=m_R407C*(h_g[1]-h_g[2])
Q_R=-Q_W_T[1]/Q_G_T[1]

"Water heat transfer coefficient"
Q_w_1_phase[1]=Q_g_1_phase[1]
Q_w_1_phase[1]=m_dot_w_pre[1]*CP_w_pre*(T_w[2]-T_wi[2])

"----------------------------Water side-----------------------------------"

"Heat Transfer Coefficient of the Water against R-407C in gas phase"
T_w_ave_1_phase[1]=(T_w[2]+T_wi[2])/2

"Prandtl number"
Pr_w_1_phase[1]=PRANDTL(Water,T=T_w_ave_1_phase[1],P=85)

"Reynolds number"
Re_w_1_phase[1]=(rho_w_1_phase[1]*V_w_1_phase[1]*D_vi)/mu_w_1_phase[1]

"Density of R-407C"
rho_w_1_phase[1]=DENSITY(Water,T=T_w_ave_1_phase[1],P=85)

"Conductivity of the water"
k_w_1_phase[1]=CONDUCTIVITY(Water,T=T_w_ave_1_phase[1],P=85)/1000

"R-407C Velocity"
m_dot_w_pre[1]= rho_w_1_phase[1]*V_w_1_phase[1]*Area_w

"Viscocity"
mu_w_1_phase[1]=VISCOSITY(Water,T=T_w_ave_1_phase[1],P=85)
```

```
"Heat Transfer Coeffieient of the water"
h_w_1_phase_heat_transfer [1]=(Nusselt_w_1_phase[1]*k_w_1_phase[1])/D_vi
Nusselt_w_1_phase[1]=Nusselt_w_gas_1(Re_w_1_phase[1],elstar,plstar,thetalstar,Pr_w_1_phase[1])

"---------- R-407C in the gas phase----------"

"Determine  Heat Transfer Coefficent of the Refrigerant"
T_g_ave_1_phase[1]=(T_gg[1]+T_g[1])/2
P_g_ave_1_phase[1]=(P_g[3]+P[1])/2

"Prandtl number"
Pr_g_1_phase[1]=PRANDTL(R407C,T=T_g_ave_1_phase[1],P=P_g_ave_1_phase[1])

"Reynolds number"
Re_g_1_phase[1]=(rho_g_1_phase[1]*V_g_1_phase[1]*Dh_g)/mu_g_1_phase[1]

"Density of R-407C"
rho_g_1_phase[1]=DENSITY(R407C,T=T_g_ave_1_phase[1],P=P_g_ave_1_phase[1])

"Conductivity of the water"
k_g_1_phase[1]=CONDUCTIVITY(R407C,T=T_g_ave_1_phase[1],P=P_g_ave_1_phase[1])/1000

"R-407C Velocity"
m_R407C= rho_g_1_phase[1]*V_g_1_phase[1]*Area_g

"Viscocity"
mu_g_1_phase[1]=VISCOSITY(R407C,T=T_g_ave_1_phase[1],P=P_g_ave_1_phase[1])
"LOG-MEAN temperature differance"
Q_UA[1]=Q_w_1_phase[1]
Q_UA[1]=UA_[1]*DELTAT_lm_1phase[1]
DELTAT_lm_1phase[1]=((T_g[1]-T_w[2])-(T_gg[1]-T_wi[2]))/(ln((T_g[1]-T_w[2])/(T_gg[1]-T_wi[2])))

"Geust Value"
Ts_ave1=((T_g_ave_1_phase[1]+T_w_ave_1_phase[1])/2+T_w_ave_1_phase[1])/2

"Determine lenght in the gas region"
Q_w_1_phase[1]=h_w_1_phase_heat_transfer [1]*A_w_hta_gas*(Ts_ave1 -T_w_ave_1_phase[1])
A_g_hta_gas=PI*D_vo*L_pre_gas
A_w_hta_gas=PI*D_vi*L_pre_gas

"Determine the heat transfer coefficient of the refrigerant"
1/(UA_[1])=1/(h_g_1_phase_heat_transfer[1]*A_g_hta_gas)+(ln(D_vo/D_vi)/(2*PI*k_copper*L_pre_gas))+1/(h_w_1_phase_
heat_transfer [1]*A_w_hta_gas)
k_copper=k_('Copper', T_g_ave_1_phase[1])/1000

"Friction factor"
f_straight[1]=0.25/(D)^2
D=log10((0.0015/(3.7*Dh_g))+(5.74/Re_g_1_phase[1]^0.9))
f_helical[1]=4*(0.079*Re_g_1_phase[1]^(-0.25)+(0.0075*(Dh_g/d_coil_T)^0.5)+(17.5782*Re_g_1_phase[1]^(
0.3137)*(Dh_g/d_coil_T)^0.361*(0.0015/Dh_g)^0.6885))
r_f_g[1]=f_helical[1]/f_straight[1]
```

```
"Nusselt number and heat transfer coefficient"
Nusselt_g_1_phase[1]=Nusselt_g_gas_1(Re_g_1_phase[1],e|star,p|star,thetalstar,r_f_g[1],e_h_1,Pr_g_1_phase[1])
h_g_1_phase_heat_transfer [1]=(Nusselt_g_1_phase[1]*k_g_1_phase[1])/Dh_g

"Pressure drops"
P_g[3]=P[1]-DELTAP_ref[1]

"Density of R-407C"
rho_g_1_phase_P_in[1]=DENSITY(R407C,T=T_g[1],P=P[1])
rho_g_1_phase_P_out[1]=DENSITY(R407C,x=1,P=P_g[3])

"Viscocity"
mu_g_1_phase_P_in[1]=VISCOSITY(R407C,T=T_g[1],P=P[1])
mu_g_1_phase_P_out[1]=VISCOSITY(R407C,x=1,P=P_g[3])

DELTAP_ref[1]=SPPD(m_R407C,Area_g,Dh_g,L_pre_gas,rho_g_1_phase_P_in[1],rho_g_1_phase_P_out[1],mu_g_1_phase_P
_in[1],mu_g_1_phase_P_out[1],f_straight[1],r_f_g[1],e_f_g[1])
e_f_g[1]=(e_f_g[5]+e_f_g[4])/2

"---------- Two-Phase region ----------"
"---------- R-407C in the two phase----------"

"Heat Transfer of the R-407C in two-phase region"
Q_g_pre_2phase[1]=m_R407C*(h_g_1_phase[1]-h_g_1_phase[2])
x_ave_2phase[1]=(x_l+x_g)/2
T_g_ave_2_phase[1]=(T_gg[1]+T_gl[1])/2

"Viscocity"
mu_g_2phase_in[1]=VISCOSITY(R407C,x=1,P=P_g[3])
mu_g_2phase_out[1]=VISCOSITY(R407C,x=0,P=P_gl[3])
mu_g_ave_2phase[1]=(mu_g_2phase_in[1]+mu_g_2phase_out[1])/2

"Reynolds number"
Re_gv_2_phase[1]=(rho_gv_2phase[1]*V_gv_2phase[1]*Dh_g)/mu_gv_2phase[1]
m_R407C= rho_gv_2phasc[1]*V_gv_2phase[1]*Area_g
rho_gv_2phase[1]=DENSITY(R407C,x=1,P=P_g[3])
mu_gv_2phase[1]=VISCOSITY(R407C,x=1,P=P_g[3])

Re_gL_2_phase[1]=(rho_gL_2phase[1]*V_gL_2phase[1]*Dh_g)/mu_gL_2phase[1]
m_R407C= rho_gL_2phase[1]*V_gL_2phase[1]*Area_g
rho_gL_2phase[1]=DENSITY(R407C,x=0,P=P_gl[3])
mu_gL_2phase[1]=VISCOSITY(R407C,x=0,P=P_gl[3])

Re_g_2phase[1]=Re_gL_2_phase[1]+mu_ref_x_2phase[1]*((1/rho_ref_x_2phase[1])^(0.5))*Re_gv_2_phase[1]
mu_ref_x_2phase[1]=mu_gv_2phase[1]/mu_gL_2phase[1]
rho_ref_x_2phase[1]=rho_gv_2phase[1]/rho_gL_2phase[1]

"Conductivity"
k_g_2phase_out[1]=CONDUCTIVITY(R407C,x=0,P=P_gl[3])/1000
k_g_2phase_in[1]=CONDUCTIVITY(R407C,x=1,P=P_g[3])/1000
k_g_ave_2phase[1]=(k_g_2phase_in[1]+k_g_2phase_out[1])/2
```

```
"Prandtl number"
Pr_g_2phase_out[1]=PRANDTL(R407C,x=0,P=P_gl[3])
Pr_g_2phase_in[1]=PRANDTL(R407C,x=1,P=P_g[3])
Pr_g_ave_2phase[1]=(Pr_g_2phase_in[1]+Pr_g_2phase_out[1])/2

"Critical Pressure Ratio"
pr1=((P_gl[3]+P_g[3])/2)/P_CRIT(R22)

"Heat transfer to the water"
Q_w_pre_2phase[1]=m_dot_w_pre[1]*CP_w_pre*(T_wi[2]-T_wo[2])
T_w_ave_2phase[1]=(T_wi[2]-T_wo[2])/2

"LOG-MEAN temperature differance"
Q_UA_pre[2]=Q_w_pre_2phase[1]
Q_UA_pre[2]=UA_pre[2]*DELTAT_pre_lm_2phase[1]
DELTAT_pre_lm_2phase[1]=((T_gg[1]-T_wi[2])-(T_gl[1]-T_wo[2]))/(ln((T_gg[1]-T_wi[2])/(T_gl[1]-T_wo[2])))

"Geust Value"
Ts_ave1_2phase=(T_g_ave_2_phase[1]+T_w_ave_2phase[1])/2
L_pre_2ph=L_pre-L_pre_gas-L_sub_1Liq

"Determine lenght in the gas region"
Q_w_pre_2phase[1]=h_w_2phase_1_heat_transfer [1]*A_w_hta_pre_2gas*(Ts_ave1_2phase -T_w_ave_2phase[1])
A_g_hta_pre_2gas=PI*D_vo*L_pre_2ph
A_w_hta_pre_2gas=PI*D_vi*L_pre_2ph

"Determine the heat transfer coefficient of the refrigerant"
(1/(UA_pre[2]))-BB-AA=1/(h_g_2phase_1_heat_transfer [1]*A_g_hta_pre_2gas)
k_copper_pre=k_('Copper', T_g_ave_2_phase[1])/1000

AA=1/(h_w_2phase_1_heat_transfer [1]*A_w_hta_pre_2gas)
BB=(ln(D_vo/D_vi)/(2*PI*k_copper_pre*L_pre_2ph))
GG=(1/(UA_pre[2]))

"Friction factor"
f_straight_pre[2]=0.25/(D_22)^2
D_22=log10((0.0015/(3.7*Dh_g))+(5.74/Re_g_2phase[1]^0.9))
f_helical_pre[2]=4*(0.079*Re_gv_2_phase[1]^(0.25)+(0.0075*(Dh_g/d_coil_T)^0.5)+(17.5782*Re_gv_2_phase[1]^(0.3137)*(D
h_g/d_coil_T)^0.361*(0.0015/Dh_g)^0.6885))
r_f_g_pre[2]=f_helical_pre[2]/f_straight_pre[2]

"Nusselt number and heat transfer coefficient"
Nusselt_g_2_phase[2]=Nusselt_g_gas_2(Re_gL_2_phase[1],elstar,plstar,thetalstar,r_f_g_pre[2],e_h_pre,Pr_g_2phase_out[1],x_a
ve_2phase[1],pr1)
h_g_2phase_1_heat_transfer [1]=Nusselt_g_2_phase[2]*(k_g_ave_2phase[1])/Dh_g

"Pressure drops"
P_g[3]=P_gl[3]+DELTAP_ref_pre[2]
x_g[1]=1
```

```
DELTAP_ref_pre[2]=TPPD(m_R407C,Area_g,d_coil_T,
Dh_g,L_pre_2ph,x_l,x_g,rho_gL_2phase[1],rho_gv_2phase[1],mu_gL_2phase[1],mu_gv_2phase[1],e_f_g_pre[2])


"---------- PRE-COOLER ----------"


" ----------(ONE - PHASE) LIQUID REGION ---------- "

"----------Heat Transfer----------"

"Determine Refrigerant Temperature"
x_l=0
T_gl[1]=TEMPERATURE(R407C,h=HL,P=P_gl[3])
HL=ENTHALPY(R407C,x=x_l,P=P_gl[3])
h_g_l_phase[2]=ENTHALPY(R407C,x=x_l,P=P_gl[3])

"Heat transfer of R-407C in the gas-one phase"
Q_g_l_phase[2]=m_R407C*(h_g_l_phase[2]-h_g[2])

"Water heat transfer coefficient"
Q_w_l_phase[2]=Q_g_l_phase[2]*Q_R
Q_w_l_phase[2]=m_dot_w_pre[1]*CP_w_pre*(T_wo[2]-T_w[1])

"---------- Water side ----------"
"Heat Transfer Coefficient of the Water against R22 in gas phase"
T_w_ave_l_phase[2]=(T_w[1]+T_wo[2])/2

"Prandtl number"
Pr_w_l_phase[2]=PRANDTL(Water,T=T_w_ave_l_phase[2],P=85)

"Reynolds number"
Re_w_l_phase[2]=(rho_w_l_phase[2]*V_w_l_phase[2]*D_vi)/mu_w_l_phase[2]

"Density of R22"
rho_w_l_phase[2]=DENSITY(Water,T=T_w_ave_l_phase[2],P=85)

"Conductivity of the water"
k_w_l_phase[2]=CONDUCTIVITY(Water,T=T_w_ave_l_phase[2],P=85)/1000

"R22 Velocity"
m_dot_w_pre[1]= rho_w_l_phase[2]*V_w_l_phase[2]*Area_w

"Viscocity"
mu_w_l_phase[2]=VISCOSITY(Water,T=T_w_ave_l_phase[2],P=85)

"Heat Transfer Coefficient of the water"
h_w_l_phase_heat_transfer [2]=(Nusselt_w_l_phase[2]*k_w_l_phase[2])/D_vi
Nusselt_w_l_phase[2]=Nusselt_w_gas_2(Re_w_l_phase[2],elstar,plstar,thetalstar,Pr_w_l_phase[2])
```

```
"---------- R-407C in the liquid phase----------"

"Determine Heat Transfer Coefficent of the Refrigerant"
T_g_ave_1_phase[2]=(T_gl[1]+T_g[2])/2
P_g_ave_1_phase[2]=(P_gl[3]+P[2])/2

"Prandtl number"
Pr_g_1_phase[2]=PRANDTL(R407C,T=T_g_ave_1_phase[2],P=P_g_ave_1_phase[2])

"Reynolds number"
Re_g_1_phase[2]=({Massflux[1]}rho_g_1_phase[2]*V_g_1_phase[2]*Dh_g)/mu_g_1_phase[2]

"Density of R-407C
rho_g_1_phase[2]=DENSITY(R407C,T=T_g_ave_1_phase[2],P=P_g_ave_1_phase[2])

"Conductivity of the water"
k_g_1_phase[2]=CONDUCTIVITY(R407C,T=T_g_ave_1_phase[2],P=P_g_ave_1_phase[2])/1000

"R-07Cocity"
m_R407C= rho_g_1_phase[2]*V_g_1_phase[2]*Area_g

"Viscocity"
mu_g_1_phase[2]=VISCOSITY(R407C,T=T_g_ave_1_phase[2],P=P_g_ave_1_phase[2])

"LOG-MEAN temperature differance"
Q_UA[3]=Q_w_1_phase[2]
Q_UA[3]=UA_[3]*DELTAT_lm_1phase[2]
DELTAT_lm_1phase[2]=((T_gl[1]-T_wo[2])-(T_g[2]-T_w[1]))/(ln((T_gl[1]-T_wo[2])/(T_g[2]-T_w[1])))

"Geust Value"
Ts_ave2_1phase22={(}(T_g_ave_1_phase[2]+T_w_ave_1_phase[2])/2{+T_w_ave_1_phase[2])/2}

"Determine lenght in the gas region"
Q_w_1_phase[2]=h_w_1_phase_heat_transfer [2]*A_w_hta_pre_1gas*(Ts_ave2_1phase22 -T_w_ave_1_phase[2])
A_g_hta_pre_1gas=PI*D_vo*L_sub_1Liq
A_w_hta_pre_1gas=PI*D_vi*L_sub_1Liq

"Determine the heat transfer coefficient of the refrigerant"
1/(UA_[3])=1/(h_g_1_phase_heat_transfer[2]*A_g_hta_pre_1gas)+(ln(D_vo/D_vi)/(2*PI*k_copper[3]*L_sub_1Liq))+1/(h_w_1
_phase_heat_transfer [2]*A_w_hta_pre_1gas)
k_copper[3]=k_('Copper', T_g_ave_1_phase[2])/1000

"Friction factor"
f_straight[3]=0.25/(D_3)^2
D_3=log10((0.0015/(3.7*Dh_g))+(5.74/Re_g_1_phase[2]^0.9))
f_helical[3]=4*(0.079*Re_g_1_phase[2]^(0.25)+(0.0075*(Dh_g/d_coil_T)^0.5)+(17.5782*Re_g_1_phase[2]^.3137)*(Dh_g/d_
coil_T)^0.361*(0.0015/Dh_g)^0.6885))
r_f_g[3]=f_helical[3]/f_straight[3]

"Nusselt number and heat transfer coefficient"
Nusselt_g_1_phase[2]=Nusselt_g_gas_3(Re_g_1_phase[2],elstar,plstar,thetalstar,r_f_g[3],e_h_3,Pr_g_1_phase[2])
```

```
h_g_1_phase_heat_transfer [2]=(Nusselt_g_1_phase[2]*k_g_1_phase[2])/Dh_g
{e_h_4=0.517}

"Pressure drops"
P[2]=P_gl[3]-DELTAP_ref[3]

"Density of R-407C
rho_g_1_phase_P_in[2]=DENSITY(R22,x=0,P=P_gl[3])
rho_g_1_phase_P_out[2]=DENSITY(R22,T=T_g[2],P=P[2])

"Viscocity"
mu_g_1_phase_P_in[2]=VISCOSITY(R22,x=0,P=P_gl[3])
mu_g_1_phase_P_out[2]=VISCOSITY(R22,T=T_g[2],P=P[2])

DELTAP_ref[3]=SPPD_2(m_R407C,Area_g,
Dh_g,L_sub_1Liq,rho_g_1_phase_P_in[2],rho_g_1_phase_P_out[2],mu_g_1_phase_P_in[2],mu_g_1_phase_P_out[2],f_straight[
3],r_f_g[3],e_f_g[3])
e_f_g[3]=(e_f_g[4]+e_f_g[5])/2



"----------TEST-COOLER----------"

"----------Water side----------"

"Heat Transfer of  Water over Test-Cooler"
"Average water temperature over test-cooler"
T_w_ave_T[2]=(T_w[3]+T_w[4])/2

"Density of water"
rho_w_T[2]=DENSITY(Water,T=T_w_ave_T[2],P=85)

"Conductivity of the water"
k_w_T[2]=CONDUCTIVITY(Water,T=T_w_ave_T[2],P=85)/1000

"Water Velocity"
m_dot_w_test[2] = rho_w_T[2]*V_water_T[2]*Area_w

"Viscocity"
mu_w_T[2]=VISCOSITY(Water,T=T_w_ave_T[2],P=85)

"Reynolds number"
Re_w_T[2]=(rho_w_T[2]*V_water_T[2]*D_vi)/mu_w_T[2]

"Prandtl number"
Pr_w_T[2]=PRANDTL(Water,T=T_w_ave_T[2],P=85)

"Heat Transfer Coefficient of the water"
hw_heat_transfer_T [2]=(Nusselt_w_T[2]*k_w_T[2])/D_vi
Nusselt_w_T[2]=Nusselt_w_1(Re_w_T[2],elstar,plstar,thetalstar,Pr_w_T[2])
```

```
"Heat Transfer"
Q_W_T[2]=m_dot_w_test[2]*CP_w_sub*(T_w[4]-T_w[3])
Q_G_T[2]=m_R407C*(h_g[2]-h_g[3])
Q_R_T[2]=Q_W_T[2]/Q_G_T[2]

"LMTD-method"
DELTAT_1[2]=(T_g[2]-T_w[4])
DELTAT_2[2]=(T_g[3]-T_w[3])
DELTAT_lm[2]=(DELTAT_1[2]-DELTAT_2[2])/(ln(DELTAT_1[2]/DELTAT_2[2]))

"U_water"
Q_W_T[2]=UA_T[2] *DELTAT_lm[2]
U_water[2]*A_w_hta_test=UA_T[2]

"---------- R22 in the liquid phase----------"

"Determine Heat Transfer Coefficent of the Refrigerant"
T_g_ave_1_phase[3]=(T_g[2]+T_g[3])/2
P_g_ave_1_phase[3]=(P[2]+P[3])/2

"Prandtl number"
Pr_g_1_phase[3]=PRANDTL(R407C,T=T_g_ave_1_phase[3],P=P_g_ave_1_phase[3])

"Reynolds number"
Re_g_1_phase[3]=({Massflux[1]}rho_g_1_phase[3]*V_g_1_phase[3]*Dh_g)/mu_g_1_phase[3]

"Density of R-407C"
rho_g_1_phase[3]=DENSITY(R407C,T=T_g_ave_1_phase[3],P=P_g_ave_1_phase[3])

"Conductivity of the water"
k_g_1_phase[3]=CONDUCTIVITY(R407C,T=T_g_ave_1_phase[3],P=P_g_ave_1_phase[3])/1000

"R-407C Velocity"
m_R407C= rho_g_1_phase[3]*V_g_1_phase[3]*Area_g

"Viscocity"
mu_g_1_phase[3]=VISCOSITY(R407C,T=T_g_ave_1_phase[3],P=P_g_ave_1_phase[3])

"Determine lenght in the gas region"
Q_W_T[2]=hw_heat_transfer_T [2]*A_w_hta_sub*(Ts_ave_1phase_test{18.5175} -T_w_ave_T[2])
A_g_hta_test=PI*D_vo*L_test

"Determine the heat transfer coefficient of the refrigerant"
1/(UA_T[2])=1/(h_g_1_phase_heat_transfer[3]*A_g_hta_test)+(ln(D_vo/D_vi)/(2*PI*k_copper[4]*L_test))+1/(hw_heat_transfer
_T [2]*A_w_hta_test)
k_copper[4]=k_('Copper', T_g_ave_1_phase[3])/1000

"Friction factor"
f_straight[4]=0.25/(D_5)^2
D_5=log10((0.0015/(3.7*Dh_g))+(5.74/Re_g_1_phase[3]^0.9))
```

```
f_helical[4]=4*(0.079*Re_g_1_phase[3]^(-0.25)+(0.0075*(Dh_g/d_coil_T)^0.5)+(17.5782*Re_g_1_phase[3]^(-
0.3137)*(Dh_g/d_coil_T)^0.361*(0.0015/Dh_g)^0.6885))
r_f_g[4]=f_helical[4]/f_straight[4]

"Nusselt number and heat transfer coefficient"
Nusselt_g_1_phase[4]=Nusselt_g_gas_4(Re_g_1_phase[3],elstar,plstar,thetalstar,r_f_g[4],e_h_4,Pr_g_1_phase[3])
h_g_1_phase_heat_transfer [3]=(Nusselt_g_1_phase[4]*k_g_1_phase[3])/Dh_g

"Pressure drops"
P[3]=P[2]-DELTAP_ref[4]

"Density of R-407C"
rho_g_1_phase_P_in[3]=DENSITY(R407C,T=T_g[2],P=P[2])
rho_g_1_phase_P_out[3]=DENSITY(R407C,T=T_g[3],P=P[3])

"Viscocity"
mu_g_1_phase_P_in[3]=VISCOSITY(R407C,T=T_g[2],P=P[2])
mu_g_1_phase_P_out[3]=VISCOSITY(R407C,T=T_g[3],P=P[3])

DELTAP_ref[4]=SPPD_3(m_R407C,Area_g,
Dh_g,L_test,rho_g_1_phase_P_in[3],rho_g_1_phase_P_out[3],mu_g_1_phase_P_in[3],mu_g_1_phase_P_out[3],f_straight[4],r_f
_g[4],e_f_g[4])


"----------SUB-COOLER----------"

"----------Water side----------"

"Heat Transfer of  Water over Test-Cooler"
"Average water temperature over test-cooler"
T_w_ave_T[3]=(T_w[5]+T_w[6])/2

"Density of water"
rho_w_T[3]=DENSITY(Water,T=T_w_ave_T[3],P=85)

"Conductivity of the water"
k_w_T[3]=CONDUCTIVITY(Water,T=T_w_ave_T[3],P=85)/1000

"Water Velocity"
m_dot_w_sub[3] = rho_w_T[3]*V_water_T[3]*Area_w

"Viscocity"
mu_w_T[3]=VISCOSITY(Water,T=T_w_ave_T[3],P=85)

"Reynolds number"
Re_w_T[3]=(rho_w_T[3]*V_water_T[3]*D_vi)/mu_w_T[3]

"Prandtl number"
Pr_w_T[3]=PRANDTL(Water,T=T_w_ave_T[3],P=85)
```

```
"Heat Transfer Coefficient of the water"
hw_heat_transfer_T [3]=(Nusselt_w_T[3]*k_w_T[3])/D_vi
Nusselt_w_T[3]=Nusselt_w_1(Re_w_T[3],elstar,plstar,thetalstar,Pr_w_T[3])

"Heat Transfer"
Q_W_T[3]=m_dot_w_sub[3]*CP_w_sub*(T_w[6]-T_w[5])
Q_G_T[3]=m_R407C*(h_g[3]-h_g[4])
Q_R_T[3]=Q_W_T[3]/Q_G_T[3]

"LMTD-method"
DELTAT_1[3]=(T_g[3]-T_w[6])
DELTAT_2[3]=(T_g[4]-T_w[5])

DELTAT_lm[3]=(DELTAT_1[3]-DELTAT_2[3])/(ln(DELTAT_1[3]/DELTAT_2[3]))

"U_water"
Q_W_T[3]=UA_T[3] *DELTAT_lm[3]
U_water[3]*A_w_hta_sub=UA_T[3]


"---------- R22 in the liquid phase----------"

"Determine  Heat Transfer Coefficent of the Refrigerant"
T_g_ave_1_phase[4]=(T_g[3]+T_g[4])/2
P_g_ave_1_phase[4]=(P[3]+P[4])/2

"Prandtl number"
Pr_g_1_phase[4]=PRANDTL(R407C,T=T_g_ave_1_phase[4],P=P_g_ave_1_phase[4])

"Reynolds number"
Re_g_1_phase[4]=({Massflux[1]}rho_g_1_phase[4]*V_g_1_phase[4]*Dh_g)/mu_g_1_phase[4]

"Density of R-407C"
rho_g_1_phase[4]=DENSITY(R407C,T=T_g_ave_1_phase[4],P=P_g_ave_1_phase[4])

"Conductivity of the water"
k_g_1_phase[4]=CONDUCTIVITY(R407C,T=T_g_ave_1_phase[4],P=P_g_ave_1_phase[4])/1000

"R-407CVelocity"
m_R407C= rho_g_1_phase[4]*V_g_1_phase[4]*Area_g

"Viscocity"
mu_g_1_phase[4]=VISCOSITY(R407C,T=T_g_ave_1_phase[4],P=P_g_ave_1_phase[4])

"Determine lenght in the gas region"
Q_W_T[3]=hw_heat_transfer_T [3]*A_w_hta_sub*(Ts_ave_1phase_sub{18.5175} -T_w_ave_T[3])
A_g_hta_sub=PI*D_vo*L_sub

"Determine the heat transfer coefficient of the refrigerant"
1/(UA_T[3])=1/(h_g_1_phase_heat_transfer[4]*A_g_hta_sub)+(ln(D_vo/D_vi)/(2*PI*k_copper[5]*L_sub))+1/(hw_heat_transfer
_T [3]*A_w_hta_sub)
```

```
k_copper[5]=k_('Copper', T_g_ave_1_phase[4])/1000

"Friction factor"
f_straight[5]=0.25/(D_6)^2
D_6=log10((0.0015/(3.7*Dh_g))+(5.74/Re_g_1_phase[4]^0.9))
f_helical[5]=4*(0.079*Re_g_1_phase[4]^(0.25)+(0.0075*(Dh_g/d_coil_T)^0.5)+(17.5782*Re_g_1_phase[4]^(0.3137)*(Dh_g/d_
coil_T)^0.361*(0.0015/Dh_g)^0.6885))
r_f_g[5]=f_helical[5]/f_straight[5]

"Nusselt number and heat transfer coefficient"
Nusselt_g_1_phase[5]=Nusselt_g_gas_5(Re_g_1_phase[4],elstar,plstar,thetalstar,r_f_g[5],e_h_5,Pr_g_1_phase[4])
h_g_1_phase_heat_transfer [4]=(Nusselt_g_1_phase[5]*k_g_1_phase[4])/Dh_g

"Pressure drops"
P[4]=P[3]-DELTAP_ref[5]

"Density of R-407C"
rho_g_1_phase_P_in[4]=DENSITY(R407C,T=T_g[3],P=P[3])
rho_g_1_phase_P_out[4]=DENSITY(R407C,T=T_g[4],P=P[4])

"Viscocity"
mu_g_1_phase_P_in[4]=VISCOSITY(R407C,T=T_g[3],P=P[3])
mu_g_1_phase_P_out[4]=VISCOSITY(R407C,T=T_g[4],P=P[4])

DELTAP_ref[5]=SPPD_4(m_R407C,Area_g,
Dh_g,L_sub,rho_g_1_phase_P_in[4],rho_g_1_phase_P_out[4],mu_g_1_phase_P_in[4],mu_g_1_phase_P_out[4],f_straight[5],r_f
_g[5],e_f_g[5])
```

APPENDIX B

R407-C Experimental data

PART A

The specific numbers, as listed in the table below, represents a measuring device which measured the experimental data of R-407C from the test facility.

Numbering of the measurement	Description
T1	Temperature: Inlet at Pre-cooler (refrigerant)
T2	Temperature: Outlet Pre-cooler / Inlet Test-cooler (refrigerant)
T3	Temperature: Outlet Test-cooler / Inlet Sub-cooler (refrigerant)
T4	Temperature: Outlet Sub-cooler (refrigerant)
T5	Pre-cooler inlet (Water)
T6	Pre-cooler outlet (Water)
T7	Test-cooler inlet (Water)
T8	Test-cooler outlet (Water)
T9	Sub-cooler inlet (Water)
T10	Sub-cooler outlet (Water)
P1	Pressure: Inlet at Pre-cooler (refrigerant)
P2	Pressure: Outlet Pre-cooler / Inlet Test-cooler (refrigerant)
P3	Pressure: Outlet Test-cooler / Inlet Sub-cooler (refrigerant)
P4	Pressure: Outlet Sub-cooler (refrigerant)
M1	Mass flow rate in Pre-cooler (water)
M2	Mass flow rate in Test-cooler (water)
M3	Mass flow rate in Sub-cooler (water)
M4	Mass flow rate in Test Condenser (refrigerant)

Fluted tube no.1: Refrigerant mass flow rate = 0.02 kg/s										
no.	**T1 (°C)**	**T2 (°C)**	**T3 (°C)**	**T4 (°C)**	**T5 (°C)**	**T6 (°C)**	**T7 (°C)**	**T8 (°C)**	**T9 (°C)**	**T10 (°C)**
1	72.02	21.59	13.31	13.21	13.45	37.62	13.27	14.40	13.00	13.15
2	72.27	22.36	16.27	16.21	16.36	39.45	16.25	17.01	16.02	16.17
3	75.00	25.47	20.39	20.38	20.34	41.78	20.25	21.05	20.29	20.38
4	72.52	15.51	13.04	12.95	13.07	31.83	13.00	13.46	12.84	12.95
5	74.19	18.23	16.23	16.19	16.35	33.55	16.05	16.57	16.01	16.12
6	73.29	21.64	19.75	19.73	19.81	35.83	19.70	20.03	19.63	19.69
7	72.83	14.29	13.17	13.16	13.19	27.18	13.08	13.36	12.95	13.07
8	73.95	16.37	15.35	15.29	15.37	28.87	15.24	15.47	15.16	15.24
9	73.64	20.49	19.46	19.43	19.68	32.34	19.31	19.57	19.38	19.41

Fluted tube no.1: Refrigerant mass flow rate = 0.02 kg/s									
no.	**M1 (kg/s)**	**M2 (kg/s)**	**M3 (kg/s)**	**M4 (kg/s)**	**P1 (kPa)**	**P2 (kPa)**	**P3 (kPa)**	**P4 (kPa)**	**P5 (kPa)**
1	0.0516	0.0495	0.0501	0.0230	1632	1597	1588	1579	514.9
2	0.0513	0.0497	0.0501	0.0223	1749	1723	1714	1706	511.4
3	0.0502	0.0544	0.0517	0.0208	1815	1796	1788	1779	510.2
4	0.0685	0.0672	0.0723	0.0232	1642	1612	1602	1597	508.1
5	0.0688	0.0723	0.0709	0.0222	1773	1748	1739	1730	512.9
6	0.0704	0.0692	0.0665	0.0213	1804	1789	1780	1772	502.3
7	0.0885	0.0907	0.0917	0.0223	1657	1633	1624	1615	502
8	0.0907	0.0929	0.0930	0.0222	1738	1716	1707	1698	509.6
9	0.0892	0.0903	0.0927	0.0213	1811	1800	1792	1783	497.8

Fluted tube no.1: Refrigerant mass flow rate = 0.03 kg/s										
no.	**T1 (°C)**	**T2 (°C)**	**T3 (°C)**	**T4 (°C)**	**T5 (°C)**	**T6 (°C)**	**T7 (°C)**	**T8 (°C)**	**T9 (°C)**	**T10 (°C)**
10	72.05	37.50	14.73	14.04	14.26	42.33	14.09	21.99	13.82	13.99
11	75.02	41.24	18.32	17.47	17.72	45.74	17.57	25.11	17.29	17.47
12	76.77	42.42	21.52	21.01	21.19	46.86	20.92	27.62	20.81	20.95
13	75.84	19.64	11.75	11.72	11.90	37.50	11.53	12.94	11.53	11.67
14	77.17	23.88	16.85	16.82	16.75	39.40	16.52	18.39	16.65	16.75
15	83.14	30.94	21.52	21.39	20.85	46.00	21.45	22.90	21.18	21.48
16	78.47	14.93	11.55	11.54	11.91	32.45	11.40	12.25	11.36	11.43
17	78.07	19.11	15.60	15.58	15.53	35.20	15.49	16.20	15.40	15.50
18	82.50	25.73	21.51	21.48	21.56	41.11	21.50	21.97	21.35	21.45

Fluted tube no.1: Refrigerant mass flow rate = 0.03 kg/s									
no.	**M1 (kg/s)**	**M2 (kg/s)**	**M3 (kg/s)**	**M4 (kg/s)**	**P1 (kPa)**	**P2 (kPa)**	**P3 (kPa)**	**P4 (kPa)**	**P5 (kPa)**
10	0.0544	0.0477	0.0491	0.0314	1650	1541	1526	1522	527.8
11	0.0510	0.0517	0.0529	0.0333	1828	1718	1703	1699	539.5
12	0.0535	0.0494	0.0486	0.0298	1845	1760	1752	1748	513.9
13	0.0685	0.0701	0.0708	0.0324	1765	1687	1669	1652	506.8
14	0.0707	0.0716	0.0725	0.0311	1888	1825	1809	1797	508
15	0.0713	0.0703	0.0731	0.0350	2125	2061	2040	2008	529.8
16	0.0914	0.0917	0.0917	0.0338	1864	1800	1782	1774	509
17	0.0886	0.0894	0.0910	0.0321	1925	1869	1852	1838	505.6
18	0.0923	0.0941	0.0942	0.0338	2077	2013	1995	1987	527.2

Fluted tube no.1: Refrigerant mass flow rate = 0.05 kg/s										
no.	**T1 (°C)**	**T2 (°C)**	**T3 (°C)**	**T4 (°C)**	**T5 (°C)**	**T6 (°C)**	**T7 (°C)**	**T8 (°C)**	**T9 (°C)**	**T10 (°C)**
19	66.05	38.24	29.90	15.00	13.49	44.63	13.79	33.44	13.54	17.00
20	67.32	40.64	32.05	18.73	16.59	46.98	16.77	39.00	16.60	19.70
21	64.46	40.87	34.25	27.09	20.64	46.68	20.88	36.31	20.55	30.72
22	72.41	40.43	13.93	11.83	11.61	44.53	11.98	21.72	11.54	12.08
23	68.00	39.57	20.70	16.85	16.55	44.44	16.78	29.07	16.49	17.80
24	63.53	37.61	31.53	21.60	20.71	42.61	20.86	31.78	20.61	24.00
25	72.90	35.08	11.50	10.63	10.43	39.19	10.82	16.30	10.40	10.65
26	69.39	39.76	17.47	16.33	16.20	42.41	16.47	22.32	16.13	16.35
27	70.13	41.85	21.62	20.06	20.04	44.83	20.20	27.36	19.87	20.09

Fluted tube no.1: Refrigerant mass flow rate = 0.05 kg/s									
no.	**M1 (kg/s)**	**M2 (kg/s)**	**M3 (kg/s)**	**M4 (kg/s)**	**P1 (kPa)**	**P2 (kPa)**	**P3 (kPa)**	**P4 (kPa)**	**P5 (kPa)**
19	0.0528	0.0523	0.0481	0.0526	1827	1523	1369	1357	510.6
20	0.0519	0.0491	0.0461	0.0531	1919	1622	1446	1434	509.5
21	0.0481	0.0504	0.0489	0.0511	1919	1639	1438	1390	500
22	0.0705	0.0708	0.0711	0.0542	1942	1679	1645	1633	523.5
23	0.0722	0.0713	0.0685	0.0540	1900	1611	1543	1532	500.3
24	0.0716	0.0736	0.0706	0.0515	1807	1510	1342	1332	494.4
25	0.0920	0.0882	0.0920	0.0536	1801	1535	1512	1501	522.5
26	0.0920	0.0901	0.0920	0.0536	1801	1542	1512	1501	522.5
27	0.0899	0.0874	0.0936	0.0538	1996	1747	1708	1698	497.3

Fluted tube no.2: Refrigerant mass flow rate = 0.02 kg/s										
no.	T1 (°C)	T2 (°C)	T3 (°C)	T4 (°C)	T5 (°C)	T6 (°C)	T7 (°C)	T8 (°C)	T9 (°C)	T10 (°C)
1	73.58	17.82	13.37	13.30	13.74	38.80	13.11	14.17	13.27	13.30
2	63.79	32.31	15.75	15.55	15.37	34.79	15.50	19.65	15.51	15.54
3	63.06	39.40	21.60	21.31	21.25	41.63	21.50	24.63	21.20	21.37
4	74.43	15.00	12.90	12.77	12.89	31.01	12.89	13.21	12.58	12.74
5	65.28	23.57	15.62	15.51	15.81	32.76	15.43	16.95	15.46	15.52
6	64.48	27.75	20.72	20.62	20.78	37.04	20.69	21.55	20.48	20.60
7	75.28	14.19	12.61	12.57	12.61	27.26	12.60	12.85	12.38	12.53
8	65.54	19.86	15.73	15.68	15.65	29.75	15.73	16.20	15.55	15.65

Fluted tube no.2: Refrigerant mass flow rate = 0.02 kg/s									
no.	M1 (kg/s)	M2 (kg/s)	M3 (kg/s)	M4 (kg/s)	P1 (kPa)	P2 (kPa)	P3 (kPa)	P4 (kPa)	P5 (kPa)
1	0.0501	0.0501	0.0513	0.0237	2085	2066	2059	481	514.9
2	0.0547	0.0511	0.0509	0.0222	1393	1341	1338	490	511.4
3	0.0504	0.0524	0.0504	0.0241	1735	1690	1691	477	510.2
4	0.0722	0.0695	0.0729	0.0240	2110	2095	2088	478	508.1
5	0.0716	0.0697	0.0693	0.0242	1488	1447	1440	492	512.9
6	0.0716	0.0726	0.0714	0.0237	1678	1644	1637	481	502.3
7	0.0908	0.0926	0.0920	0.0241	2126	2112	2105	475	502
8	0.0897	0.0923	0.0937	0.0241	1509	1475	1468	487	509.6

Fluted tube no.2: Refrigerant mass flow rate = 0.03 kg/s										
no.	T1 (°C)	T2 (°C)	T3 (°C)	T4 (°C)	T5 (°C)	T6 (°C)	T7 (°C)	T8 (°C)	T9 (°C)	T10 (°C)
9	69.66	27.21	13.38	12.94	13.24	42.17	12.94	15.95	12.76	13.05
10	70.10	40.71	16.96	16.31	16.17	44.20	16.69	21.74	16.14	16.29
11	59.35	38.45	25.43	21.20	21.02	41.85	22.20	32.38	20.93	21.40
12	69.76	17.95	12.27	12.11	12.56	34.83	12.11	13.50	11.93	12.15
13	71.32	26.87	16.04	15.82	16.09	38.42	15.68	18.29	15.75	15.86
14	60.63	37.42	21.17	20.36	20.31	39.13	20.67	25.54	20.21	20.33
15	69.78	14.90	11.68	11.62	11.80	28.68	11.52	12.35	11.44	11.66
16	71.39	21.38	15.57	15.44	15.66	33.69	15.43	16.58	15.31	15.44
17	82.50	25.73	21.51	21.48	21.56	41.11	21.50	22.00	21.35	21.45

Fluted tube no.2: Refrigerant mass flow rate = 0.03 kg/s									
no.	M1 (kg/s)	M2 (kg/s)	M3 (kg/s)	M4 (kg/s)	P1 (kPa)	P2 (kPa)	P3 (kPa)	P4 (kPa)	P5 (kPa)
9	0.0533	0.0530	0.0523	0.0310	1931	1880	1868	1857	482.5
10	0.0527	0.0528	0.0484	0.0322	1820	1746	1737	1734	516.2
11	0.0509	0.0500	0.0491	0.0328	1661	1554	1525	1522	473
12	0.0726	0.0741	0.0763	0.0311	1903	1867	1855	1839	484
13	0.0692	0.0721	0.0680	0.0316	1755	1698	1686	1684	515.6
14	0.0709	0.0720	0.0705	0.0335	1647	1550	1537	1534	465.3
15	0.0971	0.0910	0.0929	0.0311	1882	1851	1840	1824	487.1
16	0.0899	0.0929	0.0936	0.0314	1717	1667	1656	1648	514.2
17	0.0911	0.0882	0.0912	0.0340	1657	1568	1558	1557	460.8

Fluted tube no.2: Refrigerant mass flow rate = 0.05 kg/s										
no.	**T1 (°C)**	**T2 (°C)**	**T3 (°C)**	**T4 (°C)**	**T5 (°C)**	**T6 (°C)**	**T7 (°C)**	**T8 (°C)**	**T9 (°C)**	**T10 (°C)**
18	69.12	42.45	19.71	12.45	11.73	47.31	11.67	31.93	11.51	14.67
19	63.32	41.10	30.56	17.57	16.15	46.64	16.02	35.38	16.18	21.46
20	66.86	44.97	34.77	21.74	20.27	50.05	20.20	39.83	20.41	25.68
21	69.43	41.11	13.99	11.53	11.36	43.44	11.39	21.30	11.20	12.43
22	63.82	39.85	19.52	15.84	15.63	43.50	15.46	27.68	15.77	16.91
23	66.06	43.19	24.26	20.39	20.21	46.74	20.03	32.24	20.25	21.38
24	69.51	34.08	12.50	11.40	11.30	39.76	11.38	15.88	11.18	12.01
25	65.09	40.39	17.09	15.75	15.68	41.61	15.53	21.23	15.78	16.33
26	65.59	41.88	20.73	19.41	19.30	43.09	19.21	24.96	19.37	19.88

Fluted tube no.2: Refrigerant mass flow rate = 0.05 kg/s									
no.	**M1 (kg/s)**	**M2 (kg/s)**	**M3 (kg/s)**	**M4 (kg/s)**	**P1 (kPa)**	**P2 (kPa)**	**P3 (kPa)**	**P4 (kPa)**	**P5 (kPa)**
18	0.0526	0.0482	0.0503	0.0534	1962	1731	1677	1641	510.7
19	0.0513	0.0497	0.0486	0.0525	1923	1683	1590	1572	503.7
20	0.0489	0.0515	0.0489	0.0534	2115	1894	1811	1794	486.8
21	0.0726	0.0689	0.0703	0.0543	1931	1720	1694	1657	501.9
22	0.0693	0.0720	0.0739	0.0547	1906	1667	1629	1609	489.1
23	0.0713	0.0697	0.0739	0.0536	2046	1830	1790	1772	484.2
24	0.0928	0.0902	0.0889	0.0547	1909	1730	1707	1669	494.0
25	0.0914	0.0914	0.0929	0.0544	1939	1744	1721	1702	482.0
26	0.0954	0.0947	0.0903	0.0540	1995	1803	1779	1761	482.4

Fluted tube no.3: Refrigerant mass flow rate = 0.02 kg/s										
no.	**T1 (°C)**	**T2 (°C)**	**T3 (°C)**	**T4 (°C)**	**T5 (°C)**	**T6 (°C)**	**T7 (°C)**	**T8 (°C)**	**T9 (°C)**	**T10 (°C)**
1	76.37	14.59	11.98	11.74	11.84	34.88	11.57	12.21	11.66	11.75
2	77.48	20.02	16.04	15.93	15.39	38.20	15.30	16.10	15.82	15.90
3	83.78	24.90	20.63	20.57	20.65	43.78	20.00	20.81	19.97	20.46
4	71.83	14.01	11.14	11.06	11.14	30.49	10.94	11.45	10.94	10.98
5	79.82	17.42	15.81	15.81	15.85	32.89	15.69	15.89	15.30	15.70
6	84.72	22.47	20.26	20.23	20.38	38.12	20.15	20.39	19.57	20.20
7	70.32	11.93	10.61	10.54	10.40	24.11	10.43	10.70	10.45	10.58

Fluted tube no.3: Refrigerant mass flow rate = 0.02 kg/s									
no.	**M1 (kg/s)**	**M2 (kg/s)**	**M3 (kg/s)**	**M4 (kg/s)**	**P1 (kPa)**	**P2 (kPa)**	**P3 (kPa)**	**P4 (kPa)**	**P5 (kPa)**
1	0.0538	0.0544	0.0483	0.0220	1797	1774	1768	1758	412.8
2	0.0505	0.0521	0.0528	0.0215	1810	1788	1780	1771	436.3
3	0.0524	0.0518	0.0540	0.0230	2061	2038	2030	2019	453.7
4	0.0687	0.0709	0.0723	0.0237	1590	1561	1553	1543	400.1
5	0.0703	0.0737	0.0749	0.0219	1860	1844	1834	1824	432.6
6	0.0695	0.0726	0.0696	0.0231	2076	2058	2049	2039	448.6
7	0.0908	0.0931	0.0907	0.0223	1464	1441	1434	1424	387.2

Fluted tube no.3: Refrigerant mass flow rate = 0.03 kg/s										
no.	T1 (°C)	T2 (°C)	T3 (°C)	T4 (°C)	T5 (°C)	T6 (°C)	T7 (°C)	T8 (°C)	T9 (°C)	T10 (°C)
8	63.17	28.21	13.33	10.28	9.99	33.40	9.94	22.31	10.13	10.79
9	64.85	33.41	20.40	16.27	15.75	36.73	16.07	27.44	16.10	16.85
10	71.48	41.19	21.96	20.20	19.35	44.23	20.05	32.08	19.99	20.48
11	62.57	28.04	11.30	10.79	10.65	30.97	10.61	17.00	10.71	10.94
12	65.20	31.43	15.31	14.83	14.72	33.61	14.73	20.12	14.44	14.80
13	74.69	41.48	22.05	20.17	20.02	41.82	20.09	24.21	19.99	20.21
14	65.62	22.16	10.59	10.50	10.52	28.59	10.28	12.00	10.42	10.52
15	65.19	30.41	14.58	14.34	14.81	31.10	14.24	17.25	13.96	14.23

Fluted tube no.3: Refrigerant mass flow rate = 0.03 kg/s									
no.	M1 (kg/s)	M2 (kg/s)	M3 (kg/s)	M4 (kg/s)	P1 (kPa)	P2 (kPa)	P3 (kPa)	P4 (kPa)	P5 (kPa)
8	0.0501	0.0498	0.0477	0.0320	1287	1142	1110	1094	426
9	0.0522	0.0520	0.0514	0.0314	1416	1291	1256	1241	444.8
10	0.0479	0.0493	0.0498	0.0340	1733	1622	1596	1579	479
11	0.0697	0.0686	0.0679	0.0329	1295	1166	1149	1133	417.3
12	0.0706	0.0714	0.0729	0.0317	1372	1259	1240	1223	425.6
13	0.0719	0.0697	0.0748	0.0336	1770	1686	1672	1655	469.3
14	0.0928	0.0872	0.0901	0.0320	1342	1258	1245	1230	402.9
15	0.0889	0.0917	0.0928	0.0320	1354	1253	1238	1221	415.9

Fluted tube no.3: Refrigerant mass flow rate = 0.05 kg/s										
no.	T1 (°C)	T2 (°C)	T3 (°C)	T4 (°C)	T5 (°C)	T6 (°C)	T7 (°C)	T8 (°C)	T9 (°C)	T10 (°C)
16	75.77	44.69	15.76	11.28	10.85	50.26	10.65	31.15	10.83	12.24
17	66.82	40.22	33.67	17.93	16.13	46.01	16.47	35.85	16.53	21.21
18	66.49	42.35	38.70	22.14	19.88	47.51	20.50	37.16	20.52	25.99
19	77.20	42.16	12.06	10.89	10.47	44.26	10.63	18.83	10.74	11.19
20	66.45	38.05	18.67	15.46	14.82	41.89	15.17	26.95	15.19	16.20
21	67.06	40.20	25.94	20.71	19.71	44.61	20.34	32.17	20.31	21.89
22	69.33	33.57	11.78	10.82	10.67	35.73	10.65	17.03	10.69	11.04
23	66.93	37.08	16.34	15.12	14.96	38.92	14.95	22.82	14.97	15.38
24	67.26	39.59	21.52	20.06	19.89	42.03	19.88	28.03	19.86	20.35

Fluted tube no.3: Refrigerant mass flow rate = 0.05 kg/s									
no.	M1 (kg/s)	M2 (kg/s)	M3 (kg/s)	M4 (kg/s)	P1 (kPa)	P2 (kPa)	P3 (kPa)	P4 (kPa)	P5 (kPa)
16	0.0480	0.0485	0.0517	0.0517	2013	1789	1748	1715	492.7
17	0.0494	0.0525	0.0510	0.0521	1844	1567	1471	1438	475.8
18	0.0533	0.0549	0.0528	0.0526	1939	1664	1560	1524	459.5
19	0.0719	0.0699	0.0685	0.0514	1929	1750	1723	1691	477.9
20	0.0717	0.0716	0.0721	0.0530	1765	1500	1447	1414	465.8
21	0.0717	0.0723	0.0713	0.0532	1873	1610	1545	1511	458.8
22	0.0885	0.0933	0.0935	0.0516	1593	1354	1321	1288	460.2
23	0.0844	0.0928	0.0936	0.0535	1726	1488	1452	1418	459.2
24	0.0917	0.0909	0.0925	0.0535	1825	1584	1540	1506	461.7

PART B

In this section the experimental data of R22 from the test facility are listed.

Fluted tube no.3: Refrigerant mass flow rate = 0.05 kg/s										
no.	**T1 (°C)**	**T2 (°C)**	**T3 (°C)**	**T4 (°C)**	**T5 (°C)**	**T6 (°C)**	**T7 (°C)**	**T8 (°C)**	**T9 (°C)**	**T10 (°C)**
1	126.6	39.54	26.9	13.3	12.56	54.12	12.84	33.06	12.47	17.03
2	85.99	38.47	31.02	22.76	17.64	46.31	17.75	33.04	17.54	27.25
3	69.58	42.07	35.25	29.32	22.12	46.78	22.22	37.23	22.1	31.92
4	120.5	33.41	20.48	12.53	33.91	12.19	43.73	12.61	26.2	12.14
5	81.65	34.31	27.24	19.17	17.53	40.18	17.72	28.43	17.44	22.89
5	71.25	37.92	31.23	25.8	22.07	42.3	22.16	32.56	22	27.89
6	117.5	30.49	15.37	12.48	12.29	37.94	12.63	21.51	12.2	12.91
7	78.05	31.15	25.25	17.05	16.76	35.74	16.97	24.94	16.64	19.07
8	81.59	35.47	29.33	23.24	21.96	39.78	22.01	29.8	21.88	25.57

Fluted tube no.3: Refrigerant mass flow rate = 0.05 kg/s									
no.	**M1 (kg/s)**	**M2 (kg/s)**	**M3 (kg/s)**	**M4 (kg/s)**	**P1 (kPa)**	**P2 (kPa)**	**P3 (kPa)**	**P4 (kPa)**	**P5 (kPa)**
1	0.05089	0.05111	0.05465	0.05261	1767	1430	1258	1234	341.3
2	0.05126	0.05327	0.05409	0.05275	1736	1394	1151	1095	591.4
3	0.05045	0.05099	0.05121	0.0522	1806	1512	1269	1209	594.5
4	0.07169	0.07153	0.07118	0.05237	1582	1217	1064	1040	327.1
5	0.07068	0.07035	0.07063	0.05035	1574	1244	1022	987.1	569.6
5	0.0712	0.07124	0.07078	0.05182	1688	1372	1145	1093	598.2
6	0.08995	0.09295	0.09097	0.05084	1482	1123	1016	992.3	312
7	0.09238	0.09351	0.09195	0.04972	1475	1140	966.4	949	558.7
8	0.09149	0.09156	0.0909	0.05048	1605	1286	1087	1049	594.4

APPENDIX C

R407-C Experimental gained Enhancement factors

The specific numbering indication, as listed in the table below, represents the enhancement factor for a specific region.

Numbering indication	Description
$ef_{(liq)}$	Pressure drop enhancement factor for the liquid-phase region
$eh_{(liq)}$	Heat transfer enhancement factor for the liquid-phase region
$ef_{(2)}$	Pressure drop enhancement factor for the two-phase region
$eh_{(2)}$	Heat transfer enhancement factor for the two-phase region
$ef_{(gas)}$	Pressure drop enhancement factor for the gas-phase region
$eh_{(gas)}$	Heat transfer enhancement factor for the gas-phase region

Fluted tube no.1: Refrigerant mass flow rate = 0.02 kg/s

Water mass flow rate = kg/s	ef(liq)	eh(liq)	ef(2)	eh(2)	ef(gas)	eh(gas)	Inlet water temperature (°C)
0.05	3.9025	0.8838	6.68	1.77	3.9025	2.18	10
	4.103	0.8736	4.912	1.45	4.103	2.134	15
	4.106	0.5389	3.387	2.58	4.106	2.06	20
0.07	4.257	1.173	6.02	1.919	4.257	2.4	10
	4.1615	0.94	5.48	1.737	4.1615	2.28	15
	4.14	0.6225	3.57	1.827	4.14	2.24	20
0.09	4.1095	1.31	5.763	1.247	4.1095	2.89	10
	4.151	0.9355	5.381	1.278	4.151	2.77	15
	4.14	0.7581	2.5	1.591	4.14	2.69	20

Fluted tube no.1: Refrigerant mass flow rate = 0.03 kg/s

Water mass flow rate = kg/s	ef(liq)	eh(liq)	ef(2)	eh(2)	ef(gas)	eh(gas)	Inlet water temperature (°C)
0.05	4.022	0.9439	7.51	1.87	4.022	2.26	10
	4.109	0.9197	4.903	2.15	4.109	2.238	15
	4.261	0.8384	4.08	2.29	4.261	2.21	20
0.07	4.136	1.309	7.1	1.84	4.136	2.42	10
	4.154	1.129	4.7	3.034	4.154	2.38	15
	4.459	0.7933	3.077	3.48	4.459	2.34	20
0.09	4.16	1.42	4.84	1.194	4.16	2.98	10
	4.171	1.16	4.11	3.194	4.171	2.81	15
	4.16	0.9049	3.8	3.86	4.16	2.75	20

Fluted tube no.1: Refrigerant mass flow rate = 0.05 kg/s

Water mass flow rate = kg/s	ef(liq)	eh(liq)	ef(2)	eh(2)	ef(gas)	eh(gas)	Inlet water temperature (°C)
0.05	5.053	1.1464	9.6	2.18	5.053	3.21	10
	4.981	0.9904	9.5	2.65	4.981	3.92	15
							20
0.07	4.784	1.684	7.083	2.42	4.784	3.29	10
	4.431	1.21	7.2	3.05	4.431	3.16	15
	4.372	1.065	9.1	3.91	4.372	2.78	20
0.09	4.463	1.744	7.3	3.12	4.463	4.35	10
	4.482	1.267	7.86	3.42	4.482	4.09	15
	4.16	1.032	7.59	4.18	4.16	4.36	20

Fluted tube no.2: Refrigerant mass flow rate = 0.02 kg/s								
Water mass flow rate = kg/s		ef(liq)	eh(liq)	ef(2)	eh(2)	ef(gas)	eh(gas)	Inlet water temperature (°C)
	0.05	5.19	1.016	5.95	2.2769	5.19	2.49	10
		5.149	0.9017	7.9	2.06	5.149	2.4	15
		5.413	0.8044	6.26	2.1025	5.413	2.3	20
	0.07	5.081	1.245	6.92	2.45	5.081	3.5	10
		5.036	1.058	6.86	2.178	5.036	3.45	15
		5.216	0.9334	6.38	2.28	5.216	2.7	20
	0.09	5.137	1.68	6.129	3.243	5.137	3.116	10
		5.063	1.484	6.5	2.161	5.063	3.833	15
								20

Fluted tube no.2: Refrigerant mass flow rate = 0.03 kg/s								
Water mass flow rate = kg/s		ef(liq)	eh(liq)	ef(2)	eh(2)	ef(gas)	eh(gas)	Inlet water temperature (°C)
	0.05	5.512	1.235	6.4	2.91	5.512	3.9	10
		5.379	1.05	7.22	2.59	5.379	3.85	15
		5.286	0.8257	7.87	2.2	5.286	2.3	20
	0.07	5.625	1.453	6.8	2.76	5.625	3.71	10
		5.465	1.227	8.8	2.5949	5.465	2.89	15
		5.056	1.012	9.2	2.467	5.056	2.6	20
	0.09	5.153	1.75	6.08	3.26	5.153	3.32	10
		5.062	1.48	8.4	3.15	5.062	3.31	15
		5.295	1.119	6.4	3.16	5.295	3.1	20

Fluted tube no.2: Refrigerant mass flow rate = 0.05 kg/s								
Water mass flow rate = kg/s		ef(liq)	eh(liq)	ef(2)	eh(2)	ef(gas)	eh(gas)	Inlet water temperature (°C)
	0.05	6.038	1.702	13.154	4.87	6.038	5.84	10
		6.376	1.663	13.5	4.19	6.376	5.8	15
		6.073	1.253	11.8	4.05	6.073	4.62	20
	0.07	6.029	1.996	13	5.49	6.029	6.96	10
		6.708	1.783	13.22	5.39	6.708	6.02	15
		6.027	1.457	12.62	5.22	6.027	5.11	20
	0.09	6.307	2.174	12.8	6.12	6.307	6.52	10
		6.088	1.936	13.01	6.02	6.088	6.39	15
		6.614	1.749	12.7	5.32	6.614	5.74	20

Fluted tube no.3: Refrigerant mass flow rate = 0.02 kg/s								
Water mass flow rate = kg/s		ef(liq)	eh(liq)	ef(2)	eh(2)	ef(gas)	eh(gas)	Inlet water temperature (°C)
	0.05	2.034	0.49	3.97	1.486	2.034	1.53	10
		2.31	0.3054	3.159	1.816	2.31	1.51	15
		2.142	0.3026	2.191	1.908	2.141	1.47	20
	0.07	2.189	0.5301	4.002	1.36	2.189	1.75	10
		2.328	0.3299	2.375	1.01	2.328	1.72	15
		2.294	0.3134	2.278	1.14	2.294	1.721	20
	0.09	1.994	0.6375	3.736	1.322	1.994	2.084	10
								15
								20

Fluted tube no.3: Refrigerant mass flow rate = 0.03 kg/s								
Water mass flow rate = kg/s		ef(liq)	eh(liq)	ef(2)	eh(2)	ef(gas)	eh(gas)	Inlet water temperature (°C)
	0.05	2.241	0.6067	4.13	1.149	2.241	1.78	10
		2.377	0.52	4.05	1.9616	2.377	1.77	15
		2.364	0.49	3.9246	2.45	2.364	1.524	20
	0.07	2.332	0.8682	4.6575	1.6165	2.332	2.08	10
		2.148	0.7954	4.003	1.345	2.148	1.89	15
		2.219	0.7537	3.936	2.0042	2.219	1.775	20
	0.09	2.192	1.051	4.34	2.66	2.192	2.29	10
		2.111	0.9172	4.01	2.14	2.111	2.06	15
								20

Fluted tube no.3: Refrigerant mass flow rate = 0.05kg/s								
Water mass flow rate = kg/s		ef(liq)	eh(liq)	ef(2)	eh(2)	ef(gas)	eh(gas)	Inlet water temperature (°C)
	0.05	2.246	0.7606	3.5468	1.7928	2.246	1.89	10
		2.229	0.6384	4.3	1.532	2.229	1.88	15
		2.39	0.5835	4.89	1.4813	2.39	1.69	20
	0.07	2.299	1.031	4.44	2.7	2.299	2.16	10
		2.258	0.8844	4.43	2.16	2.258	2.1285	15
		2.219	0.8133	4.23	2.13	2.219	2.03	20
	0.09	2.248	1.248	4.46	3.8011	2.248	2.562	10
		2.29	1.048	4.19	3.273	2.29	2.45	15
		2.26	0.909	4.069	3.669	2.26	2.44	20

APPENDIX D

Theoretical data compared to the Experimental data

The specific numbers, listed in the table below, represents a theoretical value compared to an experimental value. The outlet values of the temperature, pressure and enthalpy are compared to the experimental outlet values of the temperature, pressure and enthalpy.

Specific Number Indication	Description
ΔP	Pressure Drop (kPa)
Δh	Enthalpy Drop (kJ/kg.K)
Q	Heat Transfer (kW)
LMTD	Log Mean Temperature Difference (°C)
1 Set	First Set of enhancement factors used
2 Set	Second Set of enhancement factors used
3 Set	Third Set of enhancement factors used

Fluted Tube no.1

Refrigerant mass flow rate = 0.02 kg/s

Water mass flow rate = 0.05 kg/s
Inlet water temperature = 10°C

Experimental Data		Theoretical Data		
		1 Set	2 Set	3 Set
ΔP	44	45	44	46
Δh	238.43	238.5	238.62	240.49
Q	4.77	4.77	4.77	4.81
LMTD	19.6	18.22	18.05	17.8

Water mass flow rate = 0.07 kg/s
Inlet water temperature = 15°C

Experimental Data		Theoretical Data		
		1 Set	2 Set	3 Set
ΔP	34	35	34	33
Δh	234.2	234.66	234.67	235.93
Q	4.68	4.69	4.69	4.72
LMTD	12.68	12.61	12.6	12.21

Water mass flow rate = 0.09 kg/s
Inlet water temperature = 20°C

Experimental Data		Theoretical Data		
		1 Set	2 Set	3 Set
ΔP	19	23.8	26	23
Δh	228.02	228.28	228.74	230.48
Q	4.56	4.57	4.57	4.61
LMTD	10.68	10.3	10.1	9.83

Refrigerant mass flow rate = 0.03 kg/s

Water mass flow rate = 0.07 kg/s
Inlet water temperature = 10°C

Experimental Data		Theoretical Data		
		1 Set	2 Set	3 Set
ΔP	96	83	77	72
Δh	242.97	243.72	243.9	242.46
Q	7.29	7.31	7.32	7.27
LMTD	21.02	21.2	20.89	20.09

Water mass flow rate = 0.09 kg/s
Inlet water temperature = 15°C

Experimental Data		Theoretical Data		
		1 Set	2 Set	3 Set
ΔP	73	65	55	61
Δh	237.06	236.98	236.9	238.69
Q	7.11	7.11	7.11	7.16
LMTD	16.68	16.76	16.84	17.04

Water mass flow rate = 0.05 kg/s
Inlet water temperature = 20°C

Experimental Data		Theoretical Data		
		1 Set	2 Set	3 Set
ΔP	97	98	96	97
Δh	228.34	228.47	228.45	228.94
Q	6.85	6.85	6.85	6.87
LMTD	30.11	30.04	30.05	29.75

Refrigerant mass flow rate = 0.05 kg/s

Water mass flow rate = 0.09 kg/s
Inlet water temperature = 10°C

Experimental Data		Theoretical Data		
		1 Set	2 Set	3 Set
ΔP	300	295	293	340
Δh	241.33	240.82	240.17	239.56
Q	12.07	12.04	12.01	11.98
LMTD	34.87	35.09	35.31	35.5

Water mass flow rate = 0.05 kg/s
Inlet water temperature = 15°C

Experimental Data		Theoretical Data		
		Data	2 Set	3 Set
ΔP	485	482	483	485
Δh	221.21	220.36	219.75	218.31
Q	11.06	11.02	10.99	10.92
LMTD	34.07	35.58	34.91	35.64

Water mass flow rate = 0.07 kg/s
Inlet water temperature = 20°C

Experimental Data		Theoretical Data		
		1 Set	2 Set	3 Set
ΔP	475	475	474	485
Δh	214.36	212.99	212.64	216.71
Q	10.72	10.65	10.63	10.84
LMTD	30.16	30.89	31.07	28.11

Fluted Tube no.2

Refrigerant mass flow rate = 0.02 kg/s

Water mass flow rate = 0.07 kg/s
Inlet water temperature = 10°C

Experimental Data		Theoretical Data		
		1 Set	2 Set	3 Set
ΔP	22	26	19	18
Δh	234.5	235.5	234.5	232.5
Q	4.691	4.709	4.685	4.649
LMTD	14	14.25	14.89	15.22

Water mass flow rate = 0.09 kg/s
Inlet water temperature = 15°C

Experimental Data		Theoretical Data		
		1 Set	2 Set	3 Set
ΔP	41	37	35	31
Δh	229.9	230.6	229.9	226.9
Q	4.598	4.612	4.553	4.538
LMTD	15.37	15.38	17.13	17.44

Water mass flow rate = 0.05 kg/s
Inlet water temperature = 20°C

Experimental Data		Theoretical Data		
		1 Set	2 Set	3 Set
ΔP	47	50	45	45
Δh	215.1	216.3	215.1	211
Q	4.302	4.326	4.254	4.221
LMTD	21.77	22.81	23.68	23.64

Refrigerant mass flow rate = 0.03 kg/s

Water mass flow rate = 0.05 kg/s
Inlet water temperature = 10°C

Experimental Data		Theoretical Data		
		1 Set	2 Set	3 Set
ΔP	63	58	55	51
Δh	231.5	232	231.5	228.2
Q	6.945	6.96	6.955	6.845
LMTD	23.44	23.79	22.75	25.98

Water mass flow rate = 0.09 kg/s
Inlet water temperature = 15°C

Experimental Data		Theoretical Data		
		1 Set	2 Set	3 Set
ΔP	61	50	53	50
Δh	233.1	233.2	233.1	234.8
Q	6.992	6.995	6.948	7.044
LMTD	18.28	18.11	19.44	17.74

Water mass flow rate = 0.07 kg/s
Inlet water temperature = 20°C

Experimental Data		Theoretical Data		
		1 Set	2 Set	3 Set
ΔP	113	115	111	109
Δh	215.6	215.8	215.6	212
Q	6.467	6.475	6.394	6.36
LMTD	23.22	23.15	24.02	24.3

Refrigerant mass flow rate = 0.05 kg/s

Water mass flow rate = 0.09 kg/s
Inlet water temperature = 10°C

Experimental Data		Theoretical Data		
		1 Set	2 Set	3 Set
ΔP	187	155	148	143
Δh	233.2	233.8	233.2	231.3
Q	11.66	11.69	11.58	11.57
LMTD	32.24	31.72	33.66	33.79

Water mass flow rate = 0.07 kg/s
Inlet water temperature = 15°C

Experimental Data		Theoretical Data		
		Data	2 Set	3 Set
ΔP	226	225	223	224
Δh	222.9	222.8	222.9	220.6
Q	11.15	11.14	11.09	11.03
LMTD	31.37	31.46	31.91	32.22

Water mass flow rate = 0.05 kg/s
Inlet water temperature = 15°C

Experimental Data		Theoretical Data		
		1 Set	2 Set	3 Set
ΔP	340	339	325	330
Δh	218.2	217.4	218.2	220.7
Q	10.91	10.87	10.81	11.03
LMTD	34.1	34.77	35.35	31.33

Fluted Tube no.3

Refrigerant mass flow rate = 0.02 kg/s

Water mass flow rate = 0.09 kg/s ***Inlet water temperature = 10°C***

Experimental Data		Theoretical Data		
		1 Set	2 Set	3 Set
ΔP	30	33	38	36
Δh	243.21	243	243.5	243.5
Q	4.86	4.86	4.87	4.87
LMTD	13.66	13.81	13.43	13.36

Water mass flow rate = 0.05 kg/s ***Inlet water temperature = 15°C***

Experimental Data		Theoretical Data		
		1 Set	2 Set	3 Set
ΔP	30	31	33	34
Δh	237.33	237.4	238.3	239.6
Q	4.75	4.75	4.77	4.79
LMTD	18.11	18.04	17.36	17

Water mass flow rate = 0.07 kg/s ***Inlet water temperature = 20°C***

Experimental Data		Theoretical Data		
		1 Set	2 Set	3 Set
ΔP	27	31	30	31
Δh	234.67	235.3	235.3	236.1
Q	4.69	4.71	4.73	4.72
LMTD	15	15.97	15	14.82

Refrigerant mass flow rate = 0.03 kg/s

Water mass flow rate = 0.05 kg/s ***Inlet water temperature = 10°C***

Experimental Data		Theoretical Data		
		1 Set	2 Set	3 Set
ΔP	162	161	172	172
Δh	237.74	237.4	237.6	237.8
Q	7.13	7.12	7.13	7.13
LMTD	27.71	27.83	27.76	27.68

Water mass flow rate = 0.09 kg/s ***Inlet water temperature = 15°C***

Experimental Data		Theoretical Data		
		1 Set	2 Set	3 Set
ΔP	133	123	148	139
Δh	233.95	232.4	234.4	234.5
Q	7.019	6.97	7.03	7.04
LMTD	27.52	27.9	27.35	27.25

Water mass flow rate = 0.07 kg/s ***Inlet water temperature = 20°C***

Experimental Data		Theoretical Data		
		1 Set	2 Set	3 Set
ΔP	115	112	121	128
Δh	228.55	228.8	229.5	230.4
Q	6.86	6.87	6.91	6.90
LMTD	35.28	35.16	34.88	34.15

Refrigerant mass flow rate = 0.05 kg/s

Water mass flow rate = 0.05 kg/s ***Inlet water temperature = 10°C***

Experimental Data		Theoretical Data		
		1 Set	2 Set	3 Set
ΔP	415	402	410	440
Δh	214.53	215.2	216.6	216.9
Q	10.73	10.76	10.83	10.84
LMTD	36.43	35.92	34.56	33.99

Water mass flow rate = 0.07 kg/s ***Inlet water temperature = 15°C***

Experimental Data		Theoretical Data		
		Data	2 Set	3 Set
ΔP	351	369	339	375
Δh	227.65	227	228.3	228.4
Q	11.38	11.35	11.42	11.42
LMTD	31.47	31.88	31.06	30.75

Water mass flow rate = 0.09 kg/s ***Inlet water temperature = 20°C***

Experimental Data		Theoretical Data		
		1 Set	2 Set	3 Set
ΔP	319	329	356	364
Δh	220.35	220.1	221.6	222
Q	11.02	11.01	11.08	11.1
LMTD	27.98	28.12	28.03	27.43

APPENDIX E

Comparing the theoretical data to experimental data on Graphs

FLUTED TUBE no. 1

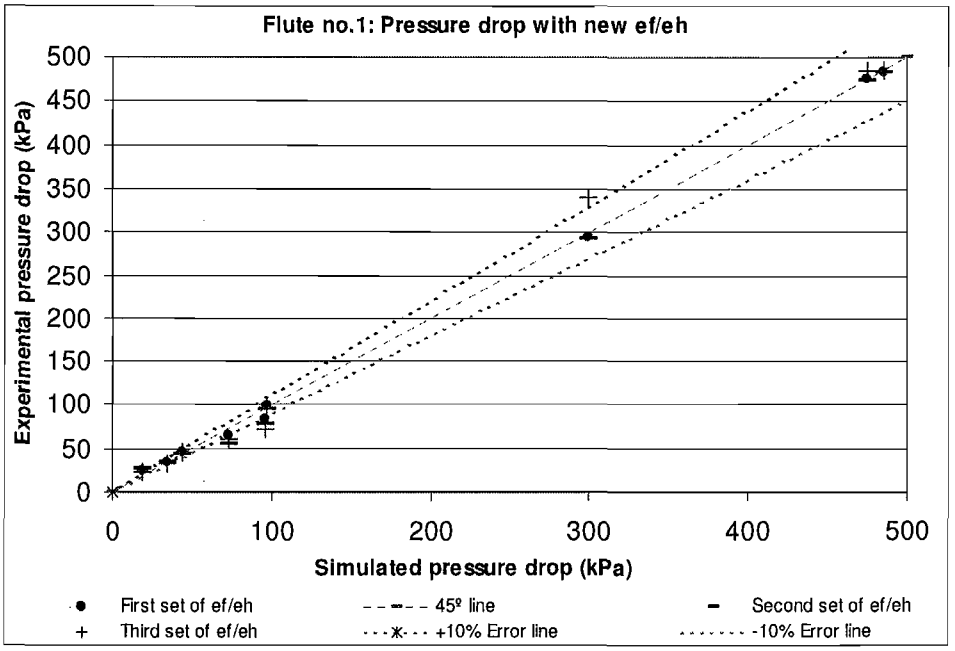


Figure E.1: Simulation of the pressure drop by using the new enhancement factors on fluted tube no.1.

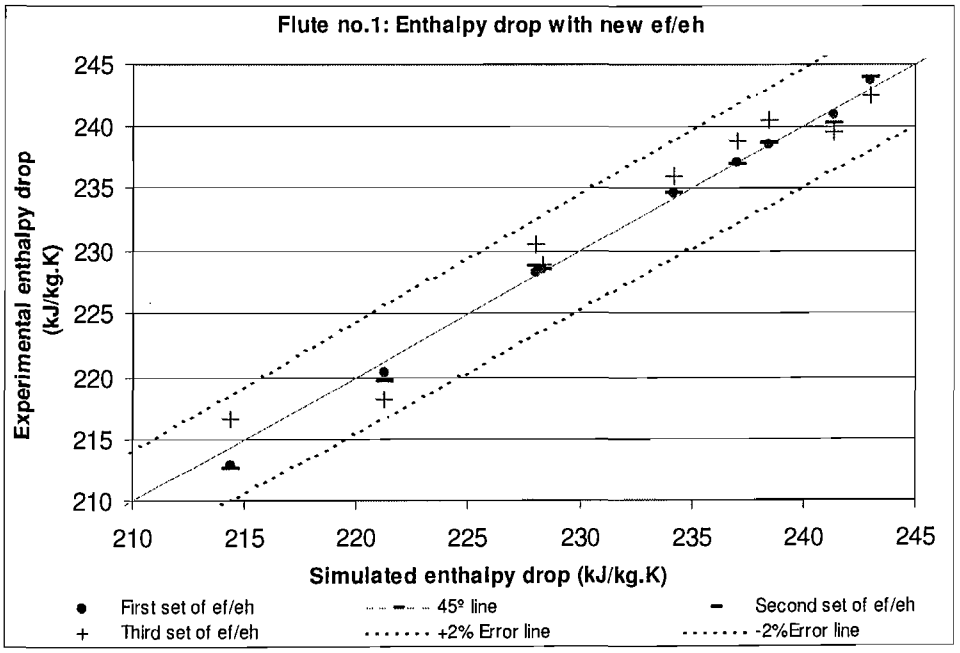


Figure E.2: Simulation of the enthalpy drop by using the new enhancement factors on fluted tube no.1.

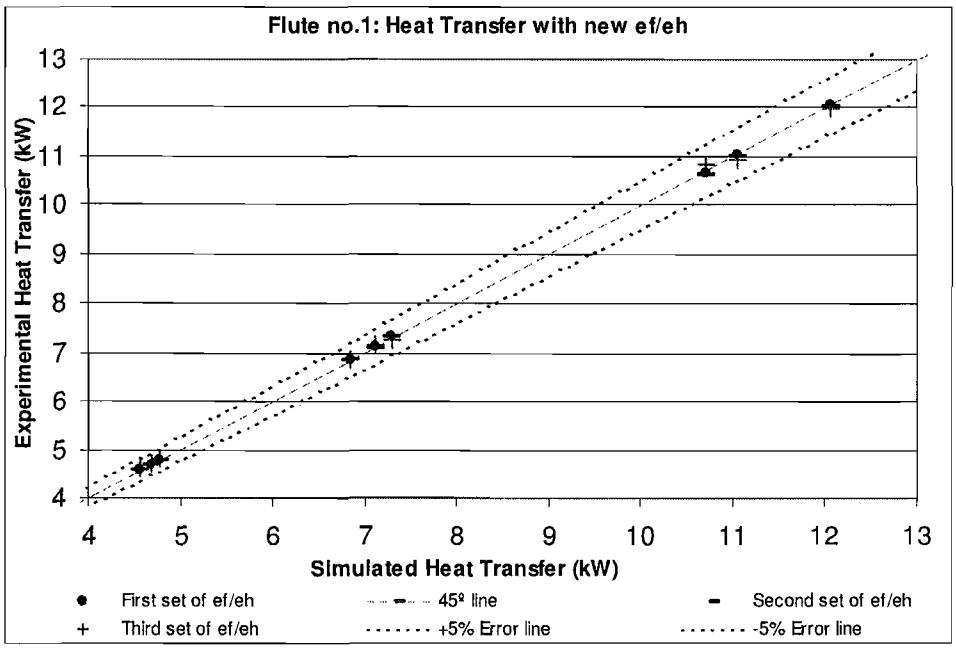


Figure E.3: Simulation of the heat transfer by using the new enhancement factors on fluted tube no.1.

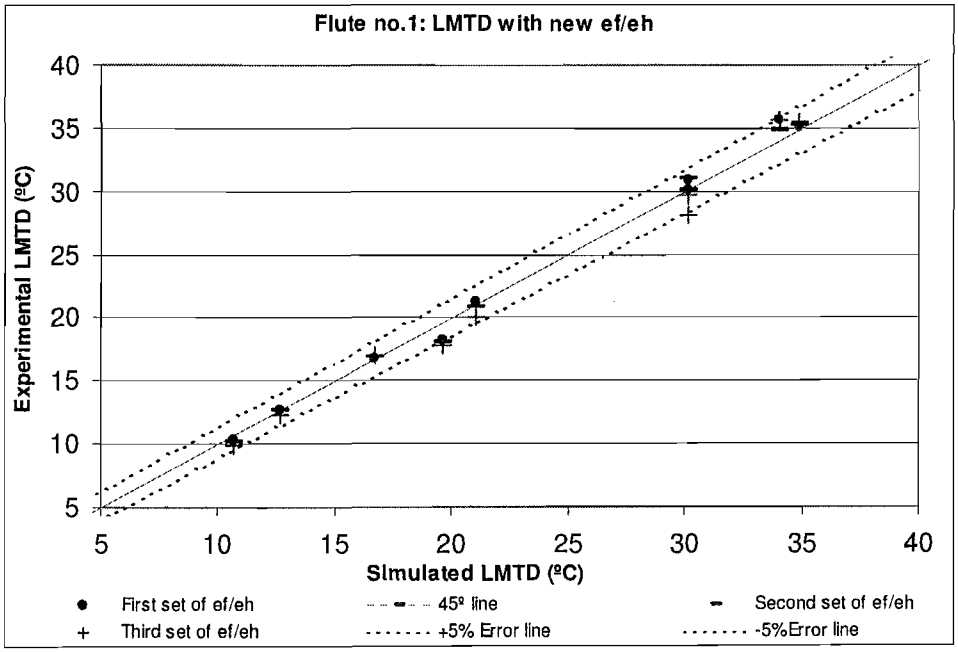


Figure E.4: Simulation of the LMTD by using the new enhancement factors on fluted tube no.1.

FLUTED TUBE no. 2

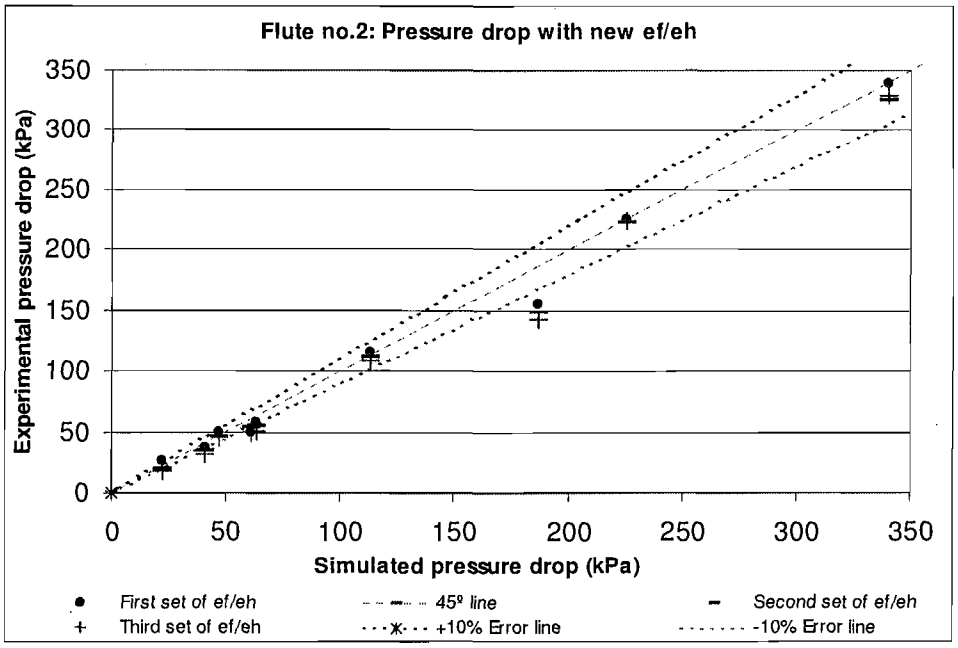


Figure E.5: Simulation of the pressure drop by using the new enhancement factors on fluted tube no.2.

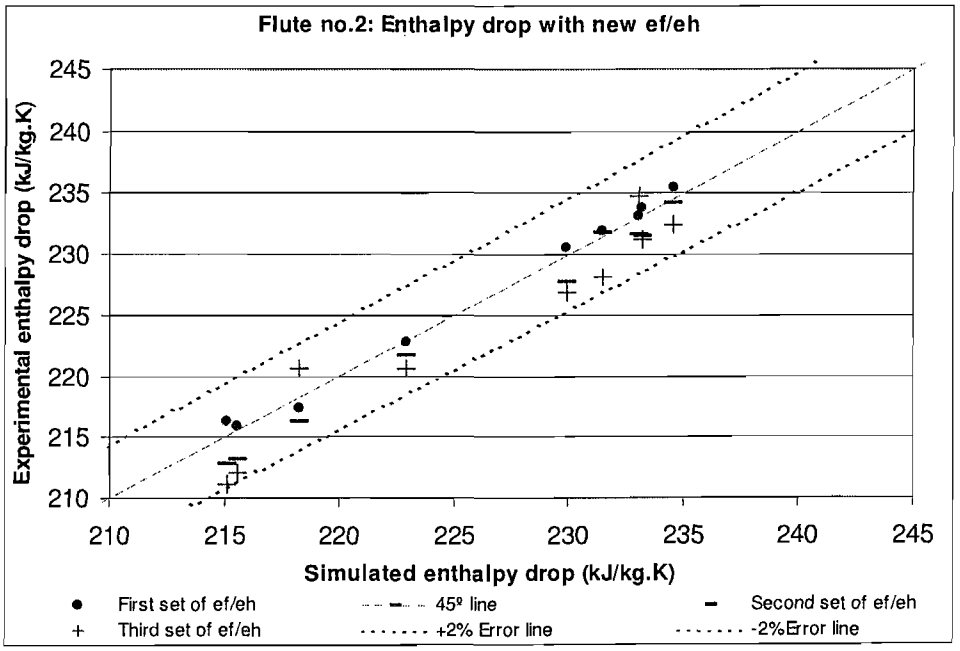


Figure E.6: Simulation of the enthalpy drop by using the new enhancement factors on fluted tube no.2.

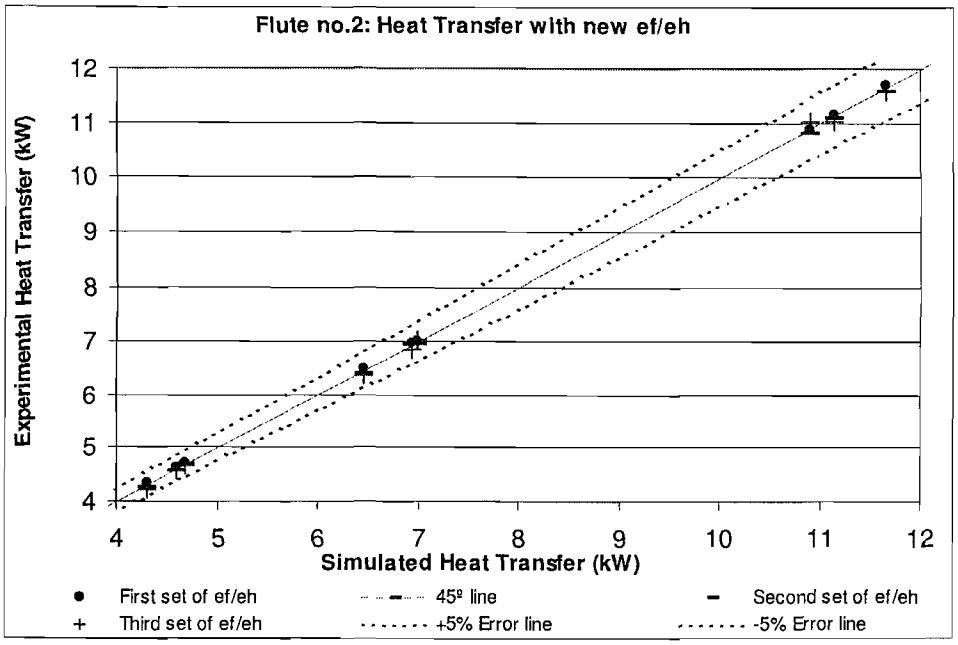


Figure E.7: Simulation of the heat transfer by using the new enhancement factors on fluted tube no.2.

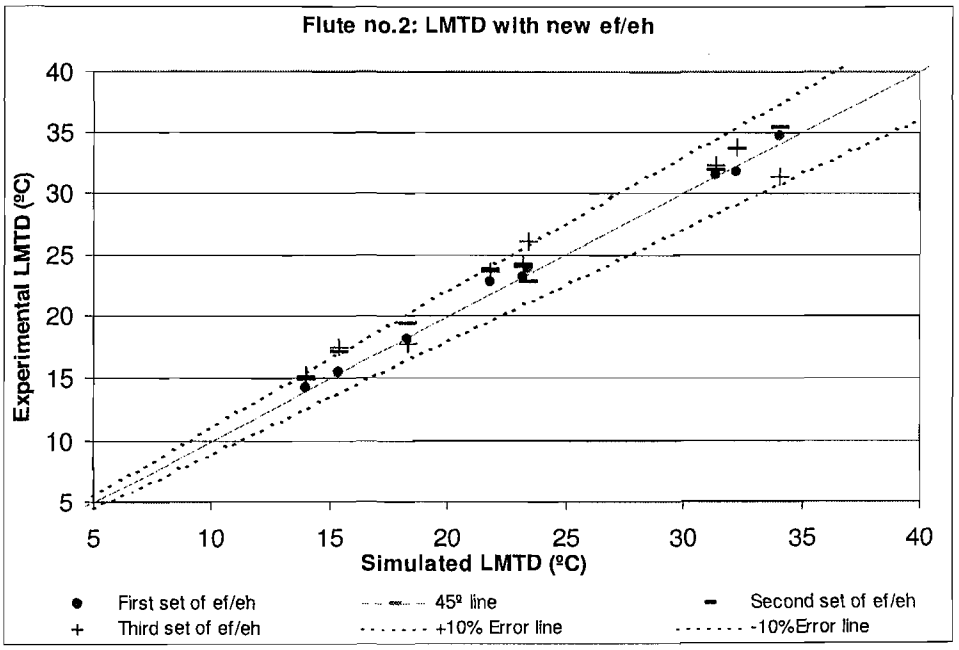


Figure E.8: Simulation of the LMTD by using the new enhancement factors on fluted tube no.2.

FLUTED TUBE no. 3

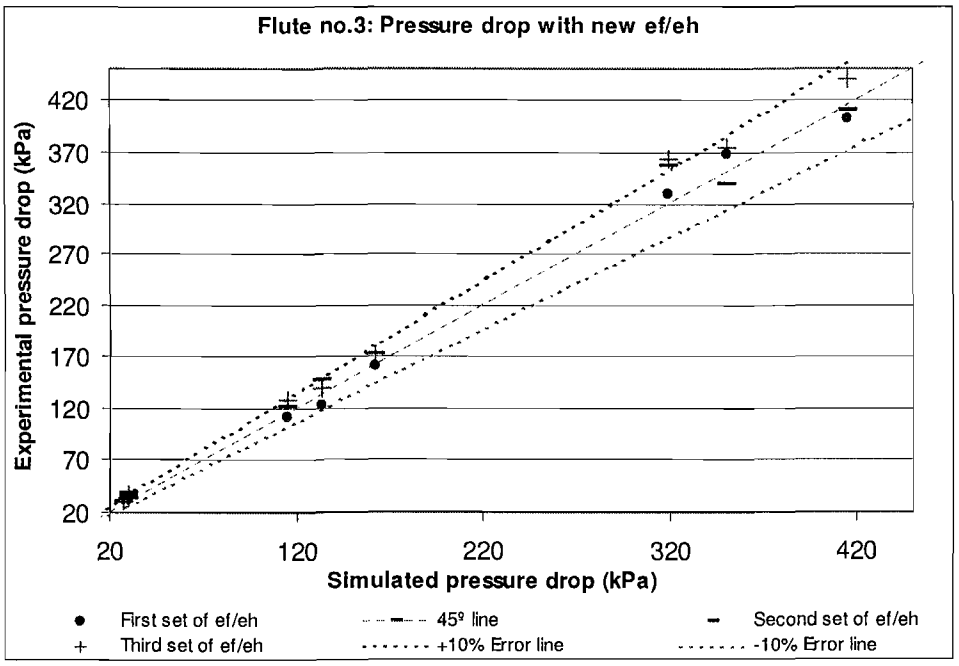


Figure E.9: Simulation of the pressure drop by using the new enhancement factors on fluted tube no.3.

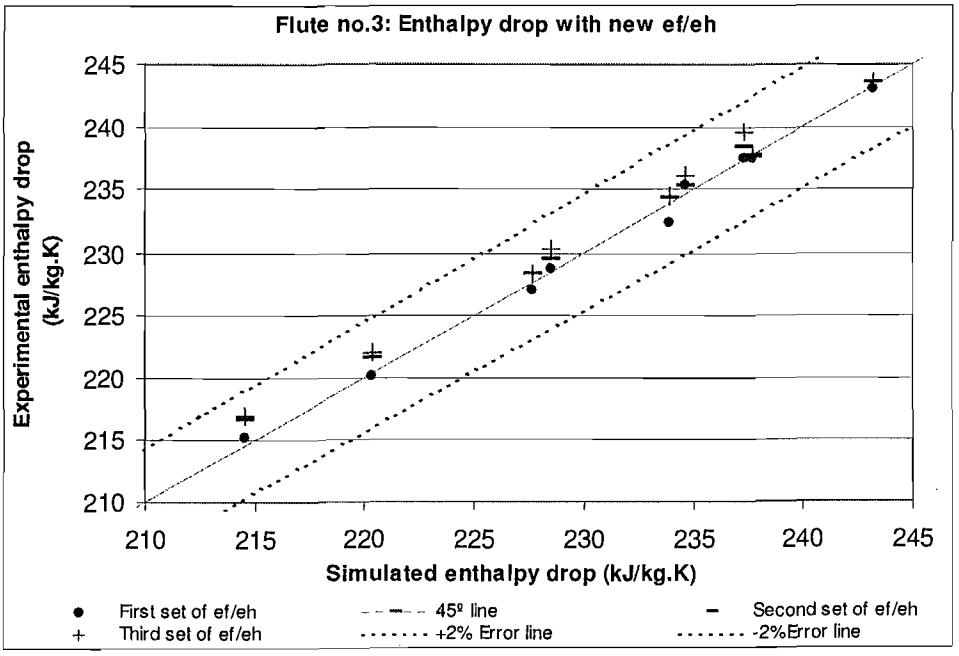


Figure E.10: Simulation of the enthalpy drop by using the new enhancement factors on fluted tube no.3.

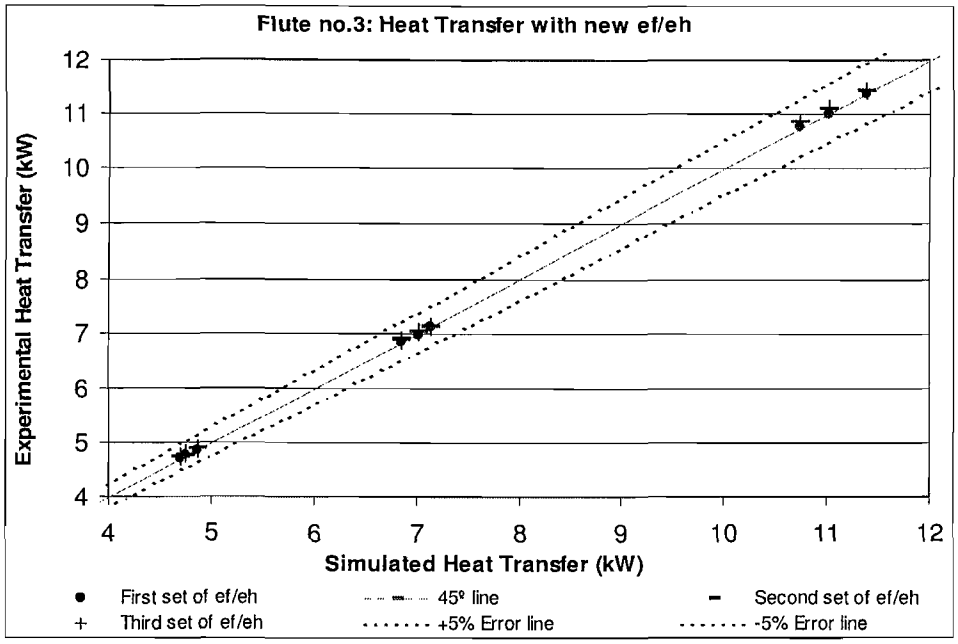


Figure E.11: Simulation of the heat transfer by using the new enhancement factors on fluted tube no.3.

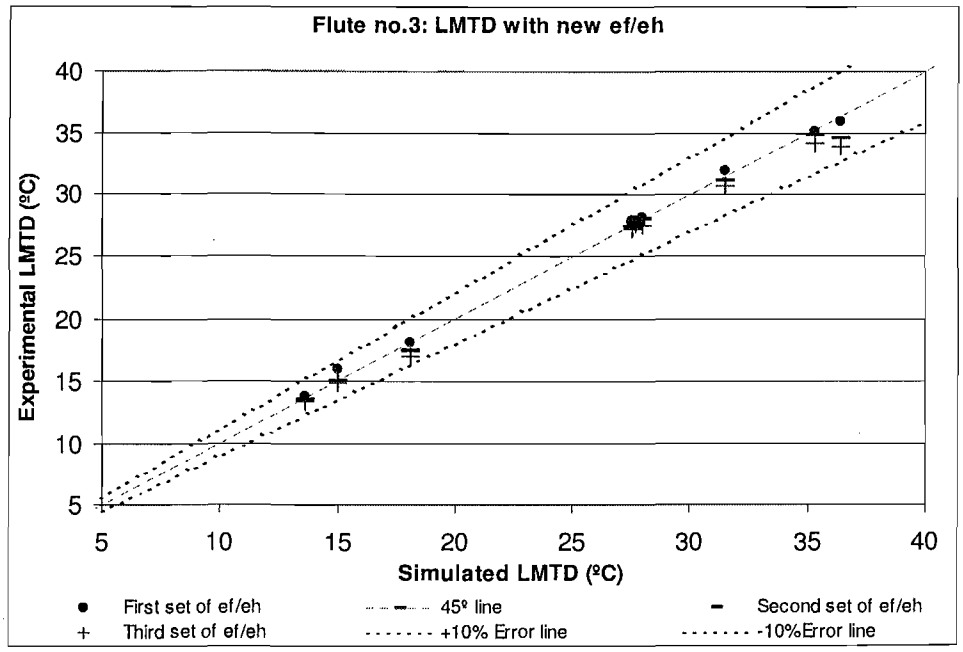


Figure E.12: Simulation of the LMTD by using the new enhancement factors on fluted tube no.3.

APPENDIX F

Uncertainty Analysis

FLUTED TUBE no. 1

		Test no.	REFRIGERANT Heat Transfer (kW)	UNCERTAINTY	%	WATER Heat Transfer (kW)	UNCERTAINTY	%
Refrigerant flow rate	0.02 kg/s	1	5.488	0.0825	1.4805	5.486	0.0687	1.2368
		2	5.186	0.0779	1.4806	5.140	0.0636	1.2219
		3	4.740	0.0713	1.4809	4.669	0.0632	1.3349
		4	5.553	0.0835	1.4805	5.535	0.0818	1.4563
		5	5.188	0.0780	1.4806	5.187	0.0817	1.5509
		6	4.841	0.0728	1.4809	4.824	0.0789	1.6091
		7	5.330	0.0801	1.4813	5.364	0.1004	1.8373
		8	5.244	0.0788	1.4808	5.244	0.1020	1.9080
		9	4.845	0.0728	1.4809	4.805	0.0987	2.0122
Refrigerant flow rate	0.03 kg/s	10	7.456	0.1121	1.4812	7.438	0.0661	0.8814
		11	7.747	0.0778	0.9948	7.703	0.0689	0.8864
		12	6.797	0.0683	0.9949	6.836	0.0646	0.9362
		13	7.872	0.0790	0.9940	7.795	0.0881	1.1180
		14	7.301	0.0734	0.9947	7.285	0.0871	1.1820
		15	8.076	0.1214	1.4810	8.013	0.0902	1.1133
		16	8.259	0.0829	0.9943	8.209	0.1088	1.3080
		17	7.621	0.1146	1.4815	7.595	0.1051	1.3649
		18	7.786	0.1171	1.4817	7.769	0.1094	1.3886
Refrigerant flow rate	0.05 kg/s	19	11.950	0.1796	1.4807	11.840	0.0772	0.6477
		20	11.740	0.1766	1.4820	11.670	0.0778	0.6623
		21	12.840	0.0654	0.5069	12.780	0.1053	0.8172
		22	12.150	0.0176	0.1446	12.140	0.0853	0.6981
		23	11.040	0.0565	0.5093	10.970	0.0833	0.7534
		24	12.930	0.1299	0.9946	12.820	0.1076	0.8323
		25	12.260	0.0173	0.1407	12.210	0.1065	0.8647
		26	11.880	0.1786	1.4811	11.840	0.1040	0.8707

FLUTED TUBE no.2

		Test no.	REFRIGERANT Heat Transfer (kW)	UNCERTAINTY	%	WATER Heat Transfer (kW)	UNCERTAINTY	%
Refrigerant flow rate	0.02 kg/s	1	5.535	0.0832	1.4813	5.480	0.0651	1.1731
		2	5.110	0.0768	1.4803	5.103	0.0623	1.2065
		3	5.180	0.0779	1.4816	5.137	0.0623	1.1984
		4	5.635	0.0847	1.4814	5.612	0.0840	1.4752
		5	5.560	0.0736	1.3057	5.539	0.0840	1.4944
		6	5.172	0.0778	1.4812	5.168	0.0822	1.5660
		7	5.678	0.0853	1.4801	5.720	0.1030	1.7688
		8	5.535	0.0832	1.4806	5.511	0.1022	1.8207
Refrigerant flow rate	0.03 kg/s	9	7.197	0.1081	1.4798	7.176	0.0728	1.0039
		10	7.373	0.1108	1.4805	7.328	0.0706	0.9545
		11	6.986	0.1051	1.4821	6.621	0.0629	0.9411
		12	7.265	0.0730	0.9950	7.264	0.0916	1.2452
		13	7.341	0.0738	0.9946	7.284	0.0866	1.1747
		14	7.210	0.0725	0.9954	7.150	0.0851	1.1761
		15	7.304	0.0734	0.9948	7.255	0.1090	1.4802
		16	7.333	0.0737	0.9944	7.280	0.1073	1.4525
		17	7.786	0.0783	0.9951	7.781	0.1113	1.4102
Refrigerant flow rate	0.05 kg/s	18	12.390	0.1246	0.9956	12.280	0.0740	0.5992
		19	11.470	0.1155	0.9969	11.370	0.0776	0.6782
		20	11.340	0.1143	0.9979	11.220	0.0774	0.6850
		21	12.710	0.1278	0.9955	12.630	0.1037	0.8144
		22	12.130	0.0621	0.5089	12.160	0.1211	0.9861
		23	11.530	0.0178	0.1541	11.630	0.0853	0.7279
		24	12.840	0.0181	0.1407	12.77	0.1077	0.8363
		25	12.130	0.0621	0.5090	12.04	0.1072	0.8825
		26	11.710	0.1178	0.9960	11.91	0.1203	1.0000

FLUTED TUBE no. 3

		Test no.	REFRIGERANT Heat Transfer (kW)	UNCERTAINTY	%	WATER Heat Transfer (kW)	UNCERTAINTY	%
Refrigerant flow	0.02 kg/s	1	5.357	0.08050	1.4805	5.352	0.06621	1.2220
		2	5.095	0.07657	1.4806	5.006	0.06422	1.2666
		3	5.369	0.08071	1.4810	5.359	0.06610	1.2184
		4	5.514	0.06857	1.2283	5.414	0.08130	1.4794
		5	5.245	0.07882	1.4805	5.195	0.08370	1.5856
		6	5.423	0.08152	1.4810	5.417	0.08204	1.4919
		7	5.416	0.08137	1.4802	5.364	0.10170	1.8607
Refrigerant flow rate	0.03 kg/s	8	7.819	0.11750	1.4805	7.758	0.08410	1.0724
		9	7.219	0.07249	0.9942	7.210	0.06442	0.8856
		10	7.627	0.07714	1.0013	7.644	0.06410	0.8316
		11	7.819	0.07847	0.9936	7.758	0.08247	1.0519
		12	7.384	0.07413	0.9939	7.344	0.08410	1.1322
		13	7.669	0.07706	0.9948	7.665	0.08671	1.1186
		14	7.696	0.07478	0.9623	7.680	0.09268	1.1924
		15	7.477	0.00922	0.1232	7.471	0.09865	1.3032
Refrigerant flow rate	0.03 kg/s	16	12.420	0.01735	0.1395	12.410	0.06774	0.5429
		17	11.620	0.01680	0.1444	11.570	0.06507	0.5593
		18	11.290	0.03640	0.3214	11.200	0.04510	0.4011
		19	12.510	0.01710	0.1365	12.480	0.08812	0.7011
		20	12.060	0.17460	1.4271	12.010	0.09298	0.7682
		21	11.610	0.17460	1.4816	11.550	0.10820	0.9281
		22	12.390	0.12440	0.9941	12.280	0.11750	0.9478
		23	12.260	0.01713	0.1395	12.240	0.10460	0.8473
		24	11.790	0.01712	0.1450	11.730	0.10410	0.8797